universität wien

DISSERTATION / DOCTORAL THESIS

Titel der Dissertation /Title of the Doctoral Thesis

„Deciphering LukGH-receptor interaction: molecular mechanisms and species specificity“

verfasst von / submitted by

Nikolina Trstenjak, BSc MSc

angestrebter akademischer Grad / in partial fulfilment of the requirements for the degree of

Doctor of Philosophy (PhD)

Wien, 2019 / Vienna 2019

Studienkennzahl lt. Studienblatt / degree programme code as it appears on the student record sheet:	A 794 685 490
Dissertationsgebiet lt. Studienblatt / field of study as it appears on the student record sheet:	Molecular Biology
Betreut von / Supervisor:	Dr. Dr. Eszter Nagy

TABLE OF CONTENTS

DEDICATION

To my five pillars of strength.

Thank you for walking this journey with me.

ACKNOWLEDGMENTS

Firstly, I would like to thank Eszter for giving me the opportunity to work on this exciting project and for accepting me into the wonderful Arsanis family. I admire your work and I am grateful I had a chance to learn from you. Thank you for your guidance.

I would like to thank Ivana, Irina, Sabine and Michele for their constant support, help with experiments, personal discussion and entertaining lunch breaks. You will always have a special place in my heart. I also want to thank the whole Arsanis team for being amazing colleagues.

My biggest gratitude goes to Adriana. You were a great and supportive teacher. Thank you for not kicking me out of the office every time I had a question (and I had a lot), but instead providing me with guidance, new ideas and excellent discussions. You helped me shape my future career and I will always be thankful to you.

Lastly, I would like to thank my entire family, my boyfriend and my friends for supporting me during this period. Most of all I would like to thank my amazing parents for all the sacrifices they have made for my siblings and me, because without them nothing I have done would be possible.

Thank you very much!
Veliko hvala svima!

ABSTRACT

Staphylococcus aureus is a major human pathogen causing a wide range of diseases due to its complex pathogenesis, arising from numerous virulence mechanisms. The leukocidins, a family of bi-component pore forming cytotoxins, are considered to be at the core of *S. aureus* immune evasion by lysing a variety of immune cells. Their contribution to *S. aureus* pathogenesis *in vitro* and *ex vivo* has been partially established, but little is known about their role *in vivo*, as they display a considerable host tropism (i.e. human specificity). This is driven by binding of leukocidins to specific cellular receptors on the surface of immune cells. For instance, the most potent and unique leukocidin, LukGH, shows limited or no activity in the rabbit and the mouse, respectively, which correlates with low affinity for the rabbit and mouse counterparts of its receptor (CD11b-I).

Research findings included in this dissertation illustrate an alternative approach towards replacing humanized animal models in staphylococcal leukocidin research. Protein engineering of leukocidins for improved affinity towards targeted receptors in different species has been used to overcome the species specificity, even in the absence of structural data on the leukocidin-receptor interaction, as illustrated with the LukGH-receptor as an example. Site-directed mutagenesis was used to map the LukGH-receptor interface and obtain recombinant LukGH variants with increased affinity for the rabbit receptor and improved activity towards rabbit neutrophils (polymorphonuclear cells or PMNs). This increased activity was maintained after chromosomal integration of LukGH variants into *S. aureus* strains lacking the natural variant(s) resulting in rabbit-PMN adapted strains that validate our approach and offer a novel option for studying the role of LukGH in *S. aureus* pathogenesis in small animal models.

Furthermore, the research resulted in the first crystal structure of the *S. aureus* leukocidin LukGH in complex with its receptor CD11b-I (human and mouse). The structures of the LukGH-receptor complex provide an invaluable insight into the structural requirements for leukocidin-receptor interaction, and the molecular basis for the contribution of receptor up-regulation and LukGH dimerization in solution before cell binding to LukGH cytotoxicity. The data illustrate the potential role of cellular receptors in the initiation of leukocidin oligomerisation, and elucidate the observed host tropism of LukGH, and the lack of cytotoxicity towards mouse cells. These findings advance our understanding of the complex mechanism of leukocidin pore formation and can aid in the development of LukGH variants, and variants of other human specific leukocidins, active in various small animal models like mouse, rat and guinea pig.

In addition to the novel insight into the LukGH host tropism and leukocidin-receptor interaction, future work and new research questions on the role of leukocidins in immune cell

signalling and immune responses during *S. aureus* infection and the potential of LukGH-receptor interaction for therapeutic use are discussed.

KURZFASSUNG

Staphylococcus aureus ist ein bedeutender, menschlicher Krankheitserreger, der aufgrund seiner komplexen Pathogenese, die sich aus zahlreichen Virulenzmechanismen ergibt, eine Vielzahl von Krankheiten verursacht. Die Leukocidine, eine Familie von bi-komponenten poren-formenden Zytotoxinen, bilden den Kern der Umgehung des Immunsystems durch *S. aureus*, indem sie eine Vielzahl von Immunzellen lysieren. Ihre Bedeutung für die Pathogenese *von S. aureus in vitro* und *ex vivo* ist nachgewiesen, über ihre Rolle in der Pathogenese ist aber wenig bekannt, da sie einen erheblichen human-spezifischen Wirts-Tropismus aufweisen. Dies wird durch die Bindung von Leukocidinen an spezifische zelluläre Rezeptoren auf der Oberfläche der Immunzelle angetrieben. So zeigt beispielsweise das potenteste und einzigartigste Leukocidin, LukGH, eine begrenzte oder gar keine Aktivität im Kaninchen bzw. der Maus, was mit einer geringen Affinität zum entsprechenden Rezeptor (CD11b-I) im Kaninchen und der Maus korreliert.

Die Forschungsergebnisse dieser Dissertation illustrieren einen Ansatz, der eine Alternative zu humanisierten Tiermodellen in der Erforschung der Leukocidine von Staphylokokken darstellt. Um die Spezies-Spezifität zu umgehen, und zur Verbesserung der Affinität gegenüber der Ziel-Rezeptoren in verschiedenen Spezies wurde ein Proteinengineering von Leukocidinen angewendet. Dies konnte trotz Mangels an Strukturdaten zu den Leukocidin-Rezeptor-Interaktionen am Beispiel des LukGH-Rezeptors gezeigt werden. Mit Hilfe zielgerichteter Mutagenese wurde die LukGH-Rezeptor-Schnittstelle kartiert und rekombinante LukGH-Varianten mit erhöhter Affinität zum Kaninchenrezeptor und verbesserter Aktivität gegenüber Kaninchen-Neutrophilen (polymorphkernige Zellen, *engl.* polymorpho-nuclear cells – PMNs) generiert. Die Aktivität wurde nach der chromosomalen Integration von LukGH-Varianten in *S. aureus*-Stämme, welche die natürlichen Varianten nicht exprimieren, beibehalten, was zu Kaninchen-PMN-angepassten Stämmen führte. Dies bestätigt unsere Strategie und ist ein vielversprechender Ansatz um die Rolle von LukGH in der *S. aureus*-Pathogenese in Kleintiermodellen zu untersuchen.

Darüber hinaus resultierte die Forschung in der ersten Kristallstruktur von *S. aureus* Leukocidin mit seinem menschlichen und murinen Rezeptor. Die Strukturen des LukGH-Rezeptor-Komplexes liefern einen wertvollen Einblick in die strukturellen Voraussetzungen für Leukocidin-Rezeptor-Interaktion und die molekulare Basis für die beobachtete Rolle der Hochregulierung des Rezeptors in der LukGH-Zytotoxizität und LukGH-Dimerisierung in Lösung,also vor der Zellbindung stattfindet. Die Daten deuten auf die potenzielle Rolle zellulärer Rezeptoren während der Initiation der Leukocidin-Oligomerisation hin und erläuternden beobachteten Wirts-Tropismus von LukGH sowie den Mangel an Zytotoxizität gegenüber Mauszellen. Diese Ergebnisse vertiefen unser Verständnis des komplexen Mechanismus der Porenbildung der

Leukocidine und können bei der Entwicklung von LukGH-Varianten und Varianten anderer humanspezifischer Leukocidine helfen, die in verschiedenen Kleintiermodellen wie Maus, Ratte und Meerschweinchen aktiv sind.

Neben den neuartigen Erkenntnissen über den LukGH-Wirt-Tropismus und die Leukocidin-Rezeptor-Interaktion werden zukünftige Studien und neue Fragestellungen bezüglich der Rolle von Leukocidinen bei der Signalweiterleitung von Immunzellen sowie Immunreaktionen während der *S. aureus*-Infektion als auch das Potenzial der LukGH-Rezeptor-Interaktion für therapeutische Zwecke diskutiert.

1. PREAMBLE

1.1. *Staphylococcus aureus*

Staphylococcus aureus is a Gram-positive pathogen and an asymptomatic, opportunistic colonizer of skin and mucosal surfaces in humans, domestic animals (e.g. livestock), and wild animals (Monecke et al, 2016; Aires-de-Sousa, 2017). Under favourable circumstances (e.g. immunosuppression, breaching of mechanical barriers, malnutrition), *S. aureus* can exert pathogenic effects and cause a range of diseases, like skin and deep tissue infections, endocarditis or life-threatening pneumonia and sepsis (Tong et al, 2015). Shortly after introduction of methicillin, outbreaks of methicillin-resistant *S. aureus* (MRSA) strains were reported, and they remain a major healthcare concern. While MRSA used to be limited to the hospitals (HA-MRSA), in the past 20 years highly virulent community-associated MRSA (CA-MRSA) strains have rapidly emerged worldwide. Antibiotic resistance and prevalence of MRSA infections in both the nosocomial and community setting, and the increased dominance of hyper-virulent clones of both MRSA (e.g. USA300) and methicillin-sensitive *S. aureus* (MSSA) (e.g. ST121), highlight the need for better understanding of *S. aureus* pathogenesis and development of effective prophylactic and therapeutic agents (Chambers & Deleo, 2009; Rao et al, 2015).

The intricate pathogenesis of *S. aureus* arises from numerous virulence mechanisms that allow the bacteria to circumvent innate and adaptive host immune systems, such as: 1) adherence to the host tissue promoted by surface factors (e.g. teichoic acids, microbial surface components recognizing adhesive matrix molecules), 2) evasion of recognition by immune cells (e.g. biofilm formation), 3) circumvention of neutrophil extravasation (e.g. staphylococcal superantigen-like 5, extracellular adherence protein Eap), chemotaxis (e.g. staphylococcal superantigen-like 5, chemotaxis inhibitory protein, formyl protein receptor-like inhibitory proteins), priming and activation (e.g. Staphopain A, staphylococcal superantigen-like family), 4) inhibition of opsonisation, phagocytosis and intracellular neutrophil killing (e.g. staphylococcal protein A, aureolysin, staphyloxanthin), and 5) invasion of immune cells and host cell injury by secreted cytotoxins (e.g. α-hemolysin, leukocidins, phenol-soluble modulins) (Rigby & DeLeo, 2012; Spaan et al, 2013a; Guerra et al, 2017). Central to the last mechanism are the bi-component leukocidins, believed to be one of the key components of *S. aureus* pathogenesis.

In the following chapters the common features of the leukocidins, with the focus on the most divergent member of the family, LukGH (also called LukAB), relevant for this PhD research project are discussed. In addition, the value of current animal models of *S. aureus* infection in

assessing the leukocidin contribution to *S. aureus* pathogenesis is debated, and a potential solution is offered.

1.2. Leukocidins

Leukocidins are members of bi-component pore forming cytotoxin (PFT) family whose binding to specific cellular receptors on the surface of immune cells, leads to the formation of the hetero-octameric, beta-barrel, membrane spanning pore, which disrupts osmotic balance and membrane potential and results in necrotic cell death (Alonso & Torres, 2014; Spaan et al, 2017). *S. aureus* strains associated with human infections can secrete up to five different leukocidins: two γ-hemolysins (HlgAB and HlgCB), LukED, LukSF-PV (PVL), and LukGH (also called LukAB) (Vandenesch et al, 2012; Alonso & Torres, 2014; Reyes-Robles & Torres, 2016) (Table 1). The leukocidins mainly target phagocytic cells (immune evasion), but also red blood cells (iron acquisition, LukED, HlgAB), T-cells (LukED, HlgAB) and endothelial cells (LukED, HlgAB) (Vandenesch et al, 2012; Berube & Wardenburg, 2013; Reyes-Robles & Torres, 2016; Spaan et al, 2017; Lubkin et al, 2019). Two more leukocidins, LukMF' and LukPQ, specific for ruminant and equine *S. aureus* strains, respectively, and not cytotoxic towards human neutrophils, have recently been identified (Vrieling et al, 2015; Koop et al, 2017).

Leukocidin-induced cell lysis triggers substantial inflammation and cellular damage through the release of pro-inflammatory mediators (e.g. IL-8 and histamine) and tissue-damaging enzymes (Alonzo & Torres, 2014). In addition to cell lysis, leukocidins can, at sublytic concentrations, act as potent activators of innate immunity; LukSF-PV and HlgAB/CB can prime neutrophils for increased bactericidal activity (Graves et al, 2012; Spaan et al, 2015a) and both LukSF-PV and LukGH can promote formation of neutrophil extracellular traps (NETs) (Pilsczek et al, 2010; Malachowa et al, 2013). Based on *in vitro* and *ex vivo* assays utilizing human phagocytes, LukGH is the most potent leukocidin in *S. aureus* mediated neutrophil killing (Ventura et al, 2010; DuMont et al, 2011; Rouha et al, 2015; Janesch et al, 2017). LukGH has a unique function, as it is the only leukocidin that enhances bacterial survival after phagocytosis by promoting bacterial escape from the neutrophils (DuMont et al, 2013a). At the late exponential phase of *S. aureus* growth, LukGH also associates with the bacterial cell membrane, the relevance of which is not clear (Ventura et al, 2010). Furthermore, the LukGH cytotoxicity is dependent on receptor up-regulation after polymorphonuclear cells (PMN) stimulation with infection-relevant stimuli (Janesch et al, 2017).

Over the last few years, significant advancement has been made regarding the different roles of leukocidins *in vitro* and *ex vivo*, but contribution of the individual leukocidins to *S. aureus* pathogenesis *in vivo* is less clear. Due to host tropism of leukocidins, discussed further in the

preamble (see Subchapter 1.5), suitable animal models of *S. aureus* infection are currently limited in application.

Table 1. Cell tropism and species specificity of the bi-component leukocidins of *Staphylococcus aureus.*

Note. Adapted from "Adaptation of the *Staphylococcus aureus* leukocidin LukGH for the rabbit host by protein engineering.", by Trstenjak et al, *Biochemical Journal* **476**, 275-292 (2019), with permission from authors.

Cytotoxin	Cellular receptors	Receptor family	Targeted cells	EC_{50} [nM]		
				Human	Rabbit	Mouse
LukSF-PV	C5aR[1], C5L2[1], CD45[2]	Chemokine receptors	monocytes, neutrophils, macrophages	0.9[1], 0.1 - 0.5[8], ~0.1 [9], ~ 1[10], ~1[11]	0.1-0.2[8], ~ 1[10]	resistant[1, 8, 10, 14]
LukED	CCR5[3], CXCR1[4], CXCR2[4]	Chemokine receptors	monocytes, neutrophils, macrophages, T cells, dendritic cells, NK cells	2.4 - 4[8], ~1[11]	0.03 - 0.04[8]	14 - 48.3[8]
	DARC[5]	Chemokine receptor	red blood cells, endothelial cells	~20[5], <15[12]		<15[12]
LukGH	CD11b-I[6]	Integrin	neutrophils, macrophages, monocytes, dendritic cells	0.01 - 0.03*[9], 0.25[13]	35[13]	550[13]
HlgAB	CXCR1[7], CXCR2[7], CCR2[7]	Chemokine receptors	monocytes, macrophages, T cells, neutrophils	0.4 - 0.6[8]	0.2[8]	resistant[7, 8]
	DARC[5]	Chemokine receptor	red blood cells, endothelial cells	~ 1[5]		
HlgCB	C5aR[7], C5L2[7]	Chemokine receptors	monocytes, macrophages, neutrophils	0.5 - 0.6[8], ~ 2.5[14]	0.1[8]	resistant[7, 8, 14]

*lipopolysaccharide (LPS) stimulated cells. [1] Spaan et al, 2013b; [2] Tromp et al, 2018; [3] Alonzo et al, 2012; [4] Reyes-Robles et al, 2013; [5] Spaan et al, 2015b; [6] DuMont et al, 2013b; [7] Spaan et al, 2014; [8] Diep et al, 2016; [9] Janesch et al, 2017; [10] Löffler et al, 2010; [11] Koop et al, 2017; [12] Yoong & Torres, 2015; [13] Malachowa et al, 2012; [14] Spaan et al, 2015a.

1.2.1. Genetic organization and amino acid sequence conservation of leukocidins

The bi-component leukocidins are comprised of S- (slow) (HlgA, HlgC, LukS-PV, LukE and LukH) and F- (fast) (HlgB, LukF-PV, LukD and LukG) components, named so based on their elution profile during ion exchange chromatography (Woodin, 1959; Woodin, 1960). The subunits are expressed as inactive, water soluble monomeric proteins of approximately 300 amino acids in length

that assemble into active toxin on the surface of the target cell (Badarau et al, 2017). Genes for HlgA, HlgB, HlgC, LukG and LukH are part of the core genome of *S. aureus* and are present in the great majority of sequenced strains, while *lukE* and *lukD* are located on the *S. aureus* pathogenicity island vSaβ, and present in 30-87% of the sequenced strains (Vandenesch et al, 2012; Alonso & Torres, 2014; Badarau et al, 2017). The *lukS-PV* and *LukF-PV* are found on the genome of the temperate phage ϕSa2 and are present in only ~2-3% of *S. aureus* isolates (Alonso & Torres, 2014). Even though genes for LukSF-PV are present in small number of isolates, over 90% of the *lukS-PV* and *lukF-PV* containing isolates are linked to severe infections (e.g. necrotizing pneumonia) and community-acquired *S. aureus* infections (Lina et al, 1999; Gillet et al, 2002; Naimi et al, 2003; Alonso & Torres, 2014). Although limited nucleotide sequence diversity was seen for *lukE*, *lukD*, *lukS-PV* and *lukF-PV* between strains, genetic diversity in the *hlg*, *lukG* and *lukH* genes is higher. The genetic diversity is also reflected at the amino acid sequence level among *S. aureus* strains (Alonso & Torres, 2014; Badarau et al, 2017).

The S- and F-components share between 65-82% amino acid sequence homology to each other, with the exception of LukH and LukG that share only 30% and 40% amino acid homology to other S- and F-components, respectively (Rouha et al, 2015; Badarau et al, 2017). Furthermore, LukH contains unique N- and C-terminal extensions, that are not present in other S-components, where glutamate 323 from this C-terminal extension is crucial for LukGH receptor binding and cytotoxicity (DuMont et al, 2014). As a result of high amino acid sequence homology, all S- and F-components, apart from LukH and LukG (Yanai et al, 2014; Adhikari et al, 2015; Badarau et al, 2015), can form non-cognate pairs with each other with a broad range of cytotoxic activities (König et al, 1997; Yanai et al, 2014; Adhikari et al, 2015). Non-cognate pairs thus expand the *S. aureus* toxin arsenal to up to 13 different leukocidins (König et al, 1997; Dalla Serra et al, 2005; Yanai et al, 2014; Adhikari et al, 2015).

1.2.2. Role of the S- and F-components

The S- and F-components play different roles during receptor recognition and pore formation. On phagocytes, the S-component mediates the cell- and species-specificity by recognizing the corresponding cellular receptor in the lipid bilayer (see Subchapter 1.3 and 1.4), and after binding to the cell, subsequently recruits the F-component. The order of S- and F-component binding is less clear on erythrocytes (Colin et al, 1994; Yokota & Kamio 2000; Nguyen et al, 2003). While the role of the S-component is established, the role of the F-component in binding and oligomerisation initiation is less understood. Except for LukG, all F-components have phosphocholine (PC) binding pocket; eliminating PC binding results in the formation of oligomeric non-lytic pre-pore

intermediates (Olson et al, 1999; Monma et al, 2004; Potrich et al, 2009). The F-components may also be involved in determining the host tropism, as seen with the recently identified equine-specific LukPQ (Koop et al, 2017). Furthermore, leukocidin cytotoxicity may also be mediated by the F-component, as LukF-PV can bind to the cellular receptor CD45 in human specific manner and independent of the S-component (Tromp et al, 2018). The affinity of this interaction is significantly lower than the affinity of the S-component-receptor interaction, thus the relevance of LukF-PV-CD45 binding *in vivo* has to be determined (Tromp et al, 2018).

1.2.3. Structure characteristics of the leukocidins

Crystal structures of all S- and F-components have been solved (Pédelacq et al, 1999; Olson et al, 1999; Guillet et al, 2004; Roblin et al, 2008; Laventie et al, 2014; Badarau et al, 2016; Nocadello et al, 2016). They share the same 3D structure and overall fold, with three distinct structural domains that do not differ by more than 1Å ($RMSD_{C\alpha}$) between different leukocidins (Badarau et al, 2017): 1) the cap or core β-sandwich domain involved in inter-monomer interactions in the pre-pore and pore structures, 2) the rim domain involved in cell binding of some leukocidins (Reyes-Robles et al, 2013; Laventie et, 2014; Peng et al, 2018), and 3) the stem domain, packed within the cap domain in soluble monomers and is forming the beta-sheet barrel structure spanning the cell membrane in the fully assembled pore (Figure 1) (Yamashita et al, 2011; Yamashita et al, 2014). Another important part of the cap domain is the so called N-terminus amino latch (Figure 1), which in the fully assembled pore forms a latch between two protomer subunits. The amino latch is believed to play an important role during pore formation by inducing stem extrusion of protomers (Yamashita et al, 2014).

In addition to the lowest amino acid sequence homology to other S- and F-components, LukGH is also unique at the structural level, as it exists as a stable heterodimer in solution even before cell binding (DuMont et al, 2014; Badarau et al, 2015). The LukGH dimer interface is stabilized by considerable interactions between the stem and rim regions of LukH and LukG (Badarau et al, 2016). In the rim region, the LukGH dimer is stabilized by polar contacts, electrostatic interactions, a hydrophobic core, and by three salt bridges between LukG and LukH (Badarau et al, 2015). The residues participating in salt bridge formation are conserved in the LukGH variant sequences, but not in the other S- and F-components (Badarau et al, 2015). While in other F-components, the stem is folded against the cap domain, in LukG the stem is extruded and interacts with the LukH monomer via electrostatic interactions, polar contacts and a hydrophobic core (Badarau et al, 2016). The difference in the 3D structures of LukGH and the other leukocidins explains the lack of non-cognate pairing observed for LukGH.

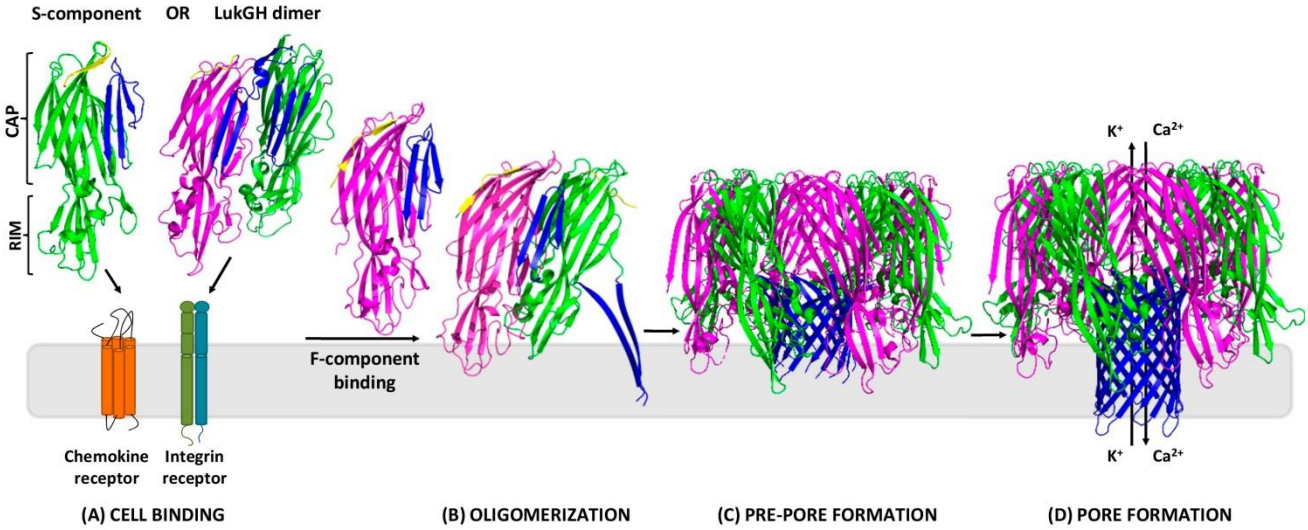

Figure 1. **Proposed mechanism of leukocidin pore formation.** The S- and F-component are shown as green and magenta cartoon, respectively. The stem domain and amino latch are shown as blue and yellow cartoon, respectively. **(A)** Binding of soluble S-component or LukGH dimer to the cellular receptor on the cell surface, followed by subsequent recruitment of F-component (or LukGH dimer). **(B)** Dimerization of the components results in amino latch release and extrusion of the stem into the cell membrane. **(C)** Further binding of S- and F-components (or LukGH dimer) leads to the formation of the pre-pore structure with 4 alternating S- and F-components and finally in the insertion of the fully formed beta-barrel pore through the cell membrane and subsequent cell death **(D)**.

1.3. Molecular mechanism of leukocidin pore formation

Crystal structures of individual S- and F-components, pre-pore (Yamashita et al, 2014) and pore (Yamashita et al, 2011; Badarau et al, 2016) structures aid the understanding of the fundamentals of molecular mechanisms of pore formation. The pore is comprised of 4 alternating S- and F-components arranged around the central axis (Figure 1). The current model of leukocidin pore formation (Figure 1) proposes that the initial binding of S-component to the cellular receptor is followed by the recruitment of the F-component, causing a release of the amino latch of the bound protomer, due to the binding of the adjacent protomer. The released amino latch interferes with the stem of the bound protomer, which triggers stem extrusion into the lipid bilayer (Yamashita et al, 2014). The initial step is different for LukGH, as LukGH already binds to the cell surface as a dimer (DuMont et al, 2014; Badarau et al, 2015). The consecutive recruitment of other S- and F-components (or LukGH dimer) and stem release of each of the protomers, leads to the formation of the non-lytic, oligomeric pre-pore structure with the transmembrane part of the pore (stems) in a highly flexible state. Final step of pore formation involves folding of extruded stems into a rigid beta-barrel pore that spans the lipid bilayer (Yamashita et al, 2011; Yamashita et al, 2014) (Figure 1).

While much is known about the structural changes occurring within leukocidins during pore formation, the role of the cytotoxin-lipid interaction, and the particular role of receptors in the intricate process of oligomerisation initiation and pore formation is unclear. Recently, LukSF-PV complexes were found in the receptor clusters, indicating possible relevance of the local density of receptors for the pore assembly initiation (Haapasalo et al, 2019). The same authors also present a model in which, after pore formation, the receptor is recycled by free LukS-PV molecules thus amplifying the cell damage (Haapasalo et al, 2019). As mentioned previously, the PC binding by F-component seems to be necessary for the active pore formation, and it is hypothesized that PC binding may play a role in disrupting the local structure of the membrane supporting the stem insertion into the membrane (Yamashita et al, 2014). Considering recent findings on LukF-PV binding to the cellular receptor, independently of the S-component (Tromp et al, 2018), a possible role of receptors in the oligomerisation initiation (Haapasalo et al, 2019) and a potential role of lipid binding in oligomerisation process, the current model of oligomerisation should be revised.

1.4. Cellular receptors of the leukocidins

The leukocidins display cell- and species-specificity, driven primarily by binding to different receptors on the cell surface, including transmembrane-spanning G protein-coupled receptors (GPCRs) and integrins (Table 1) (Alonso et al, 2012; DuMont et al, 2013b; Reyes-Robles et al, 2013; Spaan et al, 2013b; Spaan et al, 2014; Spaan et al, 2015b; Tromp et al, 2018). Intriguingly, some of the leukocidins share some of the receptors while still having receptors that are unique for each cytotoxin. The HlgAB and LukED share three receptors CXCR1, CXCR2 and DARC while, CCR2 for HlgAB and CCR5 for LukED, are unique for each leukocidin (Table 1) (Alonzo et al, 2012; Reyes-Robles et al, 2013; Spaan et al, 2014; Spaan et al, 2015a). Even though they are binding to the same receptor (DARC), they target different regions of the receptor (Spaan et al, 2015a; Spaan et al, 2015b). CCR5 and DARC are also receptors targeted by HIV virus and malaria, respectively. A CCR5 antagonist, used for treating HIV infection, can inhibit LukED pore formation by blocking the interaction of LukE with CCR5, suggesting that blocking interactions of the receptor and cytotoxin could be an effective strategy for treating *S. aureus* infections (Alonso et al, 2012). Another example of shared receptors, but targeting different binding epitopes, is the HlgCB and LukSF-PV pair (Table 1) (Spaan et al, 2015a). LukGH stands out among the leukocidins since, until now, only one receptor, which is not shared with any of the other leukocidins, has been identified (Table 1) (DuMont et al, 2013b).

1.4.1. Cellular receptor of LukGH

In addition to the lowest conservation at the sequence and structural level, LukGH is also targeting a different family of cellular receptors; the extracellular αI-domain of α_M/β_2 integrin (CD11b/CD18 also known as macrophage-1 antigen and complement receptor 3) (DuMont et al, 2013b). Integrin CD11b/CD18 is expressed on professional phagocytic cells (Ho & Springer, 1982) with a central role in immune processes and binds more than 40 reported protein ligands including human fibrinogen and complement fragment iC3b (Wright et al, 1983; Wright et al, 1988; Podolnikova et al, 2015). It is a heterodimeric protein comprised of two non-covalently linked subunits (CD11b and CD18) spanning the plasma membrane and transmitting signals from the extracellular to the intracellular space and vice versa (Figure 2A) (Shimaoka et al, 2002; Campbell & Humphries, 2011; Tan, 2012). Each subunit consists of a cytoplasmic tail, membrane spanning helixes and a multi-subunit ectodomain (Figure 2A). Although a crystal structure of the CD11b/CD18 ectodomain is not available, it is believed, based on the collected EM data (Adair et al, 2013), to resemble the solved structures of two other members of CD18 integrin family: CD11a/CD18 and CD11c/CD18 (Xie et al, 2010; Sen et al, 2013; Sen & Springer, 2016).

The main ligand binding site for most of the CD11b/CD18 binding ligands is αI-domain (CD11b-I) (Diamond et al, 1993; Podolnikova et al, 2015), located on the head of the ectodomain of the CD11b subunit (Figure 2A). DuMont et al confirmed that the main binding site of LukGH is the CD11b-I domain and that the binding is independent of the CD18 subunit (DuMont et al, 2013b). CD11b-I can be recombinantly expressed, independently of the other ectodomain subunits, and still maintain its functionality (Lee et al, 1995a). In the reported CD11b-I crystal structures two different conformations of CD11b-I were observed: inactive (closed or low affinity) and active (open or high affinity) forms of CD11b-I (Lee et al, 1995a; Lee et al, 1995b). Open conformation is characterized by the rearrangement of the metal coordinating residues at a metal ion-dependent adhesion site (MIDAS), to allow the carboxylate group of the ligand to complete the metal coordination, and a 10 Å downward shift of the C-terminal α7 helix (Figure 2B, Figure 2C) (Lee et al, 1995b; Arnout et al, 2016). Ligand associated downward shift of the CD11b-I α7 helix can induce an allosteric relay through the integrin resulting in conformational change of the CD11b/CD18 ectodomain (Arnout, 2016). The ectodomain can exist in three main conformations that, together with the conformation of the ligand binding site, characterize the integrin ligand affinity and accessibility to the ligands (Figure2A): 1) resting, bent integrin with low affinity-ligand binding site located near the cell membrane (3-7 nm), 2) extended integrin with low affinity-ligand binding site located around 20 nm from the cell membrane, and 3) extended, high affinity integrin with high affinity-ligand binding site (Campbell & Humphries, 2011; Arnaout 2016). It has also been observed that integrins can exist in a

transitional state (bent ectodomain with high affinity-ligand binding site), which can, when expressed on neutrophils, constrain inflammatory responses (Fan et al, 2015).

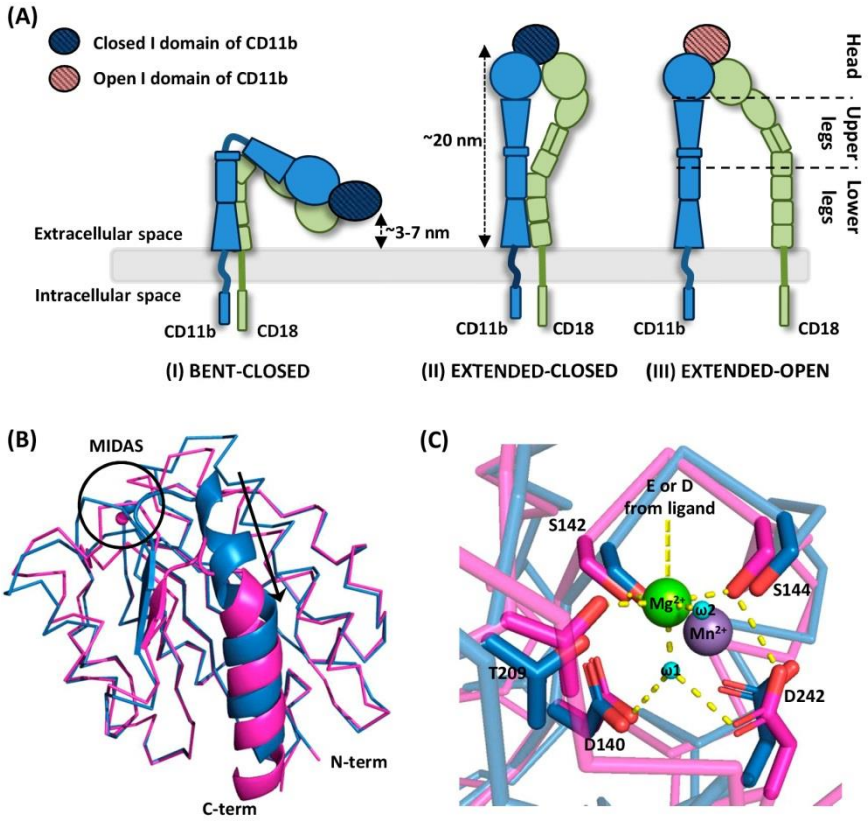

Figure 2. Ectodomain conformational changes and CD11b-I-domain changes during integrin activation. **(A)** Schematic representation of integrin activation states: (I) bent ectodomain with inactive I-domain, (II) extended ectodomain with inactive I-domain and (III) extended ectodomain with active I-domain. **(B)** Comparison of CD11b-I active (PDB 1IDO) and inactive conformation (PDB 1JLM) shown as pink and blue ribbon, respectively, with α7 helix shown as cartoon. **(C)** Comparison of active (PDB 1IDO) and inactive (PDB 1JLM) MIDAS site conformation shown as pink and blue sticks, respectively, and aligned on MIDAS residues (D140, S142, S144, T209, D242). The Mg^{2+} from 1IDO and Mn^{2+} from 1JLM conformation are shown as green and grey sphere, respectively.

The CD11b/CD18 is stored in granules of neutrophils and rapidly recruited to the cell surface after stimulation with inflammatory mediators (e.g. lipopolysaccharide, peptidoglycan, interleukin-8 (Lynn et al, 1991; Sengelov et al, 1993; Janesch et al, 2017)) resulting in increased local density of the integrin (Latger-Cannard et al, 2003). Furthermore, both LukSF-PV and LukGH can upregulate CD11b/CD18 expression (Graves et al, 2012; Malachowa et al, 2013), highlighting the possible synergistic effect between different leukocidins. As CD11b/CD18 upregulation can be directly linked to increased LukGH toxicity (Janesch et al, 2017) and can be mediated by other leukocidins, it is important to test the LukGH contribution to the *S. aureus* pathogenesis in settings that more

accurately mimic the situation *in vivo,* i.e. when leukocidins are expressed simultaneously, they are all fully functional and can form non-cognate pairs.

1.5. Leukocidin species specificity and animal models in *S. aureus* research

As the consequence of binding to specific cellular receptors, the leukocidins have significant species specificity (Table 1). Identification of the receptors helped to understand the observed species specificity, which results from: a) different level of the receptor expression between different species, b) lack of receptor expression in certain species, c) different binding affinities of the cytotoxin for the receptors from different species due to amino acid variations (lack of conservation) or d) a combination of these. Some of the most prominent examples are: LukGH, HlgCB and LukSF-PV that have no or limited activity towards mouse cells, due to molecular incompatibility of cytotoxins with their respective receptors, resulting in lower affinity or no binding of the cytotoxins to the receptor (DuMont et al, 2013b; Spaan et al, 2013b; Spaan et al, 2015a), and the HlgAB/CXCR1 pair, where the low level of receptor expression in mice seems to explain the human versus mouse preference (Spaan et al, 2015a). The only leukocidin that displays considerable cytotoxicity towards mouse phagocytes is LukED (Alonso et al, 2012). Leukocidin cytotoxicity in rabbits is more similar, but does not fully reflect cytotoxicity in human, as rabbits are much more susceptible to LukED but more resistant to LukGH (Malachowa et al, 2012; Diep et al, 2016; Trstenjak et al, 2019). Before the recognition of leukocidin species specificity, murine and rat models were broadly used for *S. aureus* pathogenesis studies and testing immune based approaches. Clearly, the value of rodent models in determining the contribution of leukocidins to *S. aureus* pathogenesis is limited (Table 1). Contradicting *in vitro* and *in vivo* data were sometimes obtained using inadequate animal models making it difficult to distinguish or assess the role of individual leukocidins in *S. aureus* pathogenesis. For instance, studies with *S. aureus ΔlukSF-PV* mutant using mouse model reported either less severe infections (Labandeira-Rey et al, 2007; Brown et al, 2009) or no change and even worsened disease outcomes, compared to the *S. aureus* wild-type (Voyich et al, 2006; Yoong & Pier, 2012). Even though LukSF-PV is active towards rabbit cells, studies of skin and soft tissue infections in rabbit models also led to ambiguous results. While some groups reported significant role of LukSF-PV in pathogenesis, others have seen no contribution (Kobayashi et al, 2011; Lipinska et al, 2011; Malachowa et al, 2012). Despite the established LukGH contribution to the *S. aureus* infection *in vitro* and *ex vivo*, contribution to the *S. aureus* virulence *in vivo* could not be uniformly confirmed. In one study, deletion of *lukGH* led to decreased bacterial load in mouse renal abscess model (DuMont et al, 2011), in another no contribution to the mouse bacteraemia model was seen, but instead deletion of *lukGH* resulted in worsened disease outcome (Malachowa et al,

2012). The same study further reports that LukGH could not enhance the virulence in the rabbit skin infection models and that the high cytotoxic capacity of LukGH towards monkey PMNs *in vitro* could not be correlated with its ability to induce inflammatory response in monkeys (Malachowa et al, 2012). This further emphasises that *in vitro* cytotoxicity may not necessarily predict the *in vivo* situation (Malachowa et al, 2012).

The contribution of leukocidins to *S. aureus* infection *in vivo* may differ from *in vitro* conditions, due to different expression levels of leukocidins during bacterial growth, non-cognate leukocidin pairs and antagonism between leukocidins (König et al, 1997; Yanai et al, 2014; Adhikari et al, 2015; Yoong & Torres, 2015). Failed clinical trials, despite the proven efficacy of drugs *in vitro* and *ex vivo* and in animal models support this notion (Fowler & Proctor, 2014; Salgado-Pabón & Schlievert, 2014). Therefore, clinically-relevant animal models that more accurately reflect the human conditions are needed. The development of such models with a focus on LukGH may be a promising starting point, due to the high cytotoxicity of LukGH *in vitro* and *ex vivo* (Ventura et al, 2010; DuMont et al, 2011; Rouha et al, 2015; Janesch et al, 2017) and as increases in its cytotoxicity is linked with receptor up-regulation upon infection-relevant stimuli (Janesch et al, 2017).

1.5.1. Overcoming LukGH species specificity

The established LukGH species specificity *in vitro* that was demonstrated to correlate with binding to CD11b-I from that species, i.e. no binding to mouse CD11b-I (moCD11b-I) and very low activity towards murine PMNs *in vitro*, is believed to be a result of lower sequence conservation of the LukGH receptor between different species (Malachowa et al, 2012; DuMont et al, 2013b; Trstenjak et al, 2019). Namely, human CD11b-I shares 86%, 79.1% and 78.1% identity with macaque, rabbit and mouse CD11b-I, respectively (DuMont et al, 2013b; own unpublished data). One of the approaches to study the contribution of species specific leukocidins, mainly LukGH, is the development of humanized mice by using immunocompromised mice reconstituted with a human hematopoietic system, or by knocking “out or in” the host factors involved in species specificity (Trstenjak et al, 2019). There is uncertainty whether transgenic CD11b/CD18 can exert all integrin related functions or if the leukocyte-dependent responses would not be compromised as seen in CD11b/CD18 deficient mice (Coxon et al, 1996; Ding et al, 1999), due to low sequence homology between human and mouse CD11b-I. Study from Prince et al (2017), using humanized mice with reconstituted human hematopoietic system, demonstrated increased susceptibility to *S. aureus* infection and they confirmed contribution of LukSF-PV to the pathogenesis, but did not observe any phenotype for LukGH. This humanized model, however, does not yet fully replicate a functioning human immune system and additional improvements are needed (Prince et al, 2017), especially

when studying the role of LukGH in the pathogenesis. Another approach in surpassing the species specificity takes advantage of structural information about bacteria-host molecular interactions. To mimic the human disease in models with non-susceptible animal species, bacteria are engineered to express virulence factors that are active towards the selected animal host. Wollert et al used this approach to adapt *Listeria monocytogenes* for mouse by improving the binding of the listerial invasion protein InlA to the murine variant of its cognate receptor E-cadherin by protein engineering (Wollert et al, 2007). Because of the central role of CD11b in immune processes, determining the binding epitope between LukGH-CD11b-I would allow us to modify the cytotoxin or to introduce minimal changes in the CD11b-I without interfering with binding of naturally occurring ligands and still preserving full function of the integrin. Even though this is an exciting approach that bypasses introduction of unwanted changes in receptors that are often important immune molecules, care should be taken as not to expand pathogenic properties of the bacterial toxins, as was observed for InlA (Tsai et al, 2013; Trstenjak et al, 2019).

1.6. Research outline

The aim of the project was to gain understanding on the molecular mechanisms and structural requirements for the leukocidin-receptor (LukGH-CD11b-I) interactions in order to design leukocidin variants that have increased potency in small animal models (rabbit or mouse).

The project started with the adaptation of LukGH for the rabbit host (**Publication I**), for three main reasons: 1) detectable LukGH cytotoxicity towards rabbit PMNs *in vitro* and *ex vivo* (still 100 fold lower than towards human neutrophils), 2) LukGH targets only one receptor and 3) cell susceptibility to LukGH is dependent on the binding affinity of LukGH to the receptor (Ventura et al, 2010; DuMont et al, 2011; Malachowa et al, 2012; DuMont et al, 2013b; Rouha et al, 2015; Janesch et al, 2017). Importantly, cytotoxicity of the other *S. aureus* leukocidins in rabbits mostly resembles their cytotoxicity towards human cells (Table 1) (Malachowa et al, 2012; Diep et al, 2016). Furthermore, rabbits are a natural host for *S. aureus* and they show a similar range of natural staphylococcal infections as humans (Viana et al, 2015). In **Publication I** we discuss the efforts to map the interaction site of CD11b-I on LukH protomer by targeted mutagenesis and report the determined binding epitope. Moreover, we illustrate how a single amino acid mutation in LukH can result in improved binding to rabbit CD11b-I and improved LukGH cytotoxicity towards rabbit PMNs when expressed from the *S. aureus* chromosome. This validates our approach and suggests that *S. aureus* strains carrying rabbit-adapted LukGH variants are attractive tools for studying the role of LukGH in *S. aureus* pathogenesis in animals (**Publication I**). Even though there was a significant (10-fold) increase in LukGH cytotoxicity towards rabbit PMNs, further targeted mutagenesis of the

epitope did not result in the same cytotoxicity levels as observed for human PMNs (still 10-fold lower).

To better understand the LukGH-CD11b-I interaction, we tried to determine the crystal structure of LukGH-CD11b-I, by using different LukGH constructs (LukGH wild-type, LukGH with an impaired oligomerisation interface (Badarau et al, 2015), and LukGH missing the unstructured N-terminus of LukH) and CD11b-I from different species. We managed to crystallize mouse CD11b-I in complex with the LukGH_K319A variant, generated in **Publication I**, that had significantly better binding to moCD11b-I but it did not show any cytotoxicity towards mouse PMNs (**Publication I, Manuscript I**). Subsequently, crystals were also obtained for huCD11b-I in complex with wild-type LukGH, within a similar crystallization conditions, but diffracting at lower resolution (**Manuscript I**). In parallel to crystallization efforts, we also collected SAXS data for LukGH-huCD11b-I complex in presence of a monoclonal antibody targeting LukGH (Badarau et al, 2016). Analysis of the LukGH-CD11b-I interaction discussed in **Manuscript I** supports the binding epitope on LukH determined in **Publication I** and it reveals a second binding epitope on LukG. Furthermore, the binding epitope on CD11b-I highlights the key integrin features necessary for interaction with LukGH and provides an insight into the species specificity of LukGH. Additionally, LukGH_K319A, as well as all other LukGH variants tested, did not form octamers in the presence of moCD11b-I in solution, explaining the lack of LukGH wild-type and LukGH_K319A cytotoxicity towards mouse PMNs despite increased affinity for the latter. In **Manuscript I,** we discuss new mechanisms of leukocidin-receptor interaction that were, so far, not reported for other leukocidins and that can explain the oligomerisation process of the leukocidins and the role of the receptor in this process. At the end, we provide the molecular basis for observed correlation between receptor upregulation and LukGH cytotoxicity and propose the mechanism of pore formation on activated PMNs (**Manuscript I)**. In conclusion, the structural features on both cytotoxin and receptor, responsible for binding and oligomerisation, open new possibilities for rational adaptation of LukGH for other species.

2. PUBLICATIONS AND MANUSCRIPTS

Publication I:

Trstenjak N., Stulik L., Rouha H., Zmajkovic J., Zerbs M., Nagy E., Badarau A. Adaptation of the *Staphylococcus aureus* leukocidin LukGH for the rabbit host by protein engineering. *Biochemical Journal* **476**, 275-292 (2019).

Personal contribution:

Performing the experiments (except generation of the mutant *S. aureus* strains), data analysis, writing of the manuscript, and preparation of the figures.

Manuscript I:

Trstenjak N., Milic, D., Graewert, M.A., Rouha, H., Svergun, D., Djinovic-Carugo, K., Nagy, E., Badarau A. Molecular mechanism of leukocidin GH - integrin CD11b/CD18 recognition and species specificity. Submitted to Nature Chemical Biology on June 28th, 2019.
currently under review (status June 28th, 2019).

Personal contribution:

Performing binding*, in vitro* and DLS experiments. Preparation of samples for SAXS and crystallization experiments. Setup and optimization of crystallization conditions. Data analysis, writing of the manuscript, and preparation of the figures.

Publication I: Adaptation of the Staphylococcus aureus leukocidin LukGH for the rabbit host by protein engineering

Biochemical Journal (2019) **476** 275–292
https://doi.org/10.1042/BCJ20180691

Research Article

Adaptation of the *Staphylococcus aureus* leukocidin LukGH for the rabbit host by protein engineering

Nikolina Trstenjak, Lukas Stulik, Harald Rouha, Jakub Zmajkovic*, Manuel Zerbs, Eszter Nagy† and Adriana Badarau

Arsanis Biosciences, Campus Vienna Biocenter, Helmut-Qualtinger-Gasse 2, Vienna, Austria

Correspondence: Adriana Badarau (adriana.badarau@arsanis.com)

Host defense against *Staphylococcus aureus* greatly depends on bacterial clearance by phagocytic cells. LukGH (or LukAB) is the most potent staphylococcal leukocidin towards human phagocytes *in vitro*, but its role in pathogenesis is obscured by the lack of suitable small animal models because LukGH has limited or no cytotoxicity towards rodent and rabbit compared with human polymorphonuclear cells (PMNs) likely due to an impaired interaction with its cellular receptor, CD11b. We aimed at adapting LukGH for the rabbit host by improving binding to the rabbit homolog of CD11b, specifically its I-domain (CD11b-I). Targeted amino acid substitutions were introduced into the LukH polypeptide to map its receptor interaction site(s). We found that the binding affinity of LukGH variants to the human and rabbit CD11b-I correlated well with their PMN cytotoxicity. Importantly, we identified LukGH variants with significantly improved cytotoxicity towards rabbit PMNs, when expressed recombinantly (10–15-fold) or by engineered *S. aureus* strains. These findings support the development of small animal models of *S. aureus* infection with the potential for demonstrating the importance of LukGH in pathogenesis.

Introduction

Staphylococcus aureus is a major human pathogen, both in the hospital setting and in the community, and it is responsible for a wide range of diseases, ranging from mild skin infections to life-threatening infections, such as pneumonia and sepsis. The bacterium can survive and multiply in various biological niches owing to an arsenal of virulence factors that mediate tissue adhesion, immune evasion, and host cell injury [1]. A central piece for the latter two mechanisms is the pore-forming cytotoxins that lyse target cells and induce inflammation: the leukocidins, which attack human phagocytic cells, some of them red blood cells and T cells as well, and α-hemolysin (Hla or α-toxin) that mainly damages epithelial and endothelial cells [2–5]. *S. aureus* produces up to five different leukocidins: γ-hemolysins HlgAB and HlgCB, LukSF-PV (PVL), LukED and LukGH (also called LukAB) [2,5,6]. The contribution of each leukocidin to the different disease types has only started to be unraveled (e.g. LukSF-PV in necrotizing pneumonia [7]), mainly due to lack of suitable animal species as model organisms [6]. The recent identification of the cellular receptors for each of the leukocidins was crucial in understanding their cell-type specificity and host tropism ([4, 8]; Table 1).

The lack of a suitable animal model for infectious diseases caused by human-adapted pathogens is an inherent challenge for pathogenesis studies and drug discovery. This is typically addressed by mouse humanization, either by knocking out/in the host factors involved in human species specificity [24] or by using immunocompromised mice reconstituted with a human hematopoietic system [25]. Another approach is to engineer the pathogen to express virulence factors that are active towards the

*Present address: Department of Biomedicine, University of Basel, Hebelstrasse 20, 4031 Basel, Switzerland.
†Present address: EveliQure Biotechnologies, Helmut-Qualtinger-Gasse 2, Vienna, Austria.

Received: 24 August 2018
Revised: 12 December 2018
Accepted: 14 December 2018

Accepted Manuscript online: 17 December 2018
Version of Record published: 25 January 2019

Biochemical Journal (2019) **476** 275–292
https://doi.org/10.1042/BCJ20180691

Table 1 Cell-tropism and species specificity of the bi-component cytotoxins of *Staphylococcus aureus*

Toxin	Cellular receptors	Targeted cells	EC_{50} (nM)		
			Human	Rabbit	Mouse
LukSF-PV	C5aR [9,10], C5L2 [9], CD45 [11]	Monocytes, neutrophils, macrophages	0.9 [9], 0.1–0.5 [12], ~0.1 [13], ~1 [14], ~1 [15]	0.1–0.2 [12], ~1 [14]	Resistant [9,12,14,16]
LukED	CCR5 [17], CXCR1 [18], CXCR2 [18]	Monocytes, neutrophils, macrophages, T cells, dendritic cells, NK cells	2.4–4 [12], ~1 [15]	0.03–0.04 [12]	14–48.3 [12]
	DARC [19]	Red blood cells	~20 [19], <15 [20]		<15 [20]
LukGH	CD11b-I [21]	Neutrophils, macrophages, monocytes, dendritic cells	0.01–0.03* [13], 0.25 [22]	35 [22]	550 [22]
HlgAB	CXCR1 [23], CXCR2 [23], CCR2 [23]	Monocytes, macrophages, T cells, neutrophils	0.4–0.6 [12]	0.2 [12]	Resistant [12, 23]
	DARC [19]	Red blood cells	~1 [19]		
HlgCB	C5aR [23], C5L2 [23]	Monocytes, macrophages, neutrophils	0.5–0.6 [12], ~2.5 [16]	0.1 [12]	Resistant [12,16,23]

*LPS-stimulated cells.

chosen animal host. The best-known example is the adaptation of *Listeria monocytogenes* to mouse by improving binding of the listerial invasion protein InlA to the murine variant of its cognate receptor E-cadherin by protein engineering [26].

LukGH is the most potent leukocidin in *in vitro* assays and *ex vivo* models [13,27–29], and is present in nearly all *S. aureus* strains [27,30]. It is expressed during human infections [31], but is inactive or displays limited activity in the established *S. aureus* models, such as mouse and rabbit [21,22] (Table 1). LukGH is also unique among the leukocidins as it is present as a dimer in solution, before it binds to the target cells [32,33], for reasons and with implications not fully understood. It is therefore conceivable that LukGH followed a distinct evolutionary path, as also suggested by the lowest sequence homology (only up to 40%) to the other leukocidins, which are otherwise up to 82% homologous to each other [34]. Moreover, the sequence conservation of LukGH among different *S. aureus* isolates is much lower (as low as 82%) than for the other leukocidins (>95% identity) with the sequence variants showing association with clonal lineages [27,30]. The cellular receptor for LukGH was identified as the α subunit of the α_M/β_2 integrin (CD11b/CD18, or macrophage-1 antigen, or complement receptor 3) [21]. It has been demonstrated that binding to the I-domain of CD11b correlates with cytotoxicity towards neutrophils, i.e. no binding to mouse CD11b-I [21] and very low activity towards murine PMNs *in vitro* [22].

In this study, we aimed at adapting LukGH to the rabbit host, which is sensitive to all the other β-barrel pore-forming cytotoxins [12] (Table 1), to allow the study of LukGH contribution to *S. aureus* pathogenesis. Our approach was to engineer LukGH for increased binding affinity to rabbit CD11b-I (rbCD11b-I) and improved activity towards rabbit PMNs (rbPMNs), which is two orders of magnitude weaker than towards human PMNs (huPMNs) [22] (Table 1). In addition, we performed a fine epitope mapping of the CD11b-I-binding site on LukGH to enable rational LukGH adaptation to other species.

Materials and methods

Production of recombinant LukGH variants

LukGH variants were produced recombinantly in *Escherichia coli*, as described previously [33], based on the wild-type sequence of the community-associated methicillin-resistant *Staphylococcus aureus* (CA-MRSA) USA300 (ST8) TCH1516 strain. The three natural sequence variants encoded by the MRSA252 (ST36), MSHR1132 (ST1850), and H19 (ST10) strains were produced as described previously [33]. The *lukG* gene was cloned into pET44a vector and was expressed as a fusion protein with NusA/His_6 at the N-terminus to allow

metal ion affinity purification of the complex, whereas LukH was expressed in the untagged form. LukH single and multiple mutants were generated with QuikChange II XL Site-Directed Mutagenesis Kit (Agilent) according to the manufacturer's instructions using the *lukH*_pET200D/TOPO (or variants thereof) as a template. Mutations to D, V, and S or to H at amino acid positions 263 and 312, respectively, were obtained by site-specific saturation mutagenesis using a QuikChange Multi Site-Directed Mutagenesis kit (Agilent) and *lukH*-PET200D/TOPO as a template. The *lukH* mutants and wild-type *lukG* were co-transformed into *E. coli* TUNER DE3 cells (Novagen), using two vectors with different antibiotic resistance markers, and protein expression was induced with isopropyl β-D-1-thiogalactopyranoside (IPTG) as described previously [33]. All LukGH variant complexes were expressed as soluble proteins, at 20°C, similarly to wild-type LukGH [33].

Recombinant LukGH proteins were purified as described previously [33] or using batch methods designed for high-throughput purification from 0.5 or 0.125 l cultures. Briefly, bacterial pellets were disrupted using either sonication (0.5 l pellet) or 0.1% *n*-dodecyl-β-D-maltoside and two freeze–thaw cycles in liquid nitrogen (0.125 l pellet). The LukGH dimers were purified from cell extracts by metal ion affinity and cation exchange chromatography using batch methods. First, soluble cell extracts (obtained by centrifugation of cell lysates) were mixed with Ni Sepharose® 6 Fast Flow beads (GE Healthcare) equilibrated in 20 mM Tris–HCl, pH 7.5 plus 50 mM imidazole. Beads were loaded either on Pierce Disposable Columns (Thermo Fisher) or on Microplate Devices UNIFILTER, 96-well plate (Whatman) and elution with 20 mM Tris–HCl, pH 7.5 plus 500 mM imidazole was performed by centrifugation. After dialyzing into buffer without imidazole, the NusA/His_6 tag on LukG was removed with enterokinase (NEB). The untagged LukGH complex was further purified using SP Sepharose® Fast Flow beads (GE Healthcare) equilibrated in 20 mM sodium phosphate, pH 7.5 plus 50 mM NaCl. Beads were treated as described for the affinity purification, and the proteins were eluted with 20 mM sodium phosphate, pH 7.5 plus NaCl (150–300 mM). Protein purity was assayed by SDS–PAGE gels, stability by differential scanning fluorimetry (DSF) and secondary structure by circular dichroism (CD).

CD and DSF analysis

Far-UV (195–250 nm) CD spectra were recorded on a Chirascan (Applied Photophysics) spectrometer in a 0.5 mm cuvette (Applied Photophysics) at 20°C with protein concentrations of 0.1–0.8 mg/ml in 20 mM sodium phosphate, pH 7.5 plus 150–300 mM NaCl. All CD spectra were normalized to a concentration of 0.3 mg/ml.

The melting points (T_m) of the proteins were determined by DSF. The proteins (0.25–0.6 mg/ml) were mixed with Sypro Orange dye and with HEPES, pH 7.5 (50 mM final concentration). The assay was conducted in a qPCR instrument (Bio-Rad CFX96) and the T_m values were determined using the Bio-Rad CFX Manager software.

Recombinant human CD11b-I (huCD11b-I) and rabbit CD11b-I (rbCD11b-I) expression and purification

The I-domains (amino acids 127–321) of huCD11b and rbCD11b (huCD11b-I and rbCD11b-I, respectively) were cloned into the pET24a (Novagen) vector at NdeI/XhoI and NdeI/BamHI sites, respectively, and the plasmids were transformed into *E. coli* TUNER DE3 cells. Protein expression was induced at 20°C for 20 h with 0.4 mM IPTG. HuCD11b-I and rbCD11b-I were purified by cation (HiTrap® SP FF, GE Healthcare) or anion (HiTrap® Q FF, GE Healthcare) exchange chromatography followed by size exclusion chromatography (HiLoad Superdex75 pg, GE Healthcare). HuCD11b-I was treated overnight with iodoacetamide (20 mM, Applichem) to alkylate-free cysteine and prevent dimer formation. Iodoacetamide was removed on PD-10 columns (GE Healthcare) equilibrated with 50 mM sodium phosphate, pH 7.5 plus 300 mM NaCl. Protein purity and monomer content were assessed by non-reducing SDS–PAGE gel.

Biotinylated huCD11b-I and rbCD11b-I were generated with the amino reactive reagent Sulfo-NHS-LC biotin (Thermo Scientific), according to the manufacturer's instructions with final biotin/protein ratios of 0.15–0.2.

Bio-layer interferometry

Binding of LukGH (wild-type and mutants) to huCD11-I or rbCD11b-I was evaluated by Bio-Layer Interferometry (BLI) (fortèBio Octet Red96 instrument, Pall Life Sciences) in assay buffer (PBS plus 1% BSA and 1 mM $MgCl_2$). Biotinylated CD11b-I (2 μg/ml) was immobilized on streptavidin sensors (fortèBio, Pall Life Sciences) to achieve a final loading of 0.6–1.6 nm. Association of LukGH (50 nM) to the immobilized receptor

Biochemical Journal (2019) **476** 275–292
https://doi.org/10.1042/BCJ20180691

and dissociation in assay buffer were monitored for 5 min each. Response units (RU) (normalized to the same loading) and, where possible (for monophasic binding curve), equilibrium dissociation constants (K_d) were determined using the Data Analysis 7 software (fortéBio, Pall Life Sciences) by simultaneously fitting the association and dissociation curves to a 1:1 binding model. Steady-state K_d values were determined for LukGH wild-type and LukGH_D312A binding to rbCD11b-I by measuring binding responses at multiple LukGH concentrations (20–400 nM) and fitting the data to the steady-state model (Forte-Bio Analysis Software, Version 7).

Cytotoxicity assays

Cell-based assays were performed using differentiated HL-60 cells, human or rabbit polymorphonuclear cells (PMNs). The HL-60 cells (ATCC® CCL-240™) were differentiated into phagocytes by treatment with 100 mM dimethylformamide in the culture media (RPMI + 20% FCS + 2 mM L-glutamine + Pen/Strep) for 3–5 days as described previously [35]. The differentiation status of HL-60 cells was confirmed by a significant reduction in CD71 and increase in CD11b expression based on staining intensity with phycoerythrin-conjugated anti-CD71 (clone OKT9, eBioscience) and Brilliant Violet 421-conjugated anti-CD11b (clone ICRF44, BioLegend) monoclonal antibodies. Human PMNs were isolated from heparinized human whole blood, obtained from healthy volunteers, using Percoll® (Percoll Plus, GE Healthcare) gradient centrifugation as described previously [33]. Rabbit PMNs were isolated from rabbit whole blood (pooled blood of three New Zealand White rabbits) anti-coagulated with citrate dextrose solution, using Histopaque®-1077 (Sigma–Aldrich) and HetaSep™ (Stemcell Technologies) as described previously [36]. For the assays with stimulated rbPMNs, purified PMNs (1×10^6 cells/ml) were pre-incubated for 1 h at 37°C, 5% CO_2 with lipopolysaccharide (LPS) purified from *E. coli* O111 (500 ng/ml, List Laboratories).

(i) Cytolytic activity of LukGH (wild-type and mutants) was assessed as described previously [13,34]. Shortly, differentiated HL-60 cells, huPMNs, non-stimulated or LPS-stimulated rbPMNs (2.5×10^4 cells/well) were treated with serial dilutions of LukGH (0.002–100 nM for human and 0.005–300 nM for rabbit cells) in RPMI + 10% FBS + L-glutamine assay medium at 37°C, 5% CO_2 for 4 h. Cell viability was determined using CellTiter-Glo® Luminescent Cell Viability Assay Kit (Promega) according to the manufacturer's instructions. The percentage viability was calculated relative to mock-treated cells (100% viability) and cytolytic activity was expressed as EC_{50} value (concentration of cytotoxin at which 50% of cells are killed) calculated by non-linear regression analysis using Prism 6 (GraphPad). Each independent experiment was performed in triplicates on different batches of PMNs or HL-60 cells.

(ii) Cell permeability, in presence of LukGH, was assessed using rbPMNs (1×10^5 cells/well) treated with serial dilutions of recombinant toxin (0.005–300 nM) in RPMI + 10% FCS + L-glutamine + 10 mM HEPES assay medium at 37°C, 5% CO_2 for 2 h. After incubation, plates were centrifuged at 1500 ***g*** for 5 min, supernatant was discarded, and pellets were re-suspended in PBS + 0.5 μM SYTOX® Green Nucleic Acid Stain (Molecular Probes). Following 10 min of incubation, fluorescence ($\lambda_{ex} = 485$ nm, $\lambda_{em} = 528$ nm) was quantified on a Synergy™HT Multi-Mode Microplate Reader (BioTek). The percentage of dead cells was calculated relative to a dead cell control (0.1% saponin) and EC_{50} values were calculated as described above. Each independent experiment was performed in triplicates on different batches of PMNs.

(iii) The cytotoxic activity of culture supernatants (CSs) was determined using huPMNs and rbPMNs. Serial dilutions of CSs from 4- to 512-fold, in RPMI plus 10% FCS and 2 mM L-glutamine assay medium, were prepared in a 96-well plate and pre-incubated for 30 min at room temperature with the monoclonal antibodies ASN-1 (1 μM), ASN-2 (1 μM), ASN-1 (1 μM) + ASN-2 (1 μM), an isotype control antibody (2 μM) or buffer. ASN-1, a human mAb that cross-neutralizes Hla and the other four leukocidins (LukED, LukSF-PV, HlgAB, and HlgCB) [34] and ASN-2, a LukGH-specific neutralizing antibody [37] were produced as described recently [29]. The supernatant–antibody mixtures were added to huPMNs or rbPMNs in 96-well, half-area luminescent plates (Greiner) at 2.5×10^4 cell density. Following incubation at 37°C, 5% CO_2 for 4 h, toxicity of CSs was assessed by measuring cellular ATP levels with CellTiter-Glo® Luminescent Cell Viability Assay Kit (Promega) and the percentage viability was calculated relative to mock-treated cells (100% viability). Each experiment was performed using 4–6 CSs prepared on different days and from different colonies.

(iv) To determine *S. aureus*-mediated killing of PMNs by extracellular bacteria, overnight cultures of *S. aureus* grown in RPMI-CAS were diluted 1:100 and grown to mid-log phase ($OD_{600\ nm} = 0.5$) at 37°C. Bacteria were harvested, washed with PBS to remove secreted toxins, re-suspended in RPMI + 10% FCS + L-glutamine + 10 mM HEPES, and added to 1×10^5 PMNs/well in a 96-well plate at different multiplicity of infection

(MOI, 50 and 100) together with ASN-1 (2 μM), ASN-2 (2 μM), ASN-1 (2 μM) + ASN-2 (2 μM), an isotype control antibody (4 μM) or buffer. Reactions were incubated for 2 h at 37°C and 5% CO_2. Fluorescence was measured using SYTOX® Green Nucleic Acid Stain (Molecular Probes) as described above. The percentage of dead cells was calculated relative to a dead cell control (0.1% saponin). Each independent experiment was performed in 2–6 replicates on different batches of PMNs.

Chromosomal integration of mutant *lukGH*

The USA300 CA-MRSA strain TCH1516 (ST8-IV-t622, BAA-1717™, ATCC®) and a clinical isolate, recovered from an endotracheal aspirate of a mechanically ventilated patient, with high LukGH expression level, LA#5 (ST8-IV-t008) [29,38], were cultured under standard microbiological conditions. *lukH*_D312K and *lukH*_E263Q-D312N were introduced by site-directed mutagenesis into the *lukGH* operon, which was subsequently cloned into the pKFT shuttle-vector at SmaI and BamHI restriction sites [39] (Supplementary Figure S1A). Gene replacement was achieved by homologous recombination according to previously published methods [39,40]. Shortly, the vector-construct was transformed into wild-type *S. aureus* by electroporation and transformants were grown at 30°C/200 rpm selecting for Tet^R. After a first temperature-based (42°C), homologous recombination event was induced, the plasmid was cured by repeated passaging at 25°C/200 rpm. The second cross-over event was induced by another temperature shift to 42°C that resulted in the excision of the integrated plasmid (Tet^S) and either the homologous insertion of the mutated *lukGH* or a reversion to wild type, which was confirmed by sequencing of the *lukGH* operon (Supplementary Figure S1B).

Strains were characterized by determining the growth curves and expression of the cytotoxins as follows: overnight cultures of the *S. aureus* strains TCH1516, LA#5 and rabbit-adapted strains, grown in RPMI + 1% Casamino acids (RPMI + 1% CAS) were diluted to an $OD_{600\ nm}$ of 0.03 and grown to a stationary phase at 37°C/200 rpm. OD_{600} was measured at regular intervals for 8 h and plotted against growth time. Cultures were centrifuged at 5000 ***g*** for 10 min and the supernatants were sterile-filtered using 0.1 μm filters (Millex Syringe Filter Units, Millipore). These CSs were further used for Western blot and PMN toxicity assays. Western blot of CSs from *S. aureus* TCH1516 and LA#5 wild-type, rabbit-adapted strains [*lukH*_D312K and *lukH*_E263Q-D312N (*lukH*_QN)], and control strain (TCH1516 Δ all cytotoxins [34]) grown in RPMI + 1% CAS, to comparable OD_{600}, was performed using same loading amount of CS and corresponding antibodies. The expressions of Hla, LukD, and HlgB were assessed using monospecific human antibodies, LukS-PV was detected with a mouse monoclonal antibody (IBT Bioservices) and LukG expression was measured using a rabbit anti-LukB polyclonal Ab (IBT Bioservices) as described recently [29].

Results

LukGH binding to human and rabbit CD11b-I

We first compared the binding strength of recombinant LukGH (derived from the genome sequence of the USA300 CA-MRSA, TCH1516 strain) to the human (huCD11b-I) and rabbit (rbCD11b-I) receptors, K_d, when LukGH was in solution and the recombinant receptor in immobilized form, using BLI. Binding of LukGH to huCD11b-I appeared to follow a 1:1 binding model, so the equilibrium dissociation constant, K_d, could be calculated from the association and dissociation progress curves, yielding a value of 7.96×10^{-9} M with an association rate constant, k_{on} of 1.0×10^5 1/Ms (Figure 1A). For rbCD11b-I, the kinetic profile was biphasic, so we were unable to determine the association and dissociation rate constants, but binding was sufficiently weak to allow determining K_d using steady-state analysis ($K_d = 9.51 \times 10^{-8}$ M, Figure 1B). In these experiments, we observed an ∼10-fold lower affinity of LukGH for rbCD11b-I compared with the human counterpart (Figure 1A,B). This difference was paralleled by the lower activity towards rbPMNs compared with huPMNs, typically by two orders of magnitude, which is in good agreement with published data [22] (Figure 1C).

We also tested the binding to rbCD11b-I and activity towards rbPMNs of three additional, most divergent, sequence variants of LukGH TCH1516 from *S. aureus* strains: MRSA252, MSHR1132, and H19 [33]. We found that the activity of these sequence variants was an order of magnitude lower (Supplementary Table S1); therefore, the TCH1516 variant was used in the subsequent rabbit adaptation studies.

Purification and characterization of LukGH variants

It was shown previously that CD11b-I interacts mainly with the LukH subunit of LukGH [21,33], and particularly with the C-terminal tail of LukH [32]. Importantly, the glutamate at position 323 (E323) in LukH was

Biochemical Journal (2019) **476** 275–292
https://doi.org/10.1042/BCJ20180691

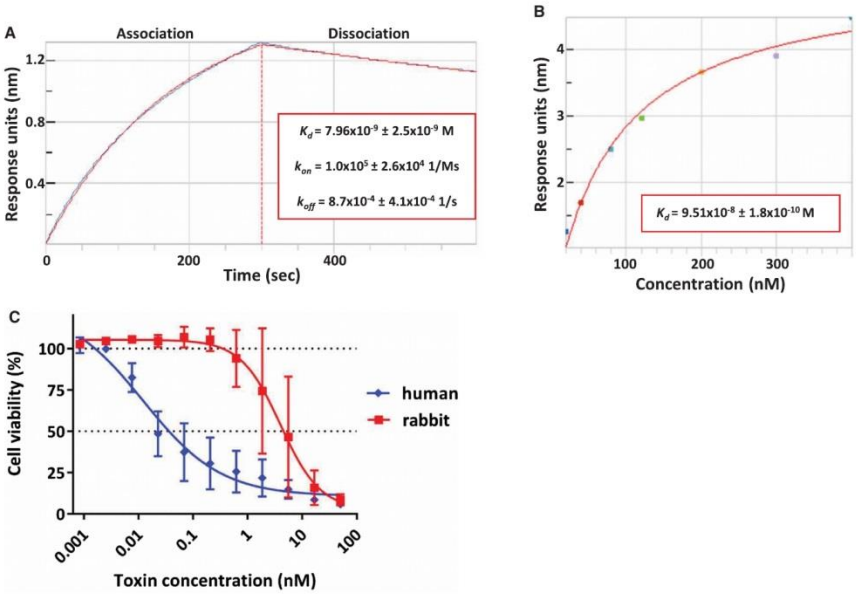

Figure 1. Binding of LukGH to hu and rbCD11b-I measured by BLI, and activity towards human and rabbit PMNs.
(**A**) Representative kinetic profile for LukGH binding to huCD11b-I. Association and dissociation steps are separated by a vertical red line. The binding curve (blue line) was fitted to a 1:1 model and the fit is shown in red. The K_d, k_{on}, and k_{off} are shown in the insert (mean of 10 independent experiments ± SD). (**B**) Steady-state analysis of LukGH binding to rbCD11b-I measured at different LukGH concentrations. The steady-state K_d is shown in the insert (mean of two independent experiments ± SD). (**C**) Activity of LukGH towards huPMNs and rbPMNs assessed in a luminescent cell viability assay measuring cellular ATP content at increasing cytotoxin concentrations (mean of two independent experiments performed in triplicates ± SEM.).

identified as being crucial for binding to huCD11b-I and activity towards huPMNs [32]. To determine the binding epitope of CD11b-I on LukGH, we investigated the involvement of residues surrounding E323 (based on the LukGH dimer [PDB 5K59] and octamer [PDB 4TW1] structures) in receptor-binding and cytotoxin activity. A total of 21 positions, mostly surface exposed, polar, and charged residues located in the cap or the rim domain of LukH, were subjected to alanine mutagenesis (Figure 2A). While most of the mutated side chains do not interact with any other residues based on the LukGH octamer structure (e.g. R121, K309), some do (e.g. D177, R207, D209, and Y314) (Figure 2A), which is presumably the reason for the decreased stability of certain Ala mutants (*vide infra*).

The LukGH complexes were purified (>95% purity) with yields varying from 0.8 to 8 mg/l culture. To exclude the possibility that protein instability and improper folding affect the binding or activity, we determined the T_m and secondary structure (far-UV CD spectra) of the variants (Figure 2B,C; Supplementary Figure S2). All variants, except the LukGH_R207A and _D209A, had T_m values ranging from 44 to 45°C, which are similar to the wild-type protein (Figure 2C). The most striking change in T_m, 10°C lower compared with the wild-type, was seen with LukGH_R207A, seemingly due to loss of interactions between A207 and the surrounding LukH residues (S109, E110, and D271) (Figure 2A). The LukGH_D209A displayed a moderately lower T_m (2.5°C). Both positions were therefore excluded from further analyses. Since no significant changes in T_m or CD spectra were observed for the other variants, we concluded that any change detected in binding to CD11b-I and in cytotoxin activity towards rabbit and human cells was not due to misfolding or decreased stability of the proteins.

Biochemical Journal (2019) **476** 275–292
https://doi.org/10.1042/BCJ20180691

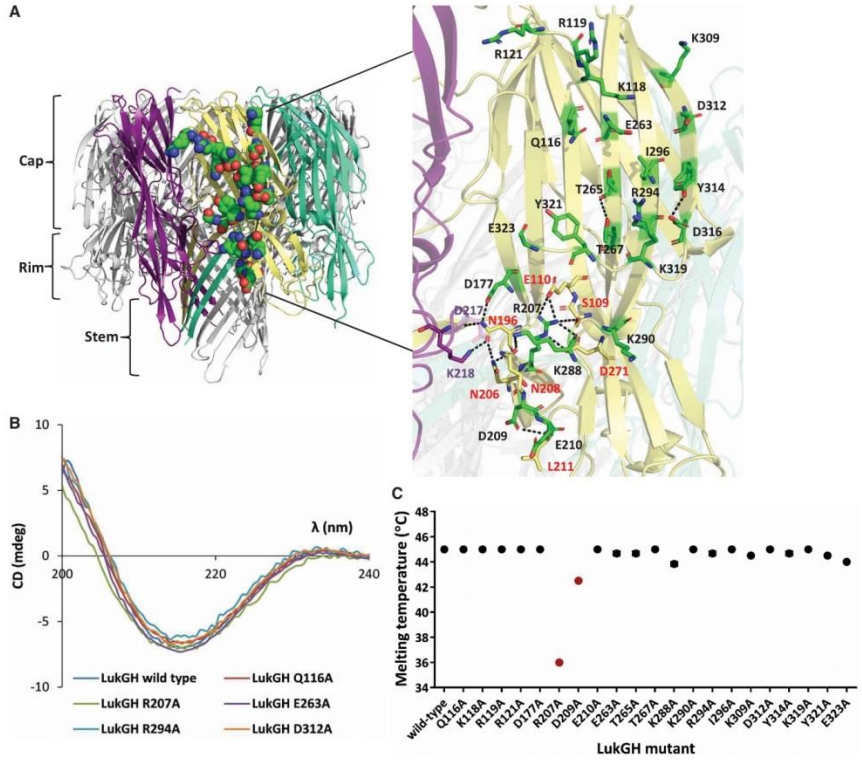

Figure 2. Amino acid positions on LukH selected for Ala screening.

(**A**) Left panel: Structure of the LukGH octamer (PDB 4TW1) with positions selected for Ala screening shown as spheres. LukG and LukH are shown as green and yellow cartoon, respectively, LukG from the neighboring dimer as purple and remaining monomers as gray cartoon. Right panel: Positions selected for Ala screening are shown as green sticks colored according to the atom (red: oxygen, blue: nitrogen). Polar contacts involving the side chains from selected positions are marked with dashed lines. Residues on LukH interacting with the positions selected for Ala screening are shown as yellow sticks and colored by atom. LukG residues involved in polar contacts are shown as purple sticks and colored by atom. (**B**) CD spectra of selected Ala mutants in 20 mM sodium phosphate, pH 7.5 plus NaCl (150–300 mM), normalized to 0.3 mg/ml. (**C**) Melting temperature of Ala mutants measured by DSF at concentrations between 0.25 and 0.6 mg/ml in 50 mM HEPES, pH 7.5. The mutants with at least 2°C difference in T_m, compared with wild-type LukGH (45°C) are marked red.

Correlation between receptor-binding and cytotoxicity of LukGH Ala variants

All alanine variants of LukGH were tested for binding to hu and rbCD11b-I to identify the residues involved in receptor recognition in both species. Most of them showed weaker binding with biphasic kinetic profiles; therefore, the binding strength was expressed as RU, which are proportional to the amount of bound cytotoxin (Figure 3A). As expected, the LukGH_E323A resulted in loss of binding (RU <0.05 nm) for both hu and rbCD11b-I. In addition, loss of binding to rbCD11b-I and a significant decrease in binding to huCD11b-I were seen with LukGH_Q116A, _T267A, _R294A, _K319A, and _Y321A (Figure 3A). The LukGH variants with K118A, R119A, and K290A mutations showed decreased binding to rbCD11b-I and huCD11b-I, although less pronounced for the latter. Notably, we have identified three variants, LukGH_E263A, _D312A, and _D316A,

Biochemical Journal (2019) **476** 275–292
https://doi.org/10.1042/BCJ20180691

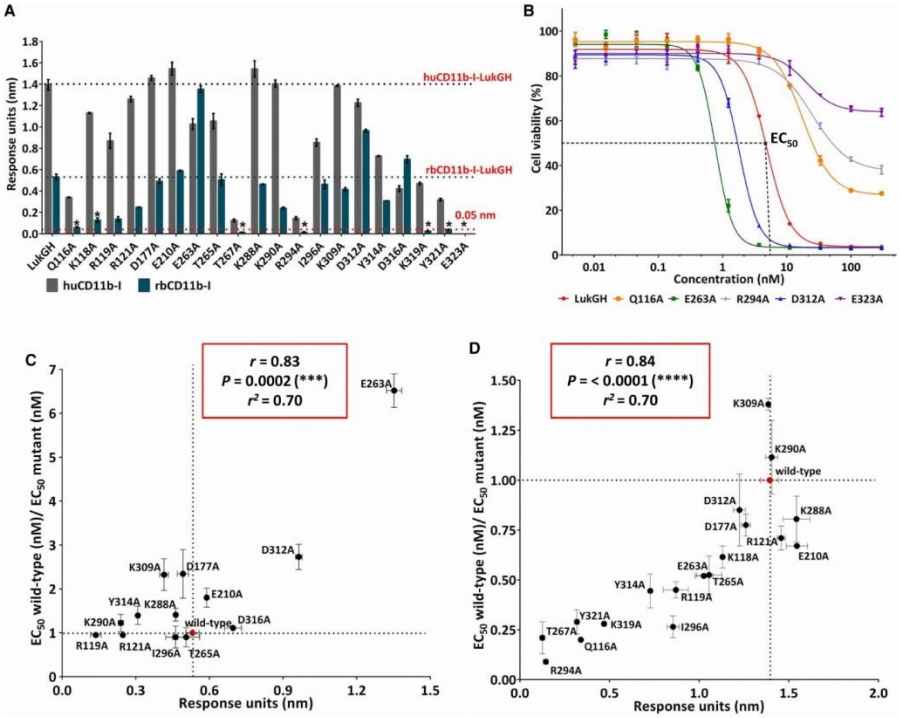

Figure 3. Cytotoxicity and receptor binding of LukGH wild-type and Ala variants.

(**A**) Binding of Ala mutants to rbCD11b-I or huCD11b-I, measured by BLI. Mutants with response units <0.05 nm (indicated by the dotted red line) are considered non-binders. Mutants that could not achieve complete cytotoxicity towards rbPMNs (cell viability >25%) at 300 nM in *in vitro* assay as shown in (**B**) are marked with stars. Data in (**A**) represent mean ± SEM of a minimum of two independent experiments. (**B**) Activity of selected LukGH mutants towards rbPMNs was assessed in a luminescent cell viability assay measuring cellular ATP content at increasing cytotoxin concentrations. Solid lines represent nonlinear fit of the data (mean of triplicates ± SEM) and the dotted line represents EC_{50} value calculated by the fit. (**C** and **D**) Correlation graphs between EC_{50} wild-type/EC_{50} mutant, obtained as shown in (**B**), and binding responses measured by BLI (**A**), for rbCD11b-I and huCD11b-I, are shown in (**C**) and (**D**), respectively. Data represent the mean ± SEM of a minimum of two independent experiments performed in triplicate; except for EC_{50} of LukGH_D316A with only one experiment performed in triplicate. Pearson correlation was calculated using Prism 6 (GraphPad) and is shown as an insert. Wild-type LukGH, as a referent value, is marked red.

which exhibited increased binding responses to rbCD11b-I. The binding to huCD11b-I was either significantly (LukGH_D316A) or only slightly (LukGH_E263A and _D312A) decreased.

To assess whether the change in binding translates into different *in vitro* toxicities, we measured the activity of all LukGH variants towards rabbit and human neutrophils in ATP-based cell viability assays. As the activity of LukGH towards huPMNs markedly depends on the activation state of the cells and is therefore subject to higher variability [13,41], we used differentiated HL-60 cells instead of huPMNs for these experiments. As there are no rabbit HL-60 counterparts, rbPMNs were used, despite showing some batch to batch variability (lower though than with huPMNs), and EC_{50} ratios between wild-type LukGH and variants were used, instead of absolute EC_{50} values, to minimize variability.

Biochemical Journal (2019) **476** 275–292
https://doi.org/10.1042/BCJ20180691

All variants showed some level of toxicity towards rbPMNs at the highest concentration tested (300 nM). While some showed improved activity towards rbPMNs (LukGH_E263A, _D312A), others, such as LukGH_E323A or _R294A, caused only a partial viability reduction (30–70%) even at the highest concentration tested (Figure 3B). The variants that showed significantly lower binding to rbCD11b-I (Figure 3A) could not achieve complete cytotoxicity (>25% of cells still viable) at 300 nM. Towards the differentiated HL-60 cells, the activity was either maintained or decreased, and no activity was seen with LukGH_E323A, in agreement with the literature [32]. The most deleterious effects in activity were observed with the mutations that were also identified using rbPMNs, namely E323A, Q116A, T267A, R294A, K319A, and Y321A, but also with I296A and Y314A that did not affect activity towards rbPMNs. When the EC_{50} values were plotted against corresponding binding responses, we observed, for most of the variants, a positive correlation between receptor-binding strength and cytotoxin activity for both differentiated HL-60 cells and rbPMNs (Figure 3C,D), indicating that the affected amino acids are indeed involved in the interaction with the cellular receptor. With some variants (LukGH_R119A, _R121A,_Y314A, and _K290A), we observed reduced binding to the rabbit receptor, but no change in activity towards rbPMNs, suggesting that binding to the recombinant domain may not necessarily reflect the binding to the cell surface or translate to cytotoxic activity.

The most interesting variants that were identified in this screening were LukGH_E263A and LukGH_D312A that showed significantly higher binding responses and ∼6- and 3-fold improved cytotoxicity towards rbPMNs, respectively (Table 2). An opposite and weaker effect for the same mutations was observed when tested with huCD11b-I and differentiated HL-60: decrease in both binding and activity. The distinct effects observed with E263A, D312A, I296A, and Y314 mutations in binding to huCD11b-I or rbCD11b-I and in their activity towards differentiated HL-60 cells or rbPMNs are likely the result of different amino acids in huCD11b-I and rbCD11b-I involved in interactions with these LukH residues.

Delineation of the CD11b-I-binding epitope on LukGH

Based on the binding and activity data, we have identified positions on LukH, which are likely, directly, or indirectly, involved in the binding of LukGH to CD11b-I with surface area of 2400 $Å^2$ (calculated using The PyMOL Molecular Graphics System, Version 2.0 Schrödinger, LLC) (Figure 4). The positions considered as

Table 2 Binding to hu and rbCD11b-I and activity of wild-type LukGH and selected LukGH variants towards differentiated HL-60 cells or rabbit PMNs

Toxin	Response $units_{max}$ (nm)*	K_d (M)*	[EC_{50} wild-type/EC_{50} mutant]*
Rabbit			
LukGH	0.53 ± 0.15	$9.51 \times 10^{-8} \pm 1.8 \times 10^{-10}$†	1.0
LukGH_E263A	1.35 ± 0.08	$4.22 \times 10^{-8} \pm 2.3 \times 10^{-8}$	6.5 ± 0.8
LukGH_D312A	0.96 ± 0.03	$8.98 \times 10^{-8} \pm 2.2 \times 10^{-9}$†	2.7 ± 0.6
LukGH_D312K	1.53 ± 0.10	$3.81 \times 10^{-8} \pm 7.8 \times 10^{-9}$	10.5 ± 1.1 (5.7 ± 1.8)‡ (12.6 ± 5.1)§
LukGH_E263Q-D312N	2.61 ± 0.37	$2.20 \times 10^{-8} \pm 2.4 \times 10^{-9}$	10.7 ± 2.1 (19.2 ± 4.0)§
LukGH_E263Q-D312K	2.49 ± 0.46	$2.10 \times 10^{-8} \pm 3.1 \times 10^{-9}$	12.7 ± 1.8 (8.6 ± 0.7)‡
LukGH_E263A-D312A	1.94 ± 0.17	$3.06 \times 10^{-8} \pm 6.3 \times 10^{-9}$	11.5 ± 2.5 (6.8 ± 0.8)‡
Human			
LukGH	1.39 ± 0.28	$7.96 \times 10^{-9} \pm 2.5 \times 10^{-9}$	1.0
LukGH_E263A	1.03 ± 0.13	$1.77 \times 10^{-8} \pm 2.8 \times 10^{-9}$	0.52 ± 0.01
LukGH_K288A	1.54 ± 0.11	$7.41 \times 10^{-9} \pm 1.6 \times 10^{-10}$	0.81 ± 0.16
LukGH_K290A	1.40 ± 0.05	$8.61 \times 10^{-9} \pm 1.1 \times 10^{-10}$	1.12 ± 0.26
LukGH_D312A	1.23 ± 0.08	$1.13 \times 10^{-8} \pm 1.4 \times 10^{-9}$	0.85 ± 0.25
LukGH_D312K	1.25 ± 0.07	$3.97 \times 10^{-9} \pm 1.2 \times 10^{-9}$	0.8 ± 0.02
LukGH_E263Q-D312N	1.13 ± 0.06	$9.61 \times 10^{-9} \pm 1.1 \times 10^{-9}$	0.58 ± 0.05

*Mean of a minimum of two independent experiments performed in triplicates ± SD; †K_d determined by steady-state analysis, ‡LPS-treated cells, §SYTOX green readout.

Biochemical Journal (2019) **476** 275–292
https://doi.org/10.1042/BCJ20180691

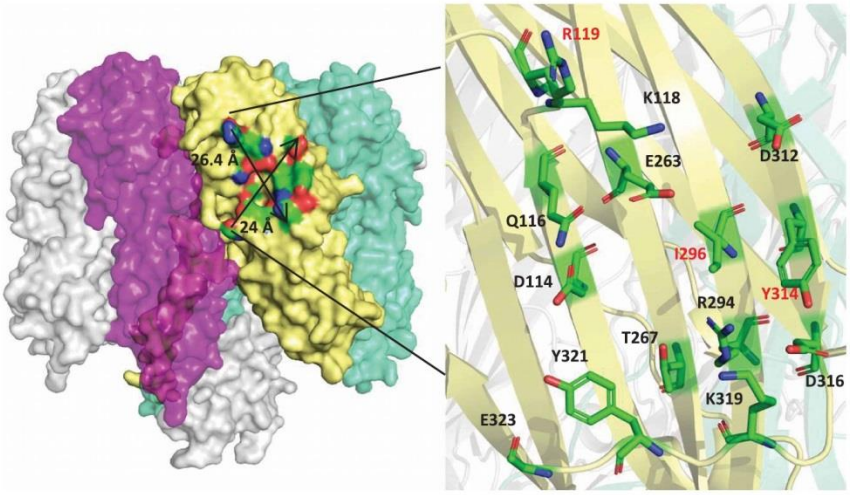

Figure 4. CD11b binding epitope on LukH based on the mutagenesis data.

Left panel: The binding epitope of CD11b-I on the LukH monomer shown on LukGH octamer structure (PDB 4TW1). LukH, LukG, and LukG from a neighboring dimer are colored yellow, green, and purple, respectively, and remaining monomers in gray. The residues involved in binding are colored by atom (red: oxygen, blue: nitrogen). Right panel: Residues in the binding epitope are shown as green sticks and colored according to the atom (red: oxygen, blue: nitrogen). The residues involved in the direct interactions are labeled black and the residues involved in indirect interactions are labeled red.

direct contacts are those where (a) binding was either improved or completely lost in at least one species and (b) binding and activity were decreased in both species. Indirect contacts were defined as positions where mutations led to at least a 2-fold effect in activity and decreased binding in at least one of the species. Nine out of the fourteen amino acids identified as part of the binding epitope are charged or polar indicating that binding occurs in the extracellular milieu, rather than at the membrane surface. Most of the positions identified as part of the binding epitope are conserved between the natural sequence variants of LukH (Supplementary Table S2).

Receptor-binding and PMN activity of LukGH variants mutated at amino acid positions 263 and 312 in the rabbit system

The increase in binding and activity of the LukGH Ala mutants at positions 263 and 312 prompted us to further screen these positions for additional improvement in activity towards rbPMNs. We tested smaller (G), positively charged (K), or the same size, polar but not charged (E263Q and D312N) amino acids at positions 263 and 312. In addition, at positions 263 and 312, five other single mutants (D, V or S and V or H, respectively) and several double mutants were generated (Figure 5A,B; Supplementary Figure S3). The variants were characterized by CD and DSF (Figure 5A; Supplementary Figures S3A and S3B). A difference in CD signals observed for two of the variants, LukGH_D312G and _D312V, indicated changes in the secondary structure relative to the wild type and these proteins were therefore excluded from further analyses (Figure 5A). The CD spectra and T_m values of all other variants, except for LukGH_E263K variant for which T_m could not be measured due to low protein yield, were comparable to those of wild-type LukGH (Supplementary Figures S3A and S3B). When these variants were tested for binding to rbCD11b-I and activity towards rbPMNs, we observed a positive correlation between activity and binding (Figure 5B), as previously seen for the Ala mutants (Figure 3C). Most of the single mutants at positions 263 and 312 had a similar or negative effect compared with the corresponding Ala variants (Figure 5B). The exception was the introduction of K at position 312, which resulted in ∼10-fold improved activity towards rbPMNs, compared with the wild-type LukGH, and an

Biochemical Journal (2019) **476** 275–292
https://doi.org/10.1042/BCJ20180691

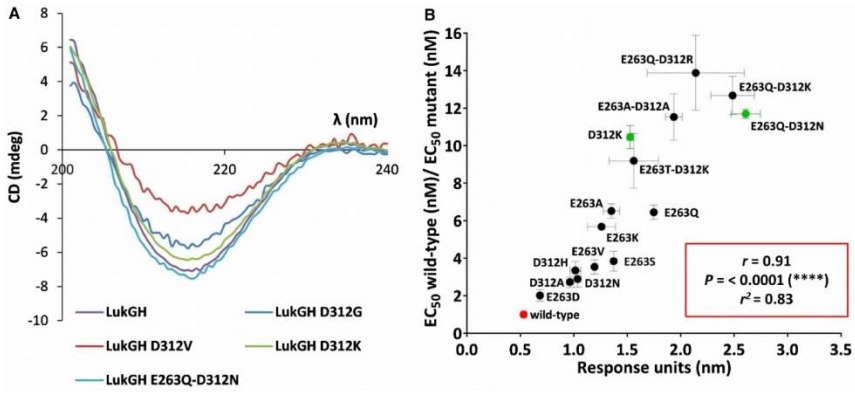

Figure 5. Targeted mutagenesis at amino acid positions 263 and 312 in LukH.

(**A**) CD spectra of selected LukGH mutants measured in 20 mM sodium phosphate, pH 7.5 plus NaCl (150–300 mM) and normalized to 0.3 mg/ml. (**B**) Correlation between EC_{50} wild-type/EC_{50} mutant towards rbPMNs and binding responses to rbCD11b-I measured by BLI. Wild-type LukGH is colored red and the LukGH variants selected for chromosomal integration are marked green. Data represent mean ± SEM of a minimum of two independent experiments performed in triplicates; except for LukGH_E263K with only one experiment for EC_{50} performed in triplicate. Pearson correlation was calculated using Prism 6 (GraphPad) and is shown as an insert.

improvement in binding kinetics that could be fitted to a K_d of 3.8×10^{-8} M (Table 2). With the double mutants, we observed, in general, an additive effect of the mutations. The LukGH_E263A-D312A variant, for example, exhibited increased binding and activity when compared with the single mutants LukGH_E263A and LukGH_D312A (Figure 5B; Table 2). However, no significant further improvement in K_d or activity could be achieved with the double mutants over the single mutants when amino acids other than Ala were introduced.

We reported recently that activation of huPMNs by LPS induced up-regulation of the CD11b receptor and resulted in increased sensitivity towards LukGH [13]. However, the ability of LPS to alter the surface expression of rbCD11b on rbPMNs and susceptibility to LukGH has not been characterized. To exclude the possibility that LPS contamination of the recombinant cytotoxins contributes to the increased activity of LukGH variants, we tested the activity of selected variants (LukGH_D312K, LukGH_E263A-D312A, and LukGH_E263Q-D312K) with LPS-stimulated rbPMNs. While we have observed that LPS increased the sensitivity of rbPMNs to LukGH (by 5–10-fold), the activity improvement obtained with these mutations was maintained in the presence of saturating amounts of LPS (6–8-fold improvement compared with wild-type LukGH) (Table 2).

Targeted mutagenesis of the CD11b-I-binding epitope

With the D312K and E263Q-D312N mutations in LukH, we were able to increase the activity towards rbPMNs by about one order of magnitude. However, this is still one order of magnitude weaker than the activity of LukGH towards huPMNs [22] (Figure 1C). To further improve the activity against rbPMNs, we generated a set of 26 triple mutants using the following backgrounds: LukGH_E263Q-D312N, _E263Q-D312K, and _E263A-D312A. We mutated LukH residues at positions which were previously identified to be important for binding and activity (i.e. 116, 118, and 294) and other proximal residues (114 and 298) to rationally selected amino acids. We introduced amino acids that appear in natural sequence variants of LukH (Supplementary Table S2), have increased or decreased size, and different charge. These triple mutants showed conserved, decreased, or lack of binding to rbCD11b-I (Figure 6A,B). Interestingly, we observed a complete loss of binding to rbCD11b-I for the triple mutants involving position 114, which was not tested as a single Ala mutant. The CD spectra and T_m values of the LukGH_E263Q-D312N-D114 mutants confirmed that folding and stability were unchanged compared with that of the wild-type LukGH, thus we concluded that the amino acid at

Biochemical Journal (2019) **476** 275–292
https://doi.org/10.1042/BCJ20180691

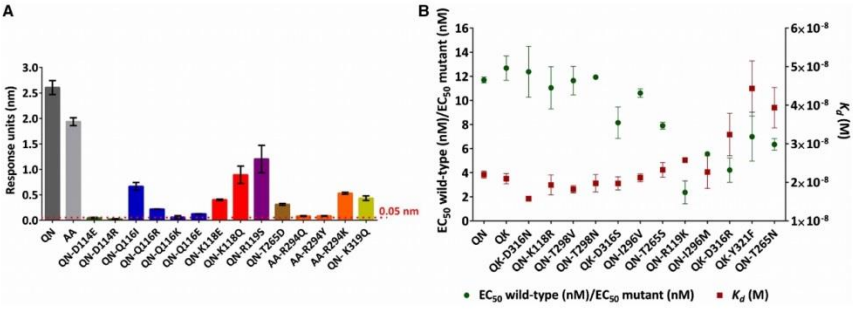

Figure 6. Binding and activity of LukGH triple mutants.

(**A**) Binding of selected triple mutants to rbCD11b-I was measured by BLI. Data represent mean ± SEM of a minimum of two independent experiments. Abbreviations: QN = LukGH_E263Q-D312N; AA = LukGH_E263A-D312A. (**B**) K_d and EC_{50}wild-type/EC_{50} mutant for triple mutants tested for activity towards rbPMNs. Data represent mean ± SEM of a minimum of two independent experiments performed in triplicates; except for LukGH E263Q-D312N-R119K with only one experiment for EC_{50} performed in triplicates. Abbreviations: QN = LukGH_E263Q-D312N; QK = LukGH_E263Q-D312K.

position 114 is part of the binding epitope (Figure 4). The variants that showed similar binding responses and K_ds as LukGH_E263Q-D312N were tested for activity towards rbPMNs. We detected no further improved activity, in agreement with the binding data. Interestingly, even small changes in K_d (<2-fold) had marked effects on activity (Figure 6B).

The best variants in terms of binding and activity, and with minimal change on protein structure, were LukGH_D312K and LukGH_E263Q-D312N, with ∼10-fold better activity towards rbPMNs and with K_d values of 20–40 nM (Table 2). We confirmed that the increased toxicity of the LukGH variants is the result of increased membrane damage of rbPMNs by employing the SYTOX green nucleic acid staining [28,42] (Table 2). Binding to huCD11b-I was unchanged and activity towards differentiated HL-60 cells was less than 2-fold reduced (Table 2). We therefore selected these two variants for replacement of the wild-type LukGH in the chromosome of *S. aureus* for further studies with natively produced cytotoxin.

Integration of rabbit-adapted *lukGH* into the *S. aureus* chromosome

Two *S. aureus* strains were selected for chromosomal integration of rabbit-adapted *lukGH* variants: a prototype USA300 CA-MRSA (TCH1516 strain) and LA#5, a clinical MSSA isolate with high LukGH expression level *in vitro* [29,38]. The mutated *S. aureus* strains were compared with the parental wild-type strains in all studies.

To confirm that the chromosomal integration did not alter protein expression, we compared expression levels for all β-barrel pore-forming cytotoxins (leukocidins and Hla) in CSs of *S. aureus* strains carrying the wild-type, the single, or double mutant LukGH variants, grown to comparable OD_{600} (Supplementary Figure S4), by Western blot. The gene replacement did not change the predicted endogenous promoter sequence and therefore LukGH expression was not expected to be affected. LukGH expression levels were comparable in the wild-type and mutant strains and in line with published data: LA#5 expressed significantly more LukGH than TCH1516 [29] (Figure 7A). Likewise, same levels of expression between wild-type and mutant strains were observed for the other cytotoxins, LukD, HlgB, Hla, and LukS-PV (present only in the TCH1516 strain), for both strains (Figure 7A).

Cytotoxicity of rabbit-adapted *S. aureus* strains towards rabbit and huPMNs

Next, we wanted to confirm that the activity improvement observed with the recombinant LukGH_D312K and _E263Q-D312N towards rbPMNs was retained with the native protein secreted into the culture medium. Testing the CS activity is important because of the different expression levels of different cytotoxins and their relative contribution to PMN killing [6,29,42]. The activity of the CSs towards rbPMNs was measured in the presence of cytotoxin-neutralizing antibodies to dissect the contribution of LukGH. We employed ASN-2, a

Biochemical Journal (2019) **476** 275–292
https://doi.org/10.1042/BCJ20180691

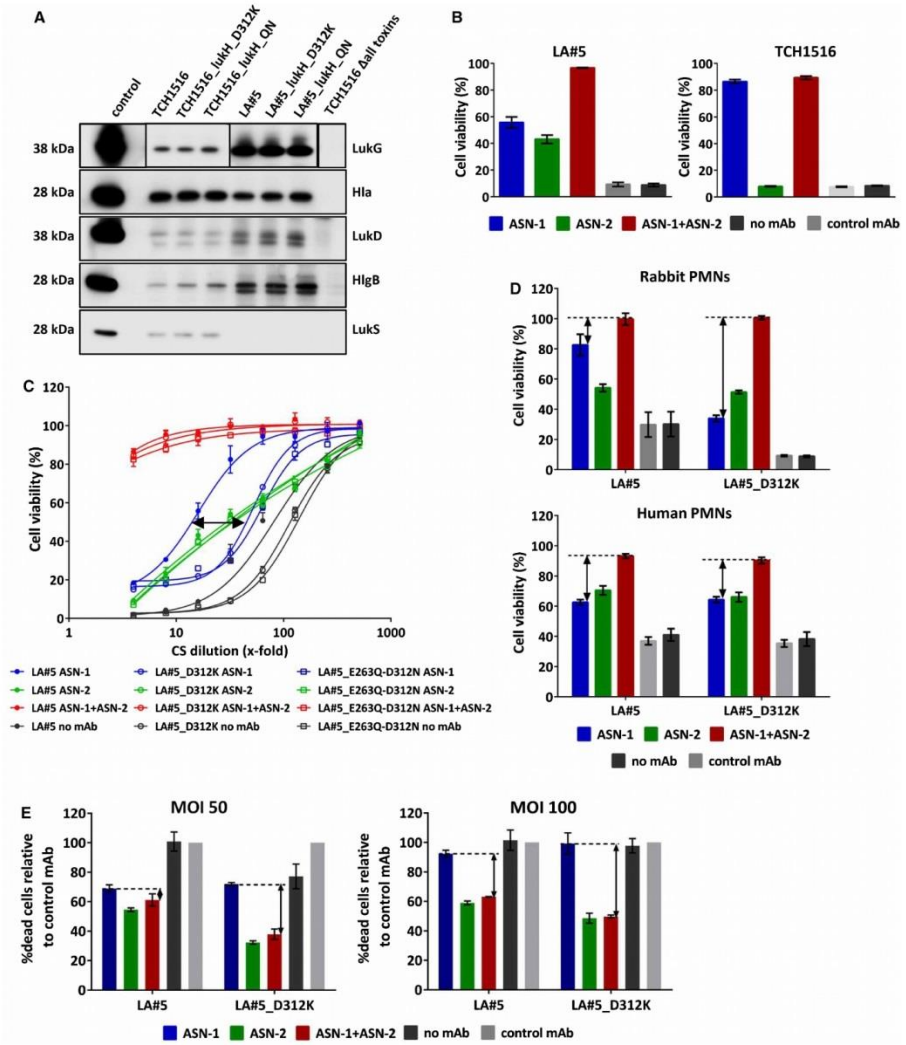

Figure 7. Characterization of *S. aureus* strains expressing the rabbit-adapted LukGH: cytotoxin expression and effect of mAbs on cytotoxin activity. Part 1 of 2

(**A**) Western blot of CSs from *S. aureus* TCH1516 and LA#5 wild-type, rabbit-adapted strains (*lukH*_D312K and *lukH*_E263Q-D312N (*lukH*_QN)), and control strain (TCH1516 Δ all cytotoxins). Control: 0.1 μg recombinant protein. (**B**) Contribution of monoclonal antibodies ASN-1 and ASN-2 to protection of rbPMNs from 16× diluted CSs prepared in RPMI + 1% CAS (mean of four to six supernatants prepared from different colonies and on different days ± SEM). (**C**) Activity of CSs of LA#5, LA#5_D312K, and LA#5_E263Q-D312N, prepared in RPMI + 1% CAS, towards rbPMNs in the presence and absence of ASN-1, ASN-2, and an equimolar mixture of both antibodies (mean of four to six supernatants prepared from different colonies and on different days ± SEM). (**D**) Comparison of protection of rb and huPMNs by the monoclonal antibodies ASN-1, ASN-2, or the equimolar mixture of the two mAbs in the presence of CSs of LA#5 and LA#5_D312K (32× dilution) prepared in RPMI + 1%

Biochemical Journal (2019) **476** 275–292
https://doi.org/10.1042/BCJ20180691

Figure 7. Characterization of *S. aureus* strains expressing the rabbit-adapted LukGH: cytotoxin expression and effect of mAbs on cytotoxin activity. Part 2 of 2

CAS (mean of four to six supernatants prepared from different colonies and on different days ± SEM). The arrow indicates the contribution of LukGH to CS toxicity. (**E**) *Ex vivo* toxicity of LA#5 and LA#5_D312K at MOI 50 (left panel) and MOI 100 (right panel) towards rbPMNs in the presence of ASN-1, ASN-2, an equimolar mixture of both antibodies, a negative control antibody and buffer alone (no mAbs) (mean of two independent experiments ± SEM). The data are expressed as % dead cells relative to control antibody and calculated as follows: [%dead cells/%dead cells$_{control\ mAb}$] × 100. The arrow indicates the contribution of LukGH to the toxicity.

LukGH-specific neutralizing antibody [37], ASN-1, a human mAb that cross-neutralizes Hla and the other four leukocidins (LukED, LukSF-PV, HlgAB, and HlgCB) [34] or an equimolar mixture of the two antibodies that allows simultaneous targeting of all five leukocidins and therefore complete inhibition of neutrophil toxicity [29]. The strains were grown in RPMI + 1% CAS to mimic the *in vivo* milieu (low iron and nutrient content); the growth kinetics and optical densities at the time point when CSs were collected were comparable (Supplementary Figure S4).

We have recently shown that full inhibition of TCH1516 and LA#5 toxicity towards huPMNs is dependent on the concerted activity of ASN-1 and ASN-2 [29]. ASN-1 alone resulted in partial inhibition of the TCH1516 CS, while for the LukSF-PV-negative strain, LA#5, inhibition was largely but not exclusively driven by ASN-2 [29]. When testing the same strains on rbPMNs, we found that ASN-2 was less critical and inhibition was almost exclusively conferred by ASN-1, a consequence of the lower sensitivity of rbPMNs to wild-type LukGH (Figure 7B).

Engineering LukGH for improved binding to rbCD11b-I resulted in increased CS toxicity for the LA#5 strain towards rbPMNs. EC_{50} values differed by a factor of 1.5 and 2 for LA#5_D312K or LA#5_E263Q-D312N, respectively (Figure 7C). In line with the data generated with huPMNs [29], the combination of the two mAbs was able to completely block toxicity towards rbPMNs (Figure 7C). The increased activity of the rabbit-adapted LukGH became apparent in the presence of ASN-1 when only LukGH was active. While the EC_{50} in the presence of ASN-1 for the LA#5 wild-type CS was 16× (dilution factor), it was ∼4-fold higher (∼64-fold) for the LA#5_D312K- and LA#5_E263Q-D312N-expressing strains. Notably, cytotoxicity in the presence of ASN-2 remained unchanged between wild-type and mutants, confirming that the expression levels of the other cytotoxins were not affected by the rabbit adaptation and that increased toxicity was a direct effect of LukGH mutagenesis. A direct comparison of the neutralization patterns of human versus rbPMNs revealed that the effect was rabbit-specific. The relative mAb and cytotoxin contribution of the parental and adapted strains were comparable with huPMNs, but differed substantially when tested with rbPMNs (Figure 7D).

Interestingly, LukGH adaptation in the TCH1516 strains, with either D312K or E263Q-D312N mutation, did not result in a significant change in CS toxicity in the absence of antibodies when tested towards either hu or rbPMNs. We observed an effect only in ASN-1 protection level towards rbPMNs for both mutants at the lowest CS dilutions tested (4–8-fold), and as expected, not towards huPMNs (Supplementary Figure S5). We speculate that this is due to the lower expression of LukGH in TCH1516 compared with LA#5 [29], and the presence of LukSF-PV, which has a significant contribution to overall *in vitro* toxicity.

We have recently shown the dominant role of LukGH during *ex vivo* infections of huPMNs [13,29] and we wanted to assess how this translates to the rabbit-adapted *S. aureus* strains with rbPMNs. Rabbit PMNs were infected with either LA#5 or LA#5_D312K at MOI 50 and 100 in the presence or absence of ASN-1 and/or ASN-2. PMN membrane damage was assessed after 2 h by SYTOX green nucleic acid staining. With both strains, we observed mostly LukGH-mediated killing as reflected by the same level of protection in the presence of ASN-2 and ASN-1 + ASN-2 (Figure 7E). Furthermore, we observed lower ASN-1 protection levels towards rbPMNs for LA#5_D312K (Figure 7E), confirming increased LukGH contribution to the killing, as seen with the CSs (Figure 7C,D).

Discussion

The most established animal models for studying *S. aureus* pathogenesis involve mice and rabbits, which are typically resistant to the bacterium, and therefore require much higher bacterial loads for disease onset and

show faster disease progression than humans [7,22,43]. Nevertheless, these models were able to pinpoint the importance of four *S. aureus* toxins: α-hemolysin, γ-hemolysin, LukED, and LukSF-PV, to *S. aureus* pathogenesis/virulence [3,7,43–47]. This is supported, at least for Hla and LukSF-PV, by clinical data, as inferred from cytotoxin expression profiles [38,46–48], presence of neutralizing antibodies and clinical outcome [49–51]. LukGH is the only *S. aureus* leukocidin whose activity and relevance *in vivo*, in these animal models, cannot be evaluated, despite its established contribution in *in vitro* and in *ex vivo* models using human cells [13,27–29,42]. It has been proposed that LukGH, alone, or in combination with Hla leads to increased organ bacterial load and biofilm formation in mouse bacteremia models [31,52]. The relevance and specificity of these effects is unclear, since mouse cells are resistant to LukGH [22], and binding of LukGH to mouse CD11b is extremely week [21]. Owing to the high cytotoxicity of LukGH and the important role of receptor up-regulation in LukGH cytotoxicity towards human cells [13,41], an *in vivo* model that reflects the human sensitivity towards LukGH is important.

The risk associated with humanizing animals for the LukGH receptor, e.g. creating a human CD11b/CD18 knock-in mouse model, is high, as CD11b, particularly its I-domain, is interacting with endogenous host factors, such as complement and blood coagulation factors [53]; the contribution of CD11b during *S. aureus* infection may be altered independent of its role as LukGH receptor. Therefore, the adaptation of LukGH to the animal hosts by *in vitro* design, as we describe here, is a closer mimic of a natural infection.

The rabbit is an ideal species for this purpose, since there is a measurable, although weak interaction between LukGH and the rabbit receptor (Figure 1B), accompanied by detectable PMN cytotoxicity (Figure 1C). By targeted mutagenesis of LukH surface-exposed residues predicted to be involved in the interaction with CD11b, we were able to increase rbPMN cytotoxicity of LukGH in a CD11b-I-dependent manner. The effects of these particular mutations are rabbit-specific, i.e. no significant change in cytotoxicity towards huPMNs, and also not related to a change in protein stability or expression level. The increased LukGH contribution to cytotoxicity towards rbPMNs in the supernatants of *S. aureus* strains expressing the rabbit-adapted LukGH mutants parallels the effects observed with the corresponding recombinant variants. This validates our approach and indicates that such rabbit-adapted strains are viable candidates for studying the role of LukGH in *S. aureus* pathogenesis in animals.

The rabbit is a suitable model organism, not only because most of the leukotoxins are active on rabbit cells, but also because rabbits are a natural host for *S. aureus*. *S. aureus* strains isolated from rabbits and humans differ by as little as one nucleotide [54]. Rabbits as well as humans show a plethora of natural staphylococcal infections: pneumonia, soft tissue infections, and bacteremia. Using a bona fide rabbit *S. aureus* strain to integrate the LukGH variants described here is another option worth considering in future experiments. The currently sequenced ST121 rabbit isolates carry *lukGH* but do not express the active LukGH dimer [54–56] — either due to stop codons in *lukG* or *lukH* or to a point mutation in LukG (E45K, WP_046463168.1), located in the LukGH dimer interface [33,37], that disrupts dimer formation (unpublished data).

It is interesting to note that none of the mutations we found to increase activity towards rbPMNs are present in over 100 published LukGH sequences [30] (Supplementary Table S2). Moreover, the three most distant sequence variants tested, including the one encoded by the livestock H19 strain, did not show any advantage, compared with TCH1516, in lysing rbPMNs. We have also tested most of the naturally occurring mutations in the epitope we have identified (Supplementary Table S2), and none of these showed significantly improved reactivity towards rbPMNs, while some decreased it. Although present in bovine strains, LukGH is not active towards bovine neutrophils [57]. It is therefore not clear if and how LukGH contributes to pathogenesis in animal hosts, which is an interesting aspect to investigate in future studies.

It has been previously demonstrated that another potent leukocidin, LukSF-PV, has an essential role in necrotizing pneumonia in rabbits, causing massive lung damage and inflammation [7]. It remains to be seen whether the same is true for rabbit-adapted LukGH. It is also noteworthy that red blood cell lysis, both by Hla and some of the leukocidins, is much more pronounced with rabbit compared with human cells. Moreover, we observed an ∼100-fold higher cytotoxicity of LukED towards rabbit compared with human neutrophils [12], and LukED is present in ∼60% of *S. aureus* isolates [30]. Despite the fact that, based on *in vitro* data, rabbits currently appear as the most suitable small animal laboratory species for studying the role of the bi-component leukocidins in *S. aureus* pathogenesis (Table 1), the prospect for additional models should not be understated.

By mapping the CD11b-I-binding site on LukH, we have identified 14 residues that are in the contact with the receptor and might be useful in similar approaches to increase LukGH susceptibility to other species, including e.g. mouse and guinea pigs. Previously, a single residue (E323) was shown to significantly affect

Biochemical Journal (2019) **476** 275–292
https://doi.org/10.1042/BCJ20180691

LukGH binding to CD11b-I and PMN activity [32]. Although the authors investigated some of the positions of the binding epitope we have delineated here (positions 316, 319, and 321 were mutated to alanine) for activity towards huPMNs (at 33 nM LukGH), they concluded these are not important for activity. Our data do not contradict their findings, but highlight possible differences in binding epitopes between hu and rbCD11b-I and indicate that lower LukGH concentrations have to be used to distinguish fine differences in activity (instead of all or none read-outs).

We demonstrated here how targeted mutagenesis can be used to expand the host receptor recognition of a bacterial toxin, even in the absence of structural information for the interaction between the toxin and its receptor. It is envisaged that the same method could be applied for other virulence factors, e.g. for the other leukocidins of *S. aureus* that bind to extracellular loops of transmembrane receptors, for which obtaining high-resolution structures to determine the exact binding interface is challenging. As this *in vitro* adaptation can be considered, in a sense, a directed evolution of an isolated toxin–receptor pair, it has significant potential over alternative approaches (such as humanization approaches that alter the host), for the *in vivo* dissection of the mode of action of drugs targeting such virulence factors in efficacy studies. However, as with any engineering effort, care must be taken that the property desired and followed is the only one affected (e.g. no expansion of the receptor-binding activity of the toxin, conferring artefactual pathogenic properties, as seen with murinized InlA from *L. monocytogenes* [58]) by such efforts. Confirming the *in vivo* phenotype with different variants, containing various amino acid substitutions (such as LukGH D312K and E263Q-D312N) for gain of function, and with controls that contain loss of function mutations, is essential.

Abbreviations

BLI, Bio-layer interferometry; CD, circular dichroism; CD11b-I, I-domain of CD11b; CS, culture supernatant; DSF, differential scanning fluorimetry; huCD11b-I, I-domain of CD11b from human; huPMNs, human polymorphonuclear cells; IPTG, isopropyl β-D-1-thiogalactopyranoside; K_d, equilibrium dissociation constant; LPS, lipopolysaccharide; PMNs, polymorphonuclear cells; rbCD11b-I, I-domain of CD11b from rabbit; rbPMNs, rabbit polymorphonuclear cells; RU, response units; T_m, melting point.

Author Contribution

A.B. and E.N. designed the study. N.T. performed the experiments, except the generation of the mutant *S. aureus* strains that was done by L.S. and M.Z. H.R. designed the cell-based experiments. J.Z. performed cloning of CD11b-I variants and preliminary binding experiments. A.B. and N.T. wrote the manuscript with input from E.N., H.R., and L.S.

Funding

This work was supported by the FFG 'Basisprogramm' Grants 832915, 837128, 841918, and 845382 from the Austrian Research Promotion Agency (awarded to Arsanis Biosciences).

Acknowledgements

The CD and DSF measurements were performed at the VBCF Protein Technologies Facility (www.vbcf.ac.at). We thank Gabor Nagy for help with designing the *S. aureus* chromosomal integration and Karin Gross and Barbara Maierhofer for their technical help with cell-based experiments.

Competing Interests

The authors declare a potential conflict of interest as the work was performed at Arsanis Biosciences GmbH (Vienna, Austria), the wholly own subsidiary of Arsanis, Inc., a biotechnology company developing a monoclonal antibody-based product targeting *S. aureus* infections. L.S., H.R, M.Z., J.Z., E.N., and A.B. declare a potential conflict of interest as they are shareholders in Arsanis, Inc.

References

1 Tong, S.Y.C., Davis, J.S., Eichenberger, E., Holland, T.L. and Fowler, Jr, V.G. (2015) *Staphylococcus aureus* infections: epidemiology, pathophysiology, clinical manifestations, and management. *Clin. Microbiol. Rev.* **28**, 603–661 https://doi.org/10.1128/CMR.00134-14

2 Vandenesch, F., Lina, G. and Henry, T. (2012) *Staphylococcus aureus* hemolysins, bi-component leukocidins, and cytolytic peptides: a redundant arsenal of membrane-damaging virulence factors? *Front. Cell. Infect. Microbiol.* **2**, 12 https://doi.org/10.3389/fcimb.2012.00012

3 Berube, B. and Wardenburg, J. (2013) *Staphylococcus aureus* α-toxin: nearly a century of intrigue. *Toxins* **5**, 1140–1166 https://doi.org/10.3390/toxins5061140

4 Spaan, A.N., van Strijp, J.A.G. and Torres, V.J. (2017) Leukocidins: staphylococcal bi-component pore-forming toxins find their receptors. *Nat. Rev. Microbiol.* **15**, 435–447 https://doi.org/10.1038/nrmicro.2017.27
5 Reyes-Robles, T. and Torres, V.J. (2017) *Staphylococcus aureus* pore-forming toxins. In *Staphylococcus aureus: Microbiology, Pathology, Immunology, Therapy and Prophylaxis* (Bagnoli, F., Rappuoli, R. and Grandi, G., eds), pp. 121–144, Springer International Publishing, Cham
6 Alonzo, F. and Torres, V.J. (2014) The bicomponent pore-forming leucocidins of *Staphylococcus aureus*. *Microbiol. Mol. Biol. Rev.* **78**, 199–230 https://doi.org/10.1128/MMBR.00055-13
7 Diep, B.A., Chan, L., Tattevin, P., Kajikawa, O., Martin, T.R., Basuino, L. et al. (2010) Polymorphonuclear leukocytes mediate *Staphylococcus aureus* Panton-Valentine leukocidin-induced lung inflammation and injury. *Proc. Natl Acad. Sci. U.S.A.* **107**, 5587–5592 https://doi.org/10.1073/pnas.0912403107
8 Seilie, E.S. and Bubeck Wardenburg, J. (2017) *Staphylococcus aureus* pore-forming toxins: the interface of pathogen and host complexity. *Semin. Cell Dev. Biol.* **72**, 101–116 https://doi.org/10.1016/j.semcdb.2017.04.003
9 Spaan, A.N., Henry, T., van Rooijen, W.J.M., Perret, M., Badiou, C., Aerts, P.C. et al. (2013) The staphylococcal toxin Panton-Valentine leukocidin targets human C5a receptors. *Cell Host Microbe* **13**, 584–594 https://doi.org/10.1016/j.chom.2013.04.006
10 Laventie, B.-J., Guérin, F., Mourey, L., Tawk, M.Y., Jover, E., Maveyraud, L. et al. (2014) Residues essential for Panton-Valentine leukocidin S component binding to its cell receptor suggest both plasticity and adaptability in its interaction surface. *PLoS ONE* **9**, e92094 https://doi.org/10.1371/journal.pone.0092094
11 Tromp, A.T., Van Gent, M., Abrial, P., Martin, A., Jansen, J.P., De Haas, C.J.C. et al. (2018) Human CD45 is an F-component-specific receptor for the staphylococcal toxin Panton–Valentine leukocidin. *Nat. Microbiol.* **3**, 708–717 https://doi.org/10.1038/s41564-018-0159-x
12 Diep, B.A., Le, V.T.M., Visram, Z.C., Rouha, H., Stulik, L., Dip, E.C. et al. (2016) Improved protection in a rabbit model of community-associated methicillin-resistant *Staphylococcus aureus* necrotizing pneumonia upon neutralization of leukocidins in addition to alpha-hemolysin. *Antimicrob. Agents Chemother.* **60**, 6333–6340 https://doi.org/10.1128/AAC.01213-16
13 Janesch, P., Rouha, H., Weber, S., Malafa, S., Gross, K., Maierhofer, B. et al. (2017) Selective sensitization of human neutrophils to LukGH mediated cytotoxicity by *Staphylococcus aureus* and IL-8. *J. Infect.* **74**, 473–483 https://doi.org/10.1016/j.jinf.2017.02.004
14 Löffler, B., Hussain, M., Grundmeier, M., Brück, M., Holzinger, D., Varga, G. et al. (2010) *Staphylococcus aureus* Panton-Valentine leukocidin is a very potent cytotoxic factor for human neutrophils. *PLoS Pathog.* **6**, e1000715 https://doi.org/10.1371/journal.ppat.1000715
15 Koop, G., Vrieling, M., Storisteanu, D.M.L., Lok, L.S., Monie, T., van Wigcheren, G. et al. (2017) Identification of LukPQ, a novel, equid-adapted leukocidin of *Staphylococcus aureus*. *Sci. Rep.* **7**, 40660 https://doi.org/10.1038/srep40660
16 Spaan, A.N., Schiepers, A., de Haas, C.J.C., van Hooijdonk, D.D.J.J., Badiou, C., Contamin, H. et al. (2015) Differential interaction of the staphylococcal toxins Panton–Valentine leukocidin and γ-hemolysin CB with human C5a receptors. *J. Immunol.* **195**, 1034–1043 https://doi.org/10.4049/jimmunol.1500604
17 Alonzo III F., Kozhaya, L., Rawlings, S.A., Reyes-Robles, T., DuMont, A.L., Myszka, D.G. et al. (2012) CCR5 is a receptor for *Staphylococcus aureus* leukotoxin ED. *Nature* **493**, 51–55 https://doi.org/10.1038/nature11724
18 Reyes-Robles, T., Alonzo, F., Kozhaya, L., Lacy, D.B., Unutmaz, D. and Torres, V.J. (2013) *Staphylococcus aureus* leukotoxin ED targets the chemokine receptors CXCR1 and CXCR2 to kill leukocytes and promote infection. *Cell Host Microbe* **14**, 453–459 https://doi.org/10.1016/j.chom.2013.09.005
19 Spaan, A.N., Reyes-Robles, T., Badiou, C., Cochet, S., Boguslawski, K.M., Yoong, P. et al. (2015) *Staphylococcus aureus* targets the Duffy antigen receptor for chemokines (DARC) to lyse erythrocytes. *Cell Host Microbe* **18**, 363–370 https://doi.org/10.1016/j.chom.2015.08.001
20 Yoong, P. and Torres, V.J. (2015) Counter inhibition between leukotoxins attenuates *Staphylococcus aureus* virulence. *Nat. Commun.* **6**, 8125 https://doi.org/10.1038/ncomms9125
21 DuMont, A.L., Yoong, P., Day, C.J., Alonzo, F., McDonald, W.H., Jennings, M.P. et al. (2013) *Staphylococcus aureus* LukAB cytotoxin kills human neutrophils by targeting the CD11b subunit of the integrin Mac-1. *Proc. Natl Acad. Sci. U.S.A.* **110**, 10794–10799 https://doi.org/10.1073/pnas.1305121110
22 Malachowa, N., Kobayashi, S.D., Braughton, K.R., Whitney, A.R., Parnell, M.J., Gardner, D.J. et al. (2012) *Staphylococcus aureus* leukotoxin GH promotes inflammation. *J. Infect. Dis.* **206**, 1185–1193 https://doi.org/10.1093/infdis/jis495
23 Spaan, A.N., Vrieling, M., Wallet, P., Badiou, C., Reyes-Robles, T., Ohneck, E.A. et al. (2014) The staphylococcal toxins γ-haemolysin AB and CB differentially target phagocytes by employing specific chemokine receptors. *Nat. Commun.* **5**, 5438 https://doi.org/10.1038/ncomms6438
24 Pan, X., Yang, Y. and Zhang, J.-R. (2014) Molecular basis of host specificity in human pathogenic bacteria. *Emerg. Microbes Infect.* **3**, e23 https://doi.org/10.1038/emi.2014.23
25 Prince, A., Wang, H., Kitur, K. and Parker, D. (2017) Humanized mice exhibit increased susceptibility to *Staphylococcus aureus* pneumonia. *J. Infect. Dis.* **215**, 1386–1395 https://doi.org/10.1093/infdis/jiw425
26 Wollert, T., Pasche, B., Rochon, M., Deppenmeier, S., van den Heuvel, J., Gruber, A.D. et al. (2007) Extending the host range of *Listeria monocytogenes* by rational protein design. *Cell* **129**, 891–902 https://doi.org/10.1016/j.cell.2007.03.049
27 Ventura, C.L., Malachowa, N., Hammer, C.H., Nardone, G.A., Robinson, M.A., Kobayashi, S.D. et al. (2010) Identification of a novel *Staphylococcus aureus* two-component leukotoxin using cell surface proteomics. *PLoS ONE* **5**, e11634 https://doi.org/10.1371/journal.pone.0011634
28 DuMont, A.L., Nygaard, T.K., Watkins, R.L., Smith, A., Kozhaya, L., Kreiswirth, B.N. et al. (2011) Characterization of a new cytotoxin that contributes to *Staphylococcus aureus* pathogenesis: the cytotoxin LukAB kills human phagocytes. *Mol. Microbiol.* **79**, 814–825 https://doi.org/10.1111/j.1365-2958.2010.07490.x
29 Rouha, H., Weber, S., Janesch, P., Maierhofer, B., Gross, K., Dolezilkova, I. et al. (2018) Disarming *Staphylococcus aureus* from destroying human cells by simultaneously neutralizing six cytotoxins with two human monoclonal antibodies. *Virulence* **9**, 231–247 https://doi.org/10.1080/21505594.2017.1391447
30 Badarau, A., Trstenjak, N. and Nagy, E. (2017) Structure and function of the two-component cytotoxins of *Staphylococcus aureus* — learnings for designing novel therapeutics. In *Protein Reviews* (Atassi, M.Z., ed.), vol. **18**, pp. 15–35, Springer, Singapore
31 Thomsen, I.P., Sapparapu, G., James, D.B.A., Cassat, J.E., Nagarsheth, M., Kose, N. et al. (2017) Monoclonal antibodies against the *Staphylococcus aureus* bicomponent leukotoxin AB isolated following invasive human infection reveal diverse binding and modes of action. *J. Infect. Dis.* **215**, 1124–1131 https://doi.org/10.1093/infdis/jix071

32 DuMont, A.L., Yoong, P., Liu, X., Day, C.J., Chumbler, N.M., James, D.B.A. et al. (2014) Identification of a crucial residue required for *Staphylococcus aureus* LukAB cytotoxicity and receptor recognition. *Infect. Immun.* **82**, 1268–1276 https://doi.org/10.1128/IAI.01444-13
33 Badarau, A., Rouha, H., Malafa, S., Logan, D.T., Håkansson, M., Stulik, L. et al. (2015) Structure-function analysis of heterodimer formation, oligomerization, and receptor binding of the *Staphylococcus aureus* bi-component toxin LukGH. *J. Biol. Chem.* **290**, 142–156 https://doi.org/10.1074/jbc.M114.598110
34 Rouha, H., Badarau, A., Visram, Z.C., Battles, M.B., Prinz, B., Magyarics, Z. et al. (2015) Five birds, one stone: Neutralization of α-hemolysin and 4 bi-component leukocidins of *Staphylococcus aureus* with a single human monoclonal antibody. *MAbs* **7**, 243–254 https://doi.org/10.4161/19420862.2014.985132
35 Romero-Steiner, S., Libutti, D., Pais, L.B., Dykes, J., Anderson, P., Whitin, J.C. et al. (1997) Standardization of an opsonophagocytic assay for the measurement of functional antibody activity against *Streptococcus pneumoniae* using differentiated HL-60 cells. *Clin. Diagn. Lab. Immunol.* **4**, 415–422 PMID: 9220157
36 Siemsen, D.W., Malachowa, N., Schepetkin, I.A., Whitney, A.R., Kirpotina, L.N., Lei, B. et al. (2014) Neutrophil isolation from nonhuman species. In *Neutrophil Methods and Protocols* (Quinn, M.T. and DeLeo, F.R., eds.), pp. 19–37, Humana Press, Totowa, NJ
37 Badarau, A., Rouha, H., Malafa, S., Battles, M.B., Walker, L., Nielson, N. et al. (2016) Context matters: The importance of dimerization-induced conformation of the LukGH leukocidin of *Staphylococcus aureus* for the generation of neutralizing antibodies. *MAbs* **8**, 1347–1360 https://doi.org/10.1080/19420862.2016.1215791
38 Stulik, L., Malafa, S., Hudcova, J., Rouha, H., Henics, B.Z., Craven, D.E. et al. (2014) α-Hemolysin activity of methicillin-susceptible *Staphylococcus aureus* predicts ventilator-associated pneumonia. *Am. J. Respir. Crit. Care Med.* **190**, 1139–1148 https://doi.org/10.1164/rccm.201406-1012OC
39 Kato, F. and Sugai, M. (2011) A simple method of markerless gene deletion in *Staphylococcus aureus*. *J. Microbiol. Methods* **87**, 76–78 https://doi.org/10.1016/j.mimet.2011.07.010
40 McNamara, P.J. (2008) Genetic manipulation of *Staphylococcus aureus*. In *Staphylococcus: Molecular Genetics* (Lindsay, J.A., ed.), 1st ed., pp. 89–130, Caister Academic Press, Norfolk
41 Malachowa, N., Kobayashi, S.D., Freedman, B., Dorward, D.W. and DeLeo, F.R. (2013) *Staphylococcus aureus* leukotoxin GH promotes formation of neutrophil extracellular traps. *J. Immunol.* **191**, 6022–6029 https://doi.org/10.4049/jimmunol.1301821
42 DuMont, A.L., Yoong, P., Surewaard, B.G.J., Benson, M.A., Nijland, R., van Strijp, J.A.G. et al. (2013) *Staphylococcus aureus* elaborates leukocidin AB to mediate escape from within human neutrophils. *Infect. Immun.* **81**, 1830–1841 https://doi.org/10.1128/IAI.00095-13
43 Kobayashi, S.D., Malachowa, N., Whitney, A.R., Braughton, K.R., Gardner, D.J., Long, D. et al. (2011) Comparative analysis of USA300 virulence determinants in a rabbit model of skin and soft tissue infection. *J. Infect. Dis.* **204**, 937–941 https://doi.org/10.1093/infdis/jir441
44 Alonzo, ,III, F., Benson, M.A., Chen, J., Novick, R.P., Shopsin, B. and Torres, V.J. (2012) *Staphylococcus aureus* leucocidin ED contributes to systemic infection by targeting neutrophils and promoting bacterial growth *in vivo*: LukED contributes to *S. aureus* bacteraemia. *Mol. Microbiol.* **83**, 423–435 https://doi.org/10.1111/j.1365-2958.2011.07942.x
45 Siqueira, J.A., Speeg-Schatz, C., Freitas, F.I.S., Sahel, J., Monteil, H. and Prevost, G. (1997) Channel-forming leucotoxins from *Staphylococcus aureus* cause severe inflammatory reactions in a rabbit eye model. *J. Med. Microbiol.* **46**, 486–494 https://doi.org/10.1099/00222615-46-6-486
46 Gillet, Y., Issartel, B., Vanhems, P., Fournet, J.C., Lina, G., Bes, M. et al. (2002) Association between *Staphylococcus aureus* strains carrying gene for Panton-Valentine leukocidin and highly lethal necrotising pneumonia in young immunocompetent patients. *Lancet* **359**, 753–759 https://doi.org/10.1016/S0140-6736(02)07877-7
47 Lina, G., Piémont, Y., Godail-Gamot, F., Bes, M., Peter, M.O., Gauduchon, V. et al. (1999) Involvement of Panton-Valentine leukocidin-producing *Staphylococcus aureus* in primary skin infections and pneumonia. *Clin. Infect. Dis.* **29**, 1128–1132 https://doi.org/10.1086/313461
48 Kuehnert, M.J., Kruszon-Moran, D., Hill, H.A., McQuillan, G., McAllister, S.K., Fosheim, G. et al. (2006) Prevalence of *Staphylococcus aureus* nasal colonization in the United States, 2001–2002. *J. Infect. Dis.* **193**, 172–179 https://doi.org/10.1086/499632
49 Adhikari, R.P., Ajao, A.O., Aman, M.J., Karauzum, H., Sarwar, J., Lydecker, A.D. et al. (2012) Lower antibody levels to *Staphylococcus aureus* exotoxins are associated with sepsis in hospitalized adults with *invasive S. aureus* infections. *J. Infect. Dis.* **206**, 915–923 https://doi.org/10.1093/infdis/jis462
50 Fritz, S.A., Tiemann, K.M., Hogan, P.G., Epplin, E.K., Rodriguez, M., Al-Zubeidi, D.N. et al. (2013) A serologic correlate of protective immunity against community-onset *Staphylococcus aureus* infection. *Clin. Infect. Dis.* **56**, 1554–1561 https://doi.org/10.1093/cid/cit123
51 Rasigade, J.P., Sicot, N., Laurent, F., Lina, G., Vandenesch, F. and Etienne, J. (2011) A history of Panton–Valentine leukocidin (PVL)-associated infection protects against death in PVL-associated pneumonia. *Vaccine* **29**, 4185–4186 https://doi.org/10.1016/j.vaccine.2011.04.033
52 Scherr, T.D., Hanke, M.L., Huang, O., James, D.B.A., Horswill, A.R., Bayles, K.W. et al. (2015) *Staphylococcus aureus* biofilms induce macrophage dysfunction through leukocidin AB and alpha-toxin. *MBio* **6**, e01021-15 https://doi.org/10.1128/mBio.01021-15
53 Takada, Y., Ye, X. and Simon, S. (2007) The integrins. *Genome Biol.* **8**, 215 https://doi.org/10.1186/gb-2007-8-5-215
54 Viana, D., Comos, M., McAdam, P.R., Ward, M.J., Selva, L., Guinane, C.M. et al. (2015) A single natural nucleotide mutation alters bacterial pathogen host tropism. *Nat. Genet.* **47**, 361–366 https://doi.org/10.1038/ng.3219
55 Guerrero, I., Ferrian, S., Penadés, M., García-Quirós, A., Pascual, J.J., Selva, L. et al. (2015) Host responses associated with chronic staphylococcal mastitis in rabbits. *Vet. J.* **204**, 338–344 https://doi.org/10.1016/j.tvjl.2015.03.020
56 Viana, D., Selva, L., Penadés, M. and Corpa, J. (2015) Screening of virulence genes in *Staphylococcus aureus* isolates from rabbits. *World Rabbit Sci.* **23**, 185–195 https://doi.org/10.4995/wrs.2015.3961
57 Vrieling, M., Boerhout, E.M., van Wigcheren, G.F., Koymans, K.J., Mols-Vorstermans, T.G., de Haas, C.J.C. et al. (2016) LukMF′ is the major secreted leukocidin of bovine *Staphylococcus aureus* and is produced *in vivo* during bovine mastitis. *Sci. Rep.* **6**, 37759 https://doi.org/10.1038/srep37759
58 Tsai, Y.-H., Disson, O., Bierne, H. and Lecuit, M. (2013) Murinization of internalin extends its receptor repertoire, altering *Listeria monocytogenes* cell tropism and host responses. *PLoS Pathog.* **9**, e1003381 https://doi.org/10.1371/journal.ppat.1003381

SUPPORTING INFORMATION

Figure S1. Design of the cloning vector and generation of *S. aureus* mutants

Figure S2. CD spectra of LukGH Ala mutants

Figure S3. Characterization of LukGH single mutants and double mutants at position LukH_263 and LukH_312

Figure S4. Growth curves of *S. aureus* strains in RPMI + 1% CAS

Figure S5. Effect of mAbs on activity of CSs from TCH1516 wild-type and rabbit adapted strains

Table S1. Binding of LukGH natural sequence variants (derived from *S. aureus* strains H19, MSHR1132 and MRSA252) to rbCD11b-I and activity towards rabbit PMNs.

LukGH variant	Response units $_{max}$ (RU) (nm) [1]	EC_{50} (nm) [3]
TCH1516	0.98 ± 0.21	1.2
MRSA252	0.61 ± 0.09	26.7
H19	1.16 ± 0.01	27.4
MSHR1132	-0.10 ± 0.05 [2]	17.7

[1] LukGH (270 nM) binding to rbCD11b-I immobilized on streptavidin sensors (loading to 5 nm) (n=2, mean +/- S.D.); [2] RU <0.05 nm: no binding; [3] Activity of LukGH variants towards rabbit PMNs (one experiment performed in triplicate).

Table S2. Sequence conservation of LukH in natural variants at the positions identified as part of the binding epitope.

TCH1516 sequence	Amino acids difference in three most divergent sequence variants (H19, MRSA252 or MSHR1132)	Amino acids present in other sequence variants (% of sequences with position different from TCH1516)
D114	conserved	conserved
Q116	conserved	R (0.7%)
K118	Q (MRSA252)	Q (9.4%)
R119	conserved	S (7.2%)
E263	conserved	conserved
T267	conserved	conserved
R294	conserved	conserved
I296	conserved	conserved
D312	E (MRSA252)	E (9.4%)
Y314	conserved	H (0.7%)
D316	conserved	conserved
K319	Q (MSHR1132)	Q (3.6%)
Y321	F (MSHR1132)	F (2.2%)
E323	conserved	conserved

Amino acid conservation in H19, MRSA252 and MSHR1132 (LukH sequences most divergent from TCH1516) and in 131 sequence variants available in NCBI database (only the sequences with≥ 90% coverage and ≥ 87% identity to TCH1516 sequence were analysed).

Figure S1

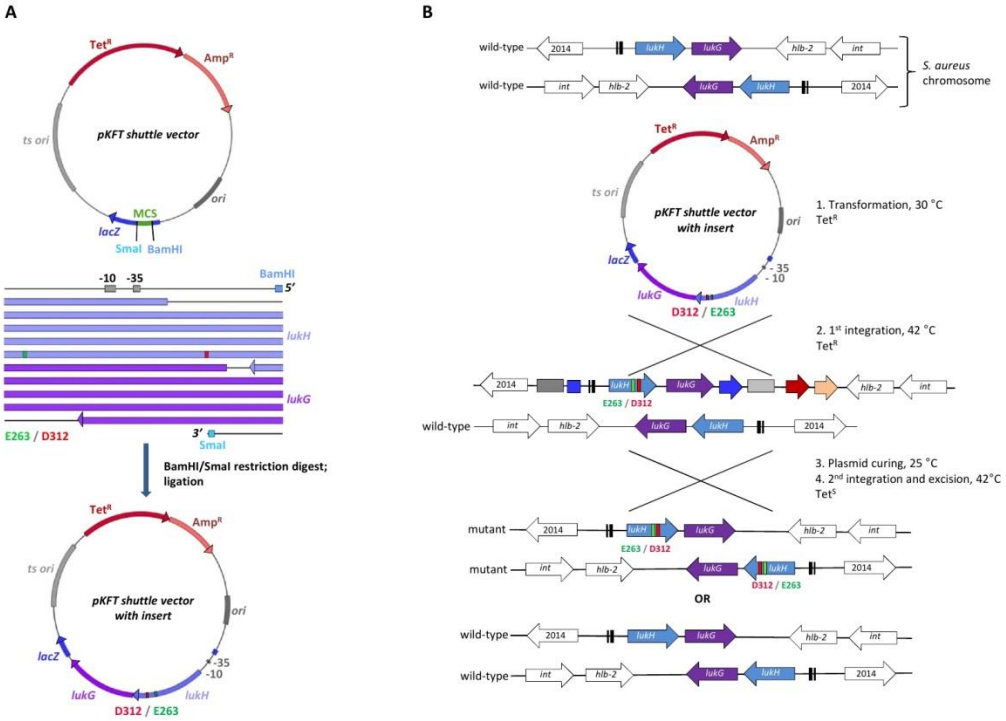
A
Tet^R
Amp^R
ts ori
pKFT shuttle vector
ori
MCS
lacZ
SmaI BamHI
-10 -35
BamHI
5'
lukH
lukG
E263 / D312
3'
SmaI
BamHI/SmaI restriction digest; ligation
pKFT shuttle vector with insert
-35
-10
D312 / E263
B
wild-type
2014
lukH
lukG
hlb-2
int
S. aureus chromosome
1. Transformation, 30 °C Tet^R
2. 1st integration, 42 °C Tet^R
3. Plasmid curing, 25 °C
4. 2nd integration and excision, 42°C Tet^S
mutant
OR

Figure S2

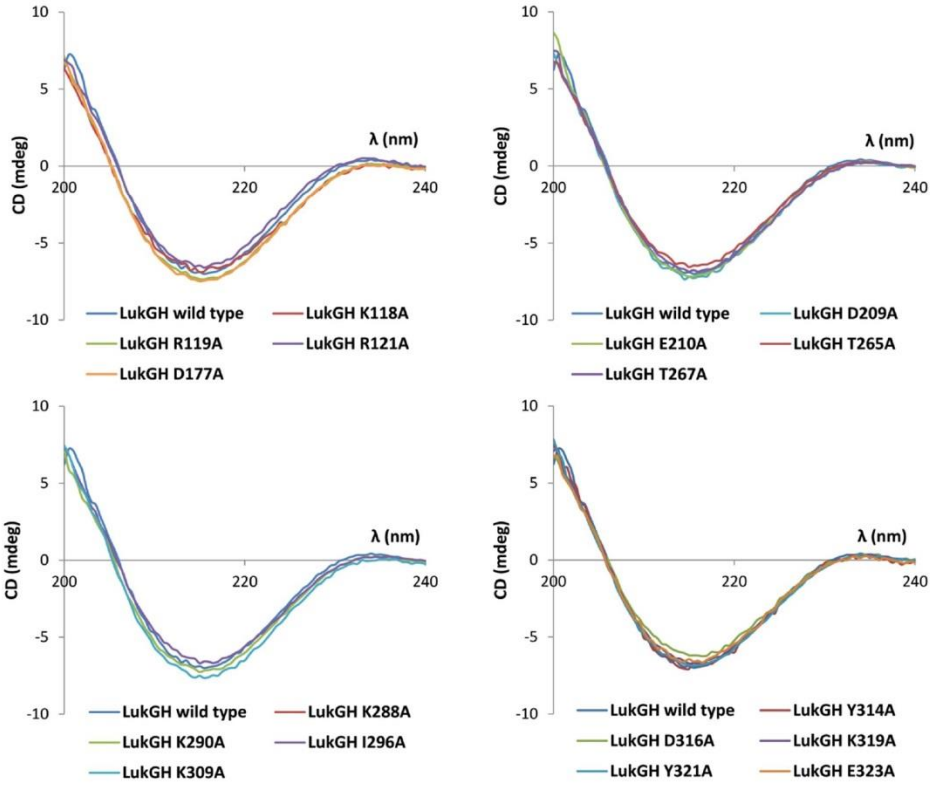
10
5
0
-5
-10
200
220
240
λ (nm)
CD (mdeg)
LukGH wild type
LukGH K118A
LukGH R119A
LukGH R121A
LukGH D177A
LukGH D209A
LukGH E210A
LukGH T265A
LukGH T267A
LukGH K288A
LukGH K290A
LukGH I296A
LukGH K309A
LukGH Y314A
LukGH D316A
LukGH K319A
LukGH Y321A
LukGH E323A

Figure S3

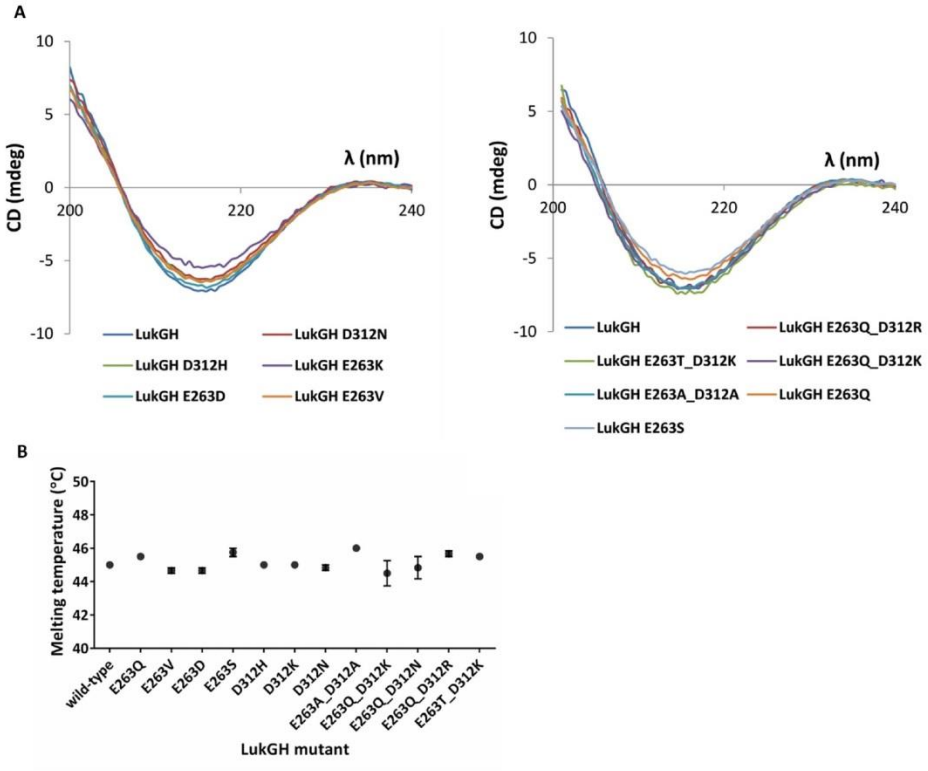
A
10
5
0
-5
-10
CD (mdeg)
200
220
240
λ (nm)
LukGH
LukGH D312N
LukGH D312H
LukGH E263K
LukGH E263D
LukGH E263V
LukGH E263Q_D312R
LukGH E263T_D312K
LukGH E263Q_D312K
LukGH E263A_D312A
LukGH E263Q
LukGH E263S
B
Melting temperature (°C)
50
48
46
44
42
40
wild-type
E263Q
E263V
E263D
E263S
D312H
D312K
D312N
E263A_D312A
E263Q_D312K
E263Q_D312N
E263Q_D312R
E263T_D312K
LukGH mutant

Figure S4

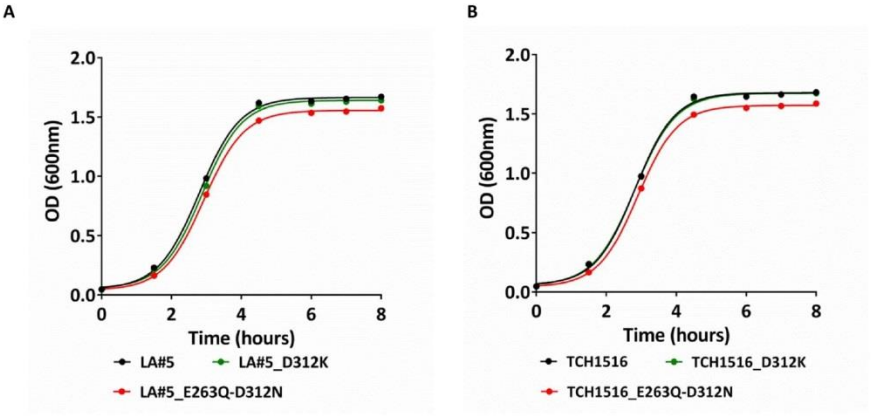
A
B
OD (600nm)
Time (hours)
LA#5
LA#5_D312K
LA#5_E263Q-D312N
TCH1516
TCH1516_D312K
TCH1516_E263Q-D312N

Figure S5

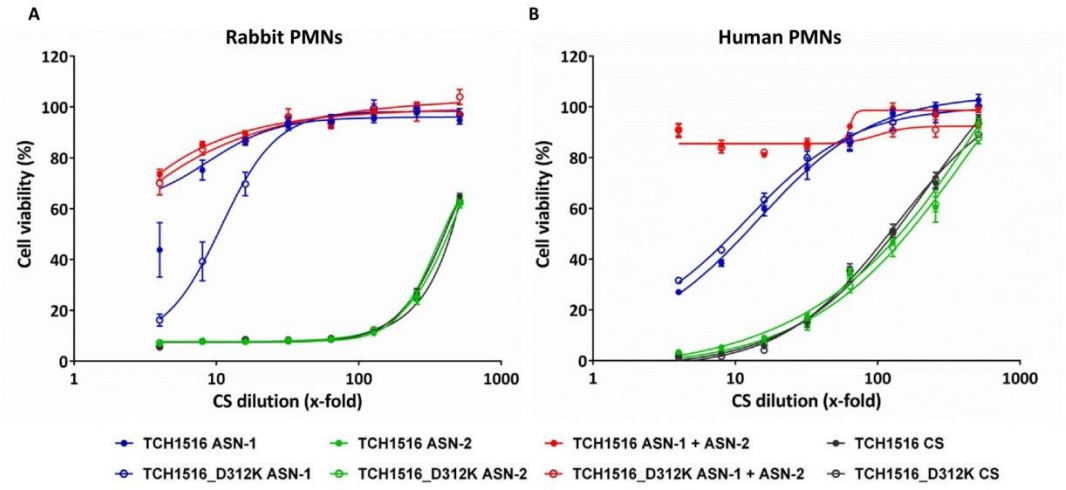
A
Rabbit PMNs
B
Human PMNs
Cell viability (%)
CS dilution (x-fold)
TCH1516 ASN-1
TCH1516 ASN-2
TCH1516 ASN-1 + ASN-2
TCH1516 CS
TCH1516_D312K ASN-1
TCH1516_D312K ASN-2
TCH1516_D312K ASN-1 + ASN-2
TCH1516_D312K CS

Manuscript I: Molecular mechanism of leukocidin GH - integrin CD11b/CD18 recognition and species specificity

Confirmation of manuscript submission:

The manuscript entitled "*Molecular mechanism of leukocidin GH - integrin CD11b/CD18 recognition and species specificity*" was submitted to Nature Chemical Biology on June 28th, 2019. It is currently under review (status June 28th, 2019). The confirmation received from the journal by e-mail (shortened for purpose of this dissertation) including the manuscript ID is shown below:

Manuscript ID: NCHEMB-A190609699

From: chembio@us.nature.com <chembio@us.nature.com>
Sent: Friday, June 28, 2019 8:25 PM
To: Adriana Badarau
Subject: NCHEMB-A190609699: All Manuscript Files Converted to PDF

Dear Dr Badarau,

The conversion of manuscript files for manuscript NCHEMB-A190609699, entitled "Molecular mechanism of leukocidin GH - integrin CD11b/CD18 recognition and species specificity", has now been completed.

Please review all the files here.
https://mts-nchemb.nature.com/cgi-bin/main.plex?el=A4O6IkW2A3CAeU5F3A9ftdtJqCtLkbH3DRubU3D20QZ

If there are any issues with the files, please contact Platform Support Helpdesk.

Your manuscript is now available to editors of Nature Chemical Biology.

Yours sincerely,

Kitty Moore
Editorial Assistant
Nature Chemical Biology

Molecular mechanism of leukocidin GH - integrin CD11b/CD18 recognition and species specificity

Nikolina Trstenjak[1*], Dalibor Milić[2*], Melissa Ann Graewert[3], Harald Rouha[1§], Dmitri Svergun[3], Kristina Djinović-Carugo[2,4], Eszter Nagy[1§], Adriana Badarau[1#§]

[1]Arsanis Biosciences, Campus Vienna Biocenter, 1030, Vienna, Austria

[2]Department of Structural and Computational Biology, Max Perutz Labs, University of Vienna, 1030 Vienna, Austria

[3]European Molecular Biology Laboratory, Hamburg Unit, c/o DESY, Notkestrasse 85, 22607 Hamburg, Germany, and BioSAXS GmbH, c/o DESY, Notkestrasse 85, 22607 Hamburg, Germany

[4]Department of Biochemistry, Faculty of Chemistry and Chemical Technology, University of Ljubljana, Večna pot 113, SI-1000 Ljubljana, Slovenia

[*] contributed equally to the work

[§] current affiliations: A.B. and H.R. – X4 Pharmaceuticals (Austria) GmbH; E. N. –CEBINA GmbH, Karl-Farkas-Gasse 22, Vienna, Austria

[#] corresponding author: adriana.badarau@x4pharma.com

ABSTRACT

Host-pathogen interactions are central to understanding microbial pathogenesis. The staphylococcal pore forming cytotoxins hijack important immune molecules but little is known about the underlying molecular mechanisms of cytotoxin–receptor interaction and host specificity. Here we report the first structures of a staphylococcal pore forming cytotoxin, leukocidin GH (LukGH), in complex with its receptor (the α-I domain of complement receptor 3, CD11b-I), both for the human and murine homologues. We observe two binding interfaces, on the LukG and the LukH protomers, and show that human CD11b-I induces LukGH oligomerisation in solution. LukGH binds murine CD11b-I weakly and is inactive towards murine neutrophils. Using a LukGH variant engineered to bind mouse CD11b-I, we demonstrate that cytolytic activity does not only require binding but also receptor-dependent oligomerisation. Our studies provide an unprecedented insight into bi-component leukocidin–host receptor interaction, enabling the development of anti-toxin approaches and improved animal models to explore these approaches.

INTRODUCTION

Staphylococcus aureus is a versatile human pathogen with the unique ability to cause a wide range of diseases, such as skin and soft tissue infections, sepsis or pneumonia, attributed to its immense diversity of host-targeting virulence factors [1]. The secreted leukocidins, a family of bi-component pore forming toxins, are believed to be at the core of *S. aureus* immune evasion by lysing phagocytic cells, mainly neutrophil granulocytes but also monocytes and macrophages [2, 3]. *S. aureus* produces up to five different leukocidins: gamma-hemolysins HlgAB and HlgCB, LukSF-PV (PVL), LukED and LukGH (also called LukAB) [2], with their cell type and species specificity driven by binding to different proteinaceous receptors on the surface of the immune cells [2, 3]. Following receptor binding, the toxins oligomerise to form a lytic, octameric, beta-barrel pore on the cell membrane. Although the steps involved in the leukocidin structural changes occurring during the pore formation are at least partly understood, less is known about the role of the receptors in this process [4, 5].

All cellular receptors of the bi-component toxins are transmembrane-spanning G protein-coupled receptors (GPCRs) [2, 3, 6], except for LukGH, which binds to the extracellular α-I domain of the α_M/β_2 integrin (CD11b/CD18, macrophage-1 antigen, or complement receptor 3) [7]. CD11b/CD18 is a member of the CD18 integrin family and is expressed on professional phagocytic cells [8] with a central role in the immune system, binding more than 40 protein ligands, including human fibrinogen and the complement fragment iC3b [9-11]. Both the α and β subunits contain large

ectodomains, one transmembrane domain each, and short cytoplasmic domains, which enable communication with the extracellular environment. The two ectodomains, supported by their upper and lower legs, come together to form the integrin head, which comprises the α-I domain, the canonical ligand binding site in the integrins. Integrin activation, the so-called 'inside-out signaling', results in an allosteric switch in the CD11b/CD18 ectodomain, from a resting, bent state to the extended form, with the corresponding activation of the α-I domain (conversion to open form, see below), and ligand recruitment [12].

The human α-I domain (CD11b-I) was expressed recombinantly, independently of the other integrin subunits [13], and to date 13 crystal structures of CD11b-I in complex with natural ligands, antagonists, antibodies, or alone, have been solved [13-20]. However, despite the critical role of CD11b-I in the immune system of different mammals [21], all available crystal structures were obtained with the human CD11b-I (huCD11b-I). Two different conformations have been observed: the so called inactive (closed or low affinity) and active (open or high affinity) forms of CD11b-I. The latter involves the rearrangement of the metal coordinating residues at the metal ion-dependent adhesion site (MIDAS), to allow a carboxylate group from the ligand to complete the metal coordination, and a 10-Å downward shift of the C-terminal α-helix [12, 14].

LukGH is expressed in human infections and appears to be the most potent *S. aureus* leukocidin based on *in vitro* and *ex vivo* data [22-25]. It is however inactive or displays limited activity in the established *S. aureus in vivo* models, such as mouse and rabbit, which hinders the study of its role in *S. aureus* pathogenesis [7, 26]. The variation in the CD11b-I sequences between different species was used to explain the LukGH species specificity, and activity was shown to correlate with binding to CD11b-I, *i.e.* no binding to mouse CD11b-I (moCD11b-I) and very low activity towards murine polymorphonuclear neutrophils (PMNs) *in vitro* [7, 26]. We have recently been able to improve LukGH cytotoxicity (~10–15-fold) towards rabbit cells by increasing binding to the rabbit CD11b-I receptor, using alanine scanning and targeted mutagenesis to map the cytotoxin-receptor interaction [27]. However, high-resolution structural data for the LukGH–CD11b-I interaction would allow rational design of LukGH variants with activity towards different species and provide mechanistic insights into receptor-mediated pore-formation.

Here, we report the crystal structure of LukGH in complex with the CD11b-I domain, which is the first structure of a *S. aureus* pore-forming cytotoxin in complex with its receptor. We use both the human and the mouse receptors, for crystal and solution structural analysis, to ascertain and characterize the two main requirements for activity: binding and oligomerisation. We find that the same receptor molecule is involved in binding and oligomerisation via interactions with the LukH and LukG

subunits, respectively. The roles of receptor cell surface expression, activation and clustering on LukGH activity and the molecular drivers of LukGH species specificity are discussed.

RESULTS

Receptor binding is necessary, but not sufficient for LukGH cytotoxicity

Using both human and rabbit cells and recombinant receptor molecules we have previously confirmed that LukGH binding to CD11b-I indeed correlated with its cytotoxic activity towards PMNs in these two species, and have identified mutations in LukGH that either decrease or enhance binding and activity [27]. The most prominent change was seen with LukGH_D312K, a variant with increased affinity towards rabbit CD11b-I (rbCD11b-I) paralleled by 10–15-fold increased cytotoxicity of recombinant LukGH towards rabbit PMNs [27]. Mouse PMNs are resistant to LukGH at concentrations up to 30 µM, and the toxin binds the mouse receptor very weakly (K_d ~1 µM, Figure 1a-c) [7]. We found two mutations in LukH, R294A and K319A (previously shown to decrease binding towards the human and rabbit receptor) [27] that significantly increase binding to moCD11b-I (K_d of 63 nM for LukGH_K319A, similar to LukGH_D312K with rbCD11b-I, Figure 1b). However, these mutants display no activity towards mouse PMNs, at concentrations up to 20 µM, which are over 3 orders of magnitude greater than the EC_{50} values of LukGH for rabbit and human PMNs (Figure 1b and 1c). Thus, the receptor binding – cytolytic activity correlation observed for human and rabbit does not apply to the mouse system and we hypothesized that another step in the pore forming process, beyond receptor binding, is responsible.

Structural insight into LukGH-CD11b-I interaction and specificity

Several attempts to crystallize huCD11b-I in complex with LukGH, including different LukGH constructs, *i.e.* LukGH wild-type, LukGH with an impaired oligomerisation interface (LukG1H) [28], and LukGH lacking the unstructured N-terminus of LukH (33 and 41 amino acids), were unsuccessful. However, we managed to crystallize murine CD11b-I (moCD11b-I) in complex with the full-length LukGH_K319A mutant (with increased affinity to moCD11b-I), with crystals diffracting to 2.29 Å resolution (Supplementary Table 1). Subsequently, crystals were also obtained for the human variant (huCD11b-I) in complex with full-length wild-type LukGH, but anisotropically diffracted to lower resolution (2.75 Å along **a*** and **b***, and 4.79 Å along **c***) (Supplementary Table 1). Both crystal structures revealed one LukG and one LukH molecule bound to the CD11b-I in the asymmetric unit, with a total binding surface area of 701 and 340 $Å^2$ for LukH_K319A/moCD11b-I and LukG/moCD11b-I, and 695 and 246 $Å^2$ for LukH/huCD11b-I and LukG/huCD11b-I interfaces, respectively. In the crystal lattice, the LukG and LukH protomers assembled into a four-fold rotationally (C_4) symmetrical

octameric pore composed of four LukG–LukH–CD11b-I heterotrimers, similar to that previously reported for LukGH alone (PDB 4TW1) [28] (Figure 1d). Interestingly, apart from the expected LukH–CD11b-I epitope, we observe a second binding site between CD11b-I and LukG from an adjacent dimer of the LukGH octamer (Figure 1d).

With the exception of the N-termini and a few loops, essentially the entire LukH and LukG subunits are visible in the electron density map. The $RMSD_{C\alpha}$ values between the LukGH from the structures reported here and each of the two crystallographically-independent LukGH octamers in PDB 4TW1 [28] are 0.88 and 1.04 Å over 2247 and 2257 superimposed Cα atoms for the mouse complex, and 0.59 and 0.73 Å over 2167 and 2161 superimposed Cα atoms for the human complex, respectively. For the moCD11b-I and huCD11b-I more than 20 amino acids of the C-terminal α-helix (α7) are not visible in the electron density maps (Figure 1e), as also seen in the structure of huCD11b-I–C3d complex (PDB 4M76) [19], which is lacking the last 11 amino acids. Similar to previously published huCD11b-I structures, moCD11b-I folds into an α/β Rossmann fold (Figure 1e), as expected due to relatively high sequence conservation between CD11b-I domains from different species (78% identity between mo and huCD11b-I) [7]. The $RMSD_{C\alpha}$ between the CD11b-I domains in the complexes and the previously published conformations of huCD11b-I: active (PDB 1IDO) [13] and inactive (PDB 1JLM) [14], are 0.62 and 1.63 Å over 169 superimposed Cα atoms for moCD11b-I, and 0.70 and 1.27 Å over 168 superimposed Cα atoms for huCD11b-I, respectively (Figure 1e). The tendency of the α7 helix for downward shift and the coordination sphere of Mg^{2+} in the MIDAS site indicate that both human and mouse CD11b-I exist in the active conformation when bound to LukGH (Figure 1e, 1f).

To explain additionally observed features in difference electron density maps, we included six discrete molecules of dimethyl sulfoxide (DMSO) per an asymmetric unit of each structure. One DMSO moiety (DMSO2) is positioned in a hydrophobic pocket in the rim of LukG, occupied by either the side chain of M103 from the antibody Fab fragment of an anti-LukGH antibody (aLukGH-mAb#5.H1H2) in the Fab-LukGH complex (PDB 5K59) [29] or the side chain of LukG_N206 in one of the four chains from the LukGH octamer (PDB 4TW1), indicating a potential lipid binding site (Figure 1d). This pocket is ~15 Å away from the canonical phosphocholine binding pocket in other beta barrel pore forming toxins [30, 31], which is occupied in all known LukGH structures by the side chain of M178.

Main interaction site of CD11b-I–LukGH and its conservation

The main interaction site of LukGH with CD11b-I is located in the cap domain of LukH, in agreement with previous binding and mutagenesis data [27, 28, 32] (Figure 2a). Interestingly, structural

superposition of the LukGH_K319A–moCD11b-I and LukGH–huCD11b-I structures over 706 Cα atoms resulted in $RMSD_{Cα}$ of 1.11 Å. The largest structural difference is due to a shift in the position of the CD11b-I main chain (mean displacement of 1.9 Å, rotation by approx. 7° about a hinge nearly parallel to the pore axis and a maximal Cα-shift of 5 Å when the superposition is performed on LukH alone; $RMSD_{Cα}$ of 0.41 Å over 270 Cα atoms), caused by different interactions at the edges of the binding epitope (*vide infra*) (Figure 2a, middle panel).

The core of the interface is well conserved between the mouse and human structures (Figure 2a, left panel, Supplementary Table 2). Central to these interactions is the MIDAS site, where the LukH residue E323 completes the octahedral coordination sphere around the metal ion, together with the conserved CD11b-I residues (S144, S142 and T209) and two water molecules, as seen for the active conformation of huCD11b-I (Figure 1f, Figure 2a, left panel) [13, 14]. The importance of this interaction is supported by the lack of receptor binding and cytolytic activity of the LukGH E323A variant [27, 32] and by the fact that Mg^{2+} substitution at the MIDAS site by Ca^{2+} impairs LukGH binding (Supplementary Table 3). Additional interactions involve the salt bridges between the side chains of E244 (CD11b-I) and R294 (LukH) and the side chain of R208 (CD11b) and the C-terminal carboxyl group of G324 (LukH). Polar contacts between R208 (CD11b-I) and H188 and Y321 (LukH), van der Waals contacts between F246 (CD11b-I) and LukH residues D114, H188 and Y321 and a hydrophobic interaction between P249 (CD11b-I) and W187 (LukH) are also observed (Figure 2a, left panel). Mutagenesis studies at these positions in LukH confirm their involvement in binding and/or activity [27]. While residues E244, R208 and F246 are conserved between human, rhesus macaque, pig, rabbit and mouse CD11b-I variants, residues R208 and F246 are replaced by Q and Y, respectively, in guinea pig (Supplementary Figure 1a), explaining the lack of binding of LukGH to the guinea pig receptor and activity towards guinea pig PMNs (unpublished data).

The LukH–CD11b-I complex is stabilized by a number of salt bridges and polar interactions (Supplementary Table 2), explaining why the LukGH affinity for CD11b-I decreases with increasing the ionic strength, even though protein stability is not affected (Supplementary Table 4, Supplementary Figure 1b). At the extremities of the interface (Figure 2a, right panel), the LukH–CD11b-I interactions vary in the two species. The main driver is the S277 huCD11b-I residue, which is K in the mouse variant. K277 forms a salt bridge with D316 in LukGH_K319A-moCD11b-I complex (not present for the human complex) (Figure 2a, right bottom panel). It appears that reduction of the size and removal of the positive charge (K319A) is needed to prevent steric clashes and electrostatic repulsion between K277 and K319, explaining the increased binding of the LukGH_K319A variant to moCD11b-I. Instead, S277 from huCD11b-I forms hydrogen bonds with the

Y314 and D316 side chains, which brings the main chain of huCD11b-I closer to LukH (Figure 2a, right bottom panel).

Since S277 is conserved between different species, except for mouse, we performed “humanizing mutations”, exchanging K277_P278 in moCD11b-I with S_E, to confirm the above hypothesis. The LukGH variants with mutations in the region involved in the interaction with K277 (R294A, K319A, D316A) showed a similar binding pattern for moCD11b-I_SE and huCD11b-I, i.e. decreased binding affinity to the R294A and K319A mutants, while mutations remote from this interaction site (R119A, R121A, D312A) were not affected by the CD11b-I variant (Figure 2b). The decreased binding affinity of K319A LukGH to huCD11b-I is probably due to loss of a salt bridge between K319 and E244 (CD11b-I). Additionally, we “humanized” the neighboring Q279 in moCD11b-I (moCD11b-I_Q279K), which makes a N-H···π interaction with the aromatic side chain of LukH_Y314 in the mouse but not in the human complex (the corresponding K279 residue is oriented away from the interface). After confirming that the protein stability of the mutants is unchanged (Supplementary Figure 1c), we measured binding of the LukGH variants to moCD11b-I_SE and _Q279K. The moCD11b-I_Q279K variant had significantly increased affinity towards LukGH_K319A (Figure 2b). Additional interactions are present in the moCD11b-I complex only, including the salt bridge at the top of the interface (D251 (moCD11b-I) – R119 (LukH)) (Figure 2a, right top panel) and a hydrogen bond at the bottom (N146 (moCD11b-I) – K322 (LukH)) (Figure 2a, right bottom panel).

While the LukH residues forming the salt bridges in human and mouse complexes are mostly conserved, with the exception of LukH_R119 and LukH_K319, only two positions from CD11b-I involved in salt bridge formation are conserved between human, rabbit, mouse, pig, rhesus macaque and guinea pig (Supplementary Table 2, Supplementary Figure 1a). The conservation of the CD11b-I residues involved in the binding epitope in mouse and human CD11b-I complex structure between different species reveals the highest similarity between human and rhesus macaque (89% identity) and the highest divergence between human and guinea pig (63% identity), which correlates with the binding and activity towards those species PMNs [26; unpublished data].

Second binding interface between LukG and CD11b-I

Unexpectedly, besides the LukH-CD11b-I epitope, we observed a second binding region between CD11b-I and LukG from an adjacent dimer of the LukGH octamer (Figure 1d, Figure 2c, Supplementary Table 5). This interface shares some conservation between the mouse and human complexes, e.g. the hydrogen bond between R66 (LukG) guanidinium group and L205 (CD11b-I) main chain carbonyl group. However, most of the residues contacting the two loops in LukG in this interface differ between the species, e.g. N33 (LukG) side chain makes a hydrogen bond with a

carboxyl group of D178 in moCD11b-I and E178 in huCD11b-I. Particularly interesting is the interaction of moCD11b-I with the loop 68–72 in LukG: due to steric hindrance by K203 in moCD11b-I, the loop is flipped by up to ~180˚ compared to the un-complexed structures (PDB 5K59 and 4TW1) and to the complex with the human receptor (Supplementary Figure 2), which in turn flips the sidechain of D69, allowing formation of a salt bridge with R181 in moCD11b-I (Figure 2c, right panel). The flip is presumably kinetically unfavorable, as D69 loses hydrogen bonds with three residues from the adjacent β-sheet. The difference electron density map suggests flexibility of this loop and the presence of some other minor alternate conformation(s), which we have not been able to model satisfactorily (Supplementary Figure 2). Such disorder is not observed in the complex with huCD11b-I, which has T at position 203 and does not appear to interact with the 69–71 loop.

All LukG residues involved in the second binding interface are variable in the currently available LukG sequences (75– 80% conservation level), in contrast to the main interface where more than half of the residues are fully conserved (the remaining show 76–99% conservation) (Supplementary Tables 2 and 5).

CD11b-I promotes LukGH oligomerisation in the absence of a cell surface

The ability of CD11b-I to bind at the oligomerisation interface indicates that the receptor alone (in absence of a cell surface) may promote oligomerisation. To further investigate this, we developed a non-invasive oligomerisation assay using dynamic light scattering (DLS), by mixing LukGH with CD11b-I in 1:1 molar ratio and monitoring the molecular size of the mixture, expressed as radius, over time. The hydrodynamic radia of LukGH and CD11b-I alone are ~5 nm and ~2 nm, and do not change for up to 36-48 h (Supplementary Figure 3a). When the two components were mixed, we observed a time-dependent increase in radius from ~5.5 nm to ~11–12 nm over several hours, after which a plateau was reached (Figure 3a). We assign the lower radius (~5.5 nm) to the LukGH–CD11b-I complex, based on data with an oligomerisation deficient variant, the LukG1H dimer, which binds huCD11b-I, but is lacking cytolytic activity [28], and shows no change in size when mixed with CD11b-I (Figure 3a). The higher (~11 nm) radius corresponds to the final oligomerisation product, a relatively stable structure that does not aggregate in the time frame of the experiment (up to 96 h), which is, most probably, an assembly similar to the octameric pore found in the crystal lattice. We observed oligomerisation of LukGH in presence of human and rabbit CD11b-I, but not mouse CD11b-I, which parallels the activity data (Figure 3a). Moreover, the LukGH K319A variant, which shows high binding to moCD11b-I is still unable to oligomerise in the presence of moCD11b-I, explaining its lack of cytolytic activity.

When the oligomerisation rate was approximated to a first-order rate constant, we observe that huCD11b-I induced oligomerisation of LukGH is ~3× faster than that induced by rbCD11b-I at physiological NaCl concentrations (150 mM) (Figure 3b, Supplementary Figure 3b). There is however a marked dependence of oligomerisation rate on NaCl concentration, i.e. it increases with increasing NaCl concentration from 0 to 150 mM, with some variations at higher salt concentrations for different receptors (Figure 3b, Supplementary Figure 3b). Although the rate limiting step in this oligomerisation process is not known, the requirement for NaCl indicates that this must happen in the extracellular space and not on the cell membrane.

In order to investigate the stoichiometry requirements for CD11b-I mediated oligomerisation of LukGH, we measured the oligomerisation efficiency and rate at different CD11b-I to LukGH ratios. The oligomerisation appears complete at ratios as low as 1:4 (1 CD11b-I molecule per LukGH octamer), with the oligomerisation rate increasing almost linearly with increasing the ratio to 1:1 (4 CD11b-I molecules per LukGH octamer), indicative of a catalytic role of CD11b-I in this process (Figure 3c).

We wanted to confirm the involvement of the individual residues of LukGH in oligomerisation and activity, and subsequently engineer LukGH that can oligomerise upon binding to moCD11b-I. We therefore generated a series of variants (Ala, natural variants and amino acid deletions, mainly in the LukH_K319A background) and measured their activity (reported as EC_{50} values or cell viability at a fixed cytotoxin concentration) towards differentiated granulocyte-like HL-60 cells and mouse neutrophils and also oligomerisation in presence of the recombinant receptors. All mutants were characterized by CD spectra and melting temperatures (T_m) to exclude false positive results due to protein instability (Supplementary Figure 3c, Supplementary Figure 4a–e). The mutants tested had T_m values similar to the wild-type, except for the L68 and D69 variants (lower T_m of D69 variants probably due to loss of stabilizing interactions with the adjacent β-sheet (Figure 2c)). Using these variants, we could clearly confirm the involvement of LukG residues N33, R66, D69, P70 and N71 in both oligomerisation and activity with the human system (Figure 3d, 3e), and for R66 and D69 also with rabbit cells (Supplementary Figure 5a), in agreement with structural data. The most striking loss of activity was seen when LukG_N33 was mutated to the negatively charged E, presumably due to repulsion at the second interface (LukG_N33 interacts with E178 in huCD11b-I) (Figure 2c right panel, Figure 3d). Importantly, all the tested variants showed no change in binding to huCD11b-I, confirming that loss of activity was not due to decreased binding affinity (Supplementary Figure 5b). Oligomerisation of the LukGH_N33E and S30N mutations could not be measured, as they showed increased aggregation when tested alone or in presence of human or mouse CD11b-I.

Importantly, none of the oligomerisation site mutants, co-expressed with LukH_K319A showed any activity towards mouse PMNs up to cytotoxin concentrations of 800–1000 nM, no improved affinity towards moCD11b-I and no increase in radius in presence of moCD11b-I, when tested by DLS (Figure 3f, Supplementary Figure 5c, Supplementary Figure 5d). Interestingly, however, the LukGH_D69A, D69N, D69E, L68Q and N71D variants, which tend to aggregate when incubated alone for up to 36 h at room temperature (Figure 3f), were stabilized in complex with both human and mouse CD11b-I (Figure 3e, 3f), as octamers or heterodimers, respectively.

Fab binding to the LukG subunit of LukGH–huCD11b-I prevents its cell membrane independent oligomerisation

In order to gain insight into the structural organization of the LukGH–receptor complex in solution, we used solution small-angle X-rays scattering (SAXS) for LukGH and the LukGH–huCD11b-I complex in presence of the Fab fragment of a LukGH neutralizing antibody (Supplementary Table 6, Figure 4a, b). The Fab was used to stabilize the dimer and to allow the elution of the complex from the size-exclusion chromatography column to ensure the sample's monodispersity. First, the complex of the Fab fragment with LukGH was analyzed in absence of the receptor, and compared to the crystal structure of the complex we have previously determined [29]. The computed distance distribution $p(r)$ (Figure 4b) indicates that the molecule is a multi-domain (distinctive bumps) and an elongated particle (skewed $p(r)$ shifted to shorter distances). Furthermore, the overall structural parameters derived from SAXS (molecular mass, *MM*, radius of gyration, R_G, and maximum dimension, D_{max}) (Supplementary Table 6) are fully compatible with a monomeric construct and strongly support that the binding of the Fab fragment prevents the oligomerisation of LukGH. Moreover, the experimental data are in good agreement with the theoretical curve calculated from a structural model derived from the available crystal structure (PDB code 5K59) with a discrepancy $\chi^2 = 1.8$ (Figure 4a).

Next, we analyzed the LukGH–Fab complex bound to huCD11b-I. Noticeable increases observed for the overall parameters (R_G, from about 4.8 to about 5.1 nm, D_{max}, from 16 to 18 nm) and an increase by about 20 kDa in the *MM* are in line with the stable 1:1 complex formation (Supplementary Table 6, Figure 4a,b) corresponding to LukGH–Fab complex bound to one huCD11b-I. No concentration dependent alterations in the SAXS data are observed indicating that the receptor is tightly bound to LukGH also in the presence of the Fab fragment. Moreover, the experimental data are in very good agreement ($\chi^2 = 1.4$, Figure 4a) with the scattering curve computed from a model combining the LukG:Fab interface (PDB 5K59) and the LukH:huCD11b-I interface (crystal structure described here, Figure 4b). To further improve the fit, the program CORAL was used. Here, the missing amino acids (44 N-terminal residues of LukH and 22 C-terminal residues of CD11b-I) were modelled as dummy

residues. With this approach, an χ^2 value of 1.0 was achieved (Supplementary Figure 6). Comparison of twenty individual runs suggests that the N-terminal of LukH is rigid and elongated.

Binding of the αLukGH-mAb#5.H1H2 Fab to the rim region of the LukG protomer (Figure 5a) [29] in the LukGH dimer did not prevent binding of CD11b-I to LukGH (*via* the LukH protomer) in solution, but prevented oligomerisation, as predicted from the crystal structure (αLukGH-mAb#5.H1H2 binds to the oligomerisation interface) [29] and confirmed by DLS measurements in presence of the Fab (Figure 5b). However, on the cell surface, when LukGH is bound to the receptor, the αLukGH-mAb#5.H1H2 epitope is no longer accessible (Figure 5a) and no αLukGH-mAb#5.H1H2 binding to cell bound LukGH was detected [29].

We have also determined the effect of anti-CD11b-I antibodies with known epitopes (Supplementary Figure 1a), on the activity of LukGH on lipopolysaccharide (LPS) activated human PMNs. In the presence of the LM2/1 antibody, whose epitope is in the proximity of the LukGH binding epitope (Supplementary Figure 1a), we observed an inhibition of LukGH activity (Figure 5c), in agreement with a previous report [7]. On the contrary, the CBRM1/5 antibody, which recognizes a conformational epitope present only on the active CD11b-I form [33], enhances LukGH activity (Figure 5d), presumably due to an allosteric activation. This is particularly interesting since an opposite effect (i.e. inhibition of binding) was observed with other CD11b ligands, ICAM-1 and fibrinogen, in the presence of CBRM1/5 [33].

DISCUSSION

LukGH is a unique member of the bi-component cytotoxin family, as it dimerizes in solution, before receptor and target cell binding [28, 32]. This feature has been proposed to be responsible for the very high cytotoxic activity of LukGH, which also correlates well with receptor up-regulation and activation on target cells [25, 28]. At 'high' receptor densities, on activated PMNs, the activity of LukGH is up to 3 orders of magnitude higher than on resting PMNs [25]. Here, we provide the molecular basis for this correlation. A single receptor molecule is able to bind two adjacent dimers in the octamer, and implicitly a single LukGH dimer can bind two receptor molecules, *via* separate LukH and LukG interfaces. In addition, LukGH binds to the active form of the I-domain of CD11b, as all the other bona fide CD11b ligands.

Using a combination of X-ray crystallography and SAXS, we were able to capture two intermediates in the receptor-mediated LukGH pore formation pathway. The LukGH dimer–CD11b-I complex, stabilized by an oligomerisation inhibitory Fab fragment, was analysed by SAXS. This ternary complex involves interactions between CD11b-I and the cap domain of the LukH subunit, close to the LukGH

oligomerisation site, also indicated by previous data generated with site-directed mutagenesis [27]. Since there are no major structural changes in the LukGH dimer compared to the un-ligated form, this is presumably one of the first intermediates in the pathway. The second intermediate is the fully formed LukGH octamer complexed with four CD11b-I molecules, which in addition to the LukH interface (the binding interface), involves interactions with two LukG loops from a neighboring LukGH dimer (across the oligomerisation interface). This is likely one of the final intermediates before insertion of the pore into the target cell membrane, although it is possible that not all four sites need to be occupied for pore formation to occur (see below). Interestingly, while the LukGH dimer–CD11b-I binding interface has six salt bridges, none is present in the oligomerisation interface, at least with the human receptor. Accordingly, the ionic strength requirements for the two processes also appear to follow different trends, i.e. increase in ionic strength favors oligomerisation but impairs binding. This corroborates the electrostatic nature of the LukGH dimer–CD11b-I interaction, and hydrophobic nature of the oligomerisation interface, and may indicate different preferences for diverse microenvironments.

Based on all the structural, mutagenesis, antibody inhibition and cytotoxicity enhancement data presented here we propose a mechanism of pore formation by LukGH on activated PMNs (Figure 6). LukGH binds to its integrin receptor, CD11b/CD18, in an extended conformation, induced as a result of inside-out signaling following activation [12]. This agrees with the potentiation of LukGH activity on LPS-stimulated PMNs by CBRM1/5, an anti-CD11b-I antibody that targets an epitope shielded in the bent integrin (Figure 5a, d). According to this model, initially LukGH binds an active CD11b-I domain on the cell surface, via its LukH subunit, presumably with concomitant recruitment of an adjacent CD11b-I domain (which may already have an occupied LukH site) via the LukG subunit (Figure 6). Homodimerization of integrin alpha domains, triggered by interactions between the homologous transmembrane domains, has been reported for the activated form of integrin αIIbβ3 [34]. Recruitment of two additional LukGH dimers to form the octamer may not necessarily involve other I-domains (Figure 6), since octameric pore formation is thought to be a highly cooperative process (as shown for *S. aureus* γ-hemolysin) [35]. Moreover, DLS oligomerisation data in solution suggests that there is no effect of additional receptor domains on oligomerisation efficacy and only a small increase in oligomerisation rate from 2 to 4 CD11b-I equivalents per LukGH octamer is observed. β-barrel pore formation is a two-step process, and the final step of insertion into the membrane is thought to occur after complete oligomerisation of the cap domain [4]. In the extended form of the integrin, the I-domain is ~20 nm from the cell surface, so the integrin would have to bend to allow for the insertion of the pore (Figure 6). Alternatively, the receptor may dissociate before pore insertion, via an unidentified mechanism, similar to the proposed receptor

dissociation after pore formation/oligomerisation in case of another bi-component leukocidins [5]. Ligand binding to the active I domain of CD11b of the bent CD11b/CD18 integrin is also not unprecedented: ICAM-1 binding was shown to have anti-inflammatory effects [36]. Another aspect is the orientation of the LukGH pore relative to the cell surface when LukGH binds the receptor, as the alignment of CD11b-I on the available ectodomain crystal structures (PDB 3K71, 5ES4, 4NEH, 3K6S) does not result in a LukGH pore oriented perpendicular to the cell membrane (Supplementary Figure 7). In principle, the region linking the I-domain with the rest of the alpha chain in integrins is flexible [37, 38] and may allow the rotation of the LukGH pore towards the membrane. An intriguing possibility is that LukGH pores are able to kill adjacent cells, or that such a mechanism is used for LukGH-dependent bacterial escape from intracellular compartments [39].

The LukGH pore formation on resting cells is more enigmatic. The receptor density itself is only ~2-fold decreased compared to LPS-activated cells [25], so it is presumably the presence of the closed conformation of the integrin I domain and the lack of clustering that limit activity. This scenario is likely less physiologically relevant at late infection time points, as the *S. aureus* extracellular components activate PMNs [25], but may become relevant at the onset of the infection. Interestingly, the killing curves are particularly flat on insensitive PMNs (i.e. little dependency of killing on LukGH concentration) [25], implying that LukGH concentration is not rate limiting in this process. In absence of any other stimuli, LukGH itself was shown to be able to prime PMNs [40]. It is thus possible that at early stages of the infection, (and LukGH is one of the earliest expressed leukocidins [7]), LukGH promotes an outside-in signalling with conversion of the integrin I domain to an open form, with binding occurring directly to the bent conformer followed by pore insertion.

Although LukGH oligomerisation in solution is a good predictor of cytolytic activity, i.e. no activity against mouse cells and no oligomerisation with the mouse receptor, the smaller surface area of the oligomeric interface in the human compared with the mouse complex, as found in the crystal structures, appears counter-intuitive. It is therefore tempting to speculate that flexibility on the outskirts of the interface is needed to promote oligomerisation (kinetically). This aspect must be considered when attempting to improve oligomerisation of LukGH towards a certain species based on the current structures. On the other hand, improving binding appears a much easier endeavor. Interestingly, the sequence conservation map of the interface (both on LukGH and CD11b-I side) also predicts higher conservation for residues forming the core of the interface, and higher diversity towards the edges (Supplementary Figure 8). In addition, the contact residues are not conserved between other CD11b integrins (CD11a, CD11c and CD11d), which explains the specificity of LukGH towards CD11b.

Being able to specifically engage activated CD11b on the PMN surface is not the only advantage of the bivalent toxin-receptor interaction. CD11b/CD18 is known to bind a variety of endogenous ligands (Supplementary Table 7), with affinities in the high nM range, some with epitopes overlapping with LukGH binding, e.g. C3d [19], iC3b [9] or human fibrinogen [10] (Supplementary Figure 1a). The concentration of these ligands varies with tissue type, but is particularly high in the blood (e.g. 1.5 – 4.0 mg/ml for fibrinogen). It is not yet clear whether LukGH is active in *S. aureus* bacterial sepsis, but the avid binding of LukGH to the CD11b receptors certainly provides a competitive advantage over the monovalent endogenous ligands. Following the same principle, the anthrax toxin protective antigen (PA) binds to its von Willebrand type I domain receptor, to the MIDAS site via the PA_IV domain, but forms additional interactions using a neighboring domain (PA_II), leading to an ~1000-fold higher affinity compared to a typical integrin–ligand complex [41]. Moreover, it was shown that the protonation of a histidine residue on the receptor, at the edge of this additional binding pocket, controls the pH-dependent dissociation from PA_II and subsequent pore formation, reminiscent of the CD11b-I interaction with LukG, where reduced interactions appear to favour oligomerisation [41].

CD11b/CD18 and the other β2 integrins (CD11a, CD11c and CD11d) play important roles in immune defense mechanisms, at the same time regulating immune responses [42]. Whereas reduction or lack of β2 integrins leads to higher susceptibility to infection and impaired inflammatory responses, increased expression or activation of integrins has been linked to autoimmune diseases such as systemic lupus erythematosus, rheumatoid arthritis, multiple sclerosis as well as inflammation aggravated conditions such as stroke [42]. The extremely high specificity and avidity of LukGH towards activated CD11b, and the availability of structural information for the interaction, make LukGH a suitable candidate for engineering potential therapeutic candidates, with or without functional pores, targeting integrins in inflammatory diseases. The caveats of using a non-human therapeutic protein, particularly for chronic indications, typically arise from the short half-life and formation of anti-drug antibodies. These could be, however, potentially circumvented for LukGH by exploiting its own ability to blunt the adaptive immunity via dendritic cell targeting [43] and by making use of its numerous and diverse natural sequence variants [44].

ONLINE METHODS

Production of recombinant LukGH variants

LukGH variants were produced recombinantly in *E. coli*, as described previously [28], based on the wild-type sequence of the community-associated methicillin resistant *S. aureus* (CA-MRSA) USA300 (ST8) TCH1516 strain. The *lukG* gene was cloned into pET44a vector and was expressed as a fusion

protein with NusA/His_6 at the N-terminus to allow metal ion affinity purification of the complex, whereas LukH was expressed in un-tagged form. LukH and LukG mutants were generated with QuikChange II XL Site-Directed Mutagenesis Kit (Agilent, according to the manufacturer instructions) using the *lukH*_pET200D/TOPO and *lukG*_pET44a as a template, respectively. The wild-type or variants *lukH* and *lukG* were co-transformed into *E. coli* TUNER DE3 cells (Novagen) and protein expression was induced with isopropyl β-D-1-thiogalactopyranoside (IPTG) as described previously [28].

Recombinant LukGH proteins were purified as described previously [28] or using batch methods designed for high-throughput purification from 0.125 L cultures as described in Trstenjak et al, 2019 [27]. Briefly, bacterial pellets were disrupted using 0.1 % *n*-dodecyl-β-D-maltoside and two freeze-thaw cycles in liquid nitrogen. The LukGH dimers were first purified from cell extracts by metal ion affinity chromatography using Ni Sepharose 6 Fast Flow beads (GE Healthcare) equilibrated in 20 mM Tris, pH 7.5 plus 50 mM imidazole. Beads were loaded on Microplate Devices UNIFILTER, 96 wells plate (Whatman) and elution with 20 mM Tris, pH 7.5 plus 500 mM imidazole was performed by centrifugation. After dialyzing into 20 mM Tris, pH 7.5 and removal of the NusA/His_6 tag on LukG with enterokinase (NEB), the untagged LukGH complex was purified using SP Sepharose Fast Flow beads (GE Healthcare) equilibrated in 20 mM sodium phosphate, pH 7.5 plus 50 mM NaCl. Beads were treated as described for the affinity purification, and the proteins were eluted with 20 mM sodium phosphate, pH 7.5 plus NaCl (150–300 mM). Protein concentration was calculated based on the UV absorbance at 280 nm using the extinction coefficient (ε_{280}= 112 000 $M^{-1}\,cm^{-1}$) calculated with ProtParam tool (ExPASy Server) [45] based on the LukGH protein sequence. Protein purity was determined by SDS-PAGE gels, stability by differential scanning fluorimetry and the secondary structure by circular dichroism.

Production of moCD11b-I variants and expression and purification of recombinant huCD11b-I, rbCD11b-I and moCD11b-I

The I-domains (amino acids 127-321) of huCD11b, rbCD11b and moCD11b (huCD11b-I, rbCD11b-I and moCD11b-I) were cloned into pET24a (Novagen) vector at NdeI/XhoI (NdeI/BamHI for rbCD11b-I) sites. MoCD11b-I variants were generated with QuikChange II XL Site-Directed Mutagenesis Kit (Agilent, according to the manufacturer instructions) using the *moCD11b-I*_pET24a as a template. All plasmids were transformed into *E. coli* TUNER DE3 cells and protein expression was induced at 20 °C for 20 hours with 0.4 mM IPTG. HuCD11b-I and rbCD11b-I were purified as described previously [27, 28]. MoCD11b-I wild-type and variants were purified by cation exchange (HiTrap SP FF, GE Healthcare) followed by size exclusion (HiLoad Superdex 75 pg, GE Healthcare) chromatography. The CD11b-I proteins were treated overnight with iodoacetamide (20 mM, Applichem) to alkylate the

free cysteine and prevent dimer formation. Iodoacetamide was removed on PD-10 columns (GE Healthcare) equilibrated with 50 mM sodium phosphate, pH 7.5 plus 300 mM NaCl. Due to the lack of tryptophan in the amino acid sequence of hu, mo and rbCD11b-I, protein concentration was determined based on the UV absorbance at 205 nm using the extinction coefficients ($\varepsilon_{205(huCD11b\text{-}I)}$= 797 420 $M^{-1}\,cm^{-1}$, $\varepsilon_{205(rbCD11b\text{-}I)}$= 790 170 $M^{-1}\,cm^{-1}$, $\varepsilon_{205(moCD11b\text{-}I)}$= 794 570 $M^{-1}\,cm^{-1}$) calculated with "A205 protein/peptide concentration webserver" [46]. Protein purity and monomer content were assessed by non-reducing SDS-PAGE gel, stability by differential scanning fluorimetry and the secondary structure by circular dichroism.

Biotinylated huCD11b-I and moCD11b-I were generated with using the sulfhydryl-reactive reagent EZ-Link BMCC-Biotin (Thermo Scientific), according to the manufacturer's instructions. For rbCD11b-I, and in some cases for huCD11b-I and moCD11b-I (e.g. when comparing with rbCD11b-I or where indicated), the amino reactive reagent Sulfo-NHS-LC biotin (Thermo Scientific) was used, yielding final biotin/protein ratios of 0.15–0.3.

Circular dichroism (CD) and differential scanning fluorimetry (DSF) analysis

Far UV (195-250 nm) CD spectra of samples were recorded on a Chirascan (Applied Photophysics) spectrometer in a 0.5 mm cuvette (Applied Photophysics) at 20°C. The LukGH and CD11b-I samples were measured at concentration of 0.2–1.0 mg/mL or 0.25–0.66 mg/mL, respectively, in 20 mM sodium phosphate, pH 7.5 plus 150–300 mM NaCl or 50 mM sodium phosphate, pH 7.5 plus 300 mM NaCl, respectively. The melting points (T_m) of the proteins were determined by differential scanning fluorimetry. The proteins were mixed with Sypro Orange dye and with corresponding buffer (either with HEPES, pH 7.5 (50 mM final concentration) or HEPES, pH 7.5 plus $MgCl_2$ (25 mM and 1 mM final concentration, respectively) and NaCl (150–1000 mM). The assay was conducted in a qPCR instrument (Bio-Rad CFX96) and the T_m values determined using the Bio-Rad CFX Manager software.

Bio-layer interferometry (BLI)

Binding of LukGH (wild-type and mutants) to huCD11b-I, rbCD11b-I or moCD11b-I (wild-type and mutants) was evaluated by Bio-Layer Interferometry (fortèBio Octet Red96 instrument, Pall Life Sciences) as described previously [27]. Shortly, biotinylated CD11b-I (2–4 µg/mL) was immobilized on streptavidin sensors (fortèBio, Pall Life Sciences). The association of LukGH [50 nM or 100 nM in assay buffer (PBS plus 1% BSA and 1mM $MgCl_2$ or $CaCl_2$, or 25 mM HEPES, pH 7.5 plus 1% BSA plus 1mM $MgCl_2$ and NaCl (150–1000 mM))] to the immobilized receptor and dissociation in assay buffer were monitored for 5 minutes each. Response units (RU) and where possible (for monophasic binding curve) equilibrium dissociation constants (K_d), were determined using the Data Analysis 7 software (fortéBio, Pall Life Sciences) by simultaneously fitting the association and dissociation

curves to a 1:1 binding model. The steady-state K_d values were determined for LukGH wild-type binding to moCD11b-I and rbCD11b-I by measuring binding at multiple LukGH concentrations (100–2200 nM and 20–400 nM, respectively) and fitting the data to a steady-state equilibrium model (Forte-Bio Analysis Software, Version 7).

Purification of LukGH–huCD11b-I–Fab and LukGH–Fab complexes and small angle X-ray scattering (SAXS) analysis

LukGH and huCD11b-I, purified as described above, and the Fab of αLukGH-mAb#5.H1H2 [29] expressed in Chinese Hamster Ovary cells and purified by LC-kappa affinity chromatography (CaptureSelect, Thermo Scientific), were mixed in 1:1:1.5 molar ratio, respectively. For the LukGH–Fab complex, LukGH and Fab were mixed in 1:1.5 molar ratio. The complexes were concentrated to approximately 10 mg/ml, and the samples were purified on size exclusion chromatography (HiLoad Superdex 200 pg, GE Healthcare) equilibrated in 20 mM HEPES, pH 7.5, 300 mM NaCl, 1 mM $MgCl_2$. The LukGH–Fab–-huCD11b-I and LukGH–Fab complexes were concentrated to 4.2 mg/mL and 4.6 mg/ml, respectively. Purity was assessed on non-reducing SDS-PAGE gel and polydispersity by dynamic light scattering (DLS). Synchrotron radiation X-ray scattering data was collected at the EMBL P12 beamline of the storage ring PETRA III (DESY, Hamburg, Germany) [47] for both complexes (LukGH–Fab and LukGH–Fab–huCD11b-I). Images were recorded using a photon counting Pilatus-2M detector at a sample to detector distance of 3.1 m and a wavelength (λ) of 0.12 nm covering the range of momentum transfer $0.08 < s < 3.5$ nm^{-1} ($s = 4\pi \sin\vartheta/\lambda$, where 2ϑ is the scattering angle). A continuous flow cell capillary was used to reduce radiation damage. The latter was monitored by collecting 20 successive 50 ms exposures, comparing the frames, and discarding those displaying significant alterations. Data was collected from a dilution series to examine concentration dependent alterations. Data reduction to produce the final scattering profiles of the complexes were performed using standard methods. Briefly, for 2D-to-1D radial averaging the SASFLOW pipeline was used [48]. Scattering profiles from the buffer without protein were used for background subtraction. The indirect inverse Fourier transform of the SAXS data and the corresponding probable real space-scattering pair distance distribution ($P(r)$ versus r profile) were calculated using GNOM [49], from which the R_g and D_{max} were determined. The $P(r)$ versus r profile was also used for volume and subsequent molecular weight estimates of the complexes as described in Hajizadeh et al (2018) [50]. CRYSOL [51] was used to calculate the scattering profiles from the atomic coordinates of available crystal structures: the Fab fragment bound to LukGH as deposited in PDB 5K59 and for the LukGH–Fab–huCD11b-I complex the interface as described in this work, was projected onto the former complex.

To account for missing residues not resolved in the crystal structure the program CORAL [52] was used. Here, additional beads representing the individual residues are added to the available crystal structures to optimize the fit to the experimental SAXS data. 44 beads were added to the N-terminus of LukH and 22 residues to the C-terminus of huCD11b-I. 20 independent calculations were performed and the models obtained were compared to each other.

To exclude any dissociation process, the program OLIGOMER [53] was used to check if the fits could be improved by additionally allowing some volume fractions of the individual subunits. This was not the case.

The SAXS data (as summarized in Supplementary Table 6) and models are deposited in SASBDB (www.sasbdb.org) with the following accession codes: SASDF45 and SASDF55 for the LukGH–Fab–huCD11b-I and the LukGH–Fab complexes, respectively.

Dynamic light scattering (DLS) and oligomerisation assay

The increase in cumulant radius of LukGH after addition of CD11b-I from different species was followed by dynamic light scattering (DLS) using a Wyatt DynaPro DLS Plate Reader II instrument at 25 °C. LukGH, CD11b-I and Fab αLukGH-mAb#5.H1H2 were dialyzed separately against 25 mM HEPES, pH 7.5 plus 1 mM $MgCl_2$ and concentrated to final concentrations of 1–5 mg/ml for LukGH, 0.5–2.5 mg/ml for CD11b-I and 1 mg/ml for Fab αLukGH-mAb#5.H1H2. After addition of NaCl (0–300 mM) to the samples, LukGH and CD11b-I were mixed either in fixed (1:1 for huCD11b-I, 1:1.2 for moCD11b-I and 1:1.4 for rbCD11b-I) or in variable (1:0.1 – 1:1 for huCD11b-I) ratios. For the experiments with the aLukGH-mAb#5.H1H2 Fab, the ratios were 1:1.5, 1.5:1 and 1:1:1.5 for LukGH:Fab, Fab:huCD11b-I and LukGH:huCD11b-I:Fab, respectively. The samples were spin filtered (Ultrafree MC, 0.1 µM, Merck) before the measurements. Duplicates of each sample were transferred into a 1536 Microplate with glass bottom (Greiner) and covered with silicone oil. Scattering data were collected at pre-set time points. The calculated autocorrelation function was analyzed by cumulant fit, assuming one population of particles with a single average diffusion coefficient and a single standard deviation about that average, using DYNAMICS 7.7.0.125 software (Wyatt Technology). The data with low intensity, or poor fits with the baseline >1.01 and the sum-of-squares error (*SOS*) > 10 were excluded from further analysis. The cumulant radii of the samples were plotted against incubation time and fitted to a 'one-phase association' function in Prism 6 (Graph Pad) with a fixed starting radius (y_0 = 5 nm).

Cytotoxicity assay

Cell-based assays were performed using either differentiated HL-60 cells or human, rabbit or mouse polymorphonuclear cells (PMNs). The HL-60 cells (ATCC® CCL-240™) were differentiated into granulocyte-like cells using dimethylformamide (DMF) as described previously [27]. Human PMNs were isolated from heparinized human whole blood, obtained from healthy volunteers, using Percoll® (Percoll Plus, GE Healthcare) gradient centrifugation as described previously [28]. Rabbit PMNs were isolated from rabbit whole blood (New Zealand White rabbits) anti-coagulated with citrate dextrose solution, using Histopaque 1077 (Sigma-Aldrich) and HetaSep (Stemcell Technologies) as described previously [54]. Mouse PMNs were purified from mouse whole blood with acid-citrate-dextrose anti-coagulant (ACD), obtained from BALB/C mice, using EasySep™ Mouse Neutrophil Enrichment Kit (Stemcell Technologies), according to manufacturer's instruction. Cytolytic activity of LukGH (wild-type and variants) was assessed as described previously [24, 25]. Shortly, human, rabbit (both at $2.5x10^4$ cells/well) or mouse PMNs ($1x10^4$ – $2.5x10^4$ cells/well) were exposed to serial dilutions (0.002 to 100 nM for human and 0.005 to 300 nM for rabbit cells) or fixed concentration (800 nM, 1000 nM, 20 µM, 30 µM for mouse PMNs) of LukGH or LukED (0.002 to 100 nM) in assay medium (RPMI plus 10% FBS and L-Glutamine) at 37 °C, 5% CO_2 for 4 h. Cell viability was determined with a Cell Titer-Glo® Luminescent Cell Viability Assay Kit (Promega) according to manufacturer's instructions. Percent viability was calculated relative to mock-treated cells (100% viability). Data were analyzed by non-linear regression using Prism 6 (Graph Pad) and toxin activity is given as EC_{50} value (half maximal effective concentration).

To determine LukGH competition with the LM2/1 (a-huCD11b (Mac-1a), eBioscience) and CBRM1/5 (Anti-HumanCD11b, Clone: CBRM1/5, eBioscience) antibodies, LPS treated human PMNs (as described in [27]), at a concentration of $2.5x10^4$ cells/well in the assay medium, were pre-incubated with corresponding antibody (10 µg/ml) or assay buffer for 30 minutes. After pre-incubation, LukGH (at final concentrations of 0.031, 0.125, 0.5 or 2 nM) was added to the well and mixture was incubated at 37 °C, 5% CO_2 for 4 hours. Cell viability was determined with Cell Titer-Glo® Luminescent Cell Viability Assay Kit (Promega) as described above.

Protein crystallization

LukGH_K319A with moCD11b-I or LukGH wild-type with huCD11b-I (all proteins were purified as described above) were mixed in 1:1.2 and 1:1 molar ratio, respectively, after dialyzing the individual proteins in 25 mM HEPES, pH 7.5. The mixtures were concentrated, and the complexes purified on a cation exchange column (SP FF, GE Healthcare) equilibrated in 20 mM sodium phosphate, pH 7.5, 50 mM NaCl plus 1 mM $MgCl_2$ using a 0–0.95 M linear gradient of NaCl in the same buffer. The complexes eluted at ~300 mM NaCl and fractions containing both proteins, based on the SDS-PAGE

gel, were combined and buffer exchanged (PD-10 column, GE Healthcare) into 25 mM HEPES, pH 7.5 plus 1 mM $MgCl_2$ (and 50 mM NaCl for the mouse complex). The complexes were concentrated to a final concentration of 5 mg/ml and 5.2 mg/ml for LukGH_K319A–moCD11b-I and LukGH–huCD11b-I, respectively, and characterized by DLS and reducing SDS-PAGE gel. Diffraction quality crystals were obtained using hanging drop vapor diffusion at 20 °C, in a drop containing 1 µL complex in 1 µL reservoir solution (25–30% (v/v) Jeffamine-600, 5–10% (v/v) DMSO) or 1 µL complex in 0.5 µL reservoir solution (30% (v/v) Jeffamine-600, 10% (v/v) DMSO), for LukGH_K319A–moCD11b-I and LukGH–huCD11b-I, respectively. The crystals were harvested from the crystallization drop using a nylon loop and frozen directly in liquid nitrogen without addition of a cryoprotectant.

Diffraction data collection, structure determination, refinement and interpretation

Diffraction data were collected at 100 K at the European Synchrotron Radiation Facility at beamline ID30A-1 (MASSIF-1; wavelength 0.966 Å) for the LukGH_K319A–moCD11b-I complex and beamline ID29 (wavelength 1.072 Å) for the LukGH–huCD11b-I complex. Both datasets were processed using the XDS program package [55]. Due to significant anisotropic diffraction, the LukGH–huCD11b-I dataset was corrected and merged using the STARANISO Server [56] incorporating programs autoPROC [57], POINTLESS [58] and AIMLESS [59].

The LukGH_K319A–moCD11b-I structure was solved by molecular replacement in *Phaser* [60] using LukG and LukH structures from their complex with a Fab fragment (PDB code 5K59, chains A and C; [29]) as independent search models. After initial model building of LukGH in *Coot* [61] and 10 cycles of restrained refinement in REFMAC5 [62, 63], additional electron density corresponding to moCD11b-I domain could be identified clearly and the missing component built in *Coot* and *Buccaneer* [64, 65]. The structure of LukGH–huCD11b-I was solved by molecular replacement in *Phaser* [60] by searching sequentially with the LukGH dimer from the refined LukGH_K319A–moCD11b-I structure and then with the modified huCD11b-I domain (PDB code 1IDO) [13] lacking the C-terminal α7-helix (residues 303–315). Both structures of the complexes were finalized by model building and refinement in *Coot* and *Phenix* [66]. Due to the anisotropic low-resolution diffraction data, the LukGH–huCD11b-I structure was refined by applying additional dihedral-angle restraints derived from the refined LukGH_K319A–moCD11b-I structure as a reference model. The data collection, refinement and validation statistics are shown in Supplementary Table 1. The molecular interfaces and oligomeric states were analyzed in PISA [67] and the structures were superposed in program LSQKAB [68] as a part of the CCP4 program suite [69].

ACKNOWLEDGEMENTS

We are grateful to M. Bowler and D. de Sanctis at the European Synchrotron Radiation Facility (ESRF), Grenoble, France for providing assistance in using beamlines ID30A-1 (MASSIF-1) and ID29, respectively, and other ESRF staff members for their excellent support. We thank I. Grishkovskaya and G. Mlynek for initial crystal screening, J. Zmajkovic for cloning the CD11b-I variants and S. Maier for technical assistance. The DLS, CD and DSF measurements were performed at the VBCF Protein Technologies Facility (www.vbcf.ac.at). We thank D. Mantus and L. Stulik for critical reading of the manuscript. KDC research was supported by Christian Doppler Laboratory for Knowledge-based structural biology and biotechnology, Federal Ministry of Economy, Family and Youth through the initiative “Laura Bassi Centres of Expertise”, funding the Centre of Optimized Structural Studies, N°253275, COST action BM1405 - Non-globular proteins, and by the University of Vienna.

AUTHOR CONTRIBUTIONS

AB and NT designed the study. AB, EN, KDC, DS and HR provided supervision. NT performed all experiments except for the crystallography work performed by DM and the SAXS study by MG. AB, NT, DM and MG analyzed the data. All authors contributed to interpreting the data. AB and NT wrote the manuscript with input from DM and MG, and all authors have reviewed the manuscript.

AUTHOR INFORMATION

The atomic coordinates and structure factors have been deposited in the Protein Data Bank (PDB) under the accession codes 6RHV (LukGH_K319A–moCD11b-I) and 6RHW (LukGH–huCD11b-I).
The SAXS data and models are deposited in the Small Angle Scattering Biological Data Bank (SASBDB) with the following accession codes SASDF55 (LukGH–Fab) and SASDF45 (LukGH–Fab–huCD11b-I).

COMPETING INTERESTS

AB and HR are employees of X4 Pharmaceuticals (Austria) GmbH, the legal successor of Arsanis Biosciences GmbH, which has developed an anti-LukGH antibody.

REFERENCES

[1] Tong, S. Y. C., Davis, J. S., Eichenberger, E., Holland, T. L. & Fowler, V. G. *Staphylococcus aureus* infections: epidemiology, pathophysiology, clinical Manifestations, and management. *Clinical Microbiology Reviews* **28**, 603–661 (2015).

[2] Alonzo, F. & Torres, V. J. The bicomponent pore-forming leucocidins of *Staphylococcus aureus*. *Microbiology and Molecular Biology Reviews* **78,** 199–230 (2014).

[3] Spaan, A. N., van Strijp, J. A. G. & Torres, V. J. Leukocidins: staphylococcal bi-component pore-forming toxins find their receptors. *Nature Reviews Microbiology* **15**, 435-447 (2017).

[4] Yamashita, D. *et al.* Molecular basis of transmembrane beta-barrel formation of staphylococcal pore-forming toxins. *Nature Communications* **5**, 4897 (2014).

[5] Haapasalo, K. *et al. Staphylococcus aureus* toxin LukSF dissociates from its membrane receptor target to enable renewed ligand sequestration. *The FASEB Journal* **33**, 3807-3824 (2019)

[6] Tromp, A. T. *et al*. Human CD45 is an F-component-specific receptor for the staphylococcal toxin Panton–Valentine leukocidin. *Nature Microbiology* **3**, 708–717 (2018).

[7] DuMont, A. L. *et al. Staphylococcus aureus* LukAB cytotoxin kills human neutrophils by targeting the CD11b subunit of the integrin Mac-1. *Proceedings of the National Academy of Sciences* **110**, 10794–10799 (2013).

[8] Ho, M.-K. & Springer, T. A. Biosynthesis and assembly of the α and β subunits of Mac-1, a macrophage glycoprotein associated with complement receptor function. *The Journal of Biological Chemistry* **258**, 2766-2769 (1983).

[9] Zhang, L. & Plow, E. F. Amino acid sequences within the α subunit of integrin $\alpha_M\beta_2$ (Mac-1) critical for specific recognition of C3bi. *Biochemistry* **38**, 8064–8071 (1999).

[10] Yakubenko, V. P., Lishko, V. K., Lam, S. C.-T. & Ugarova, T. P. A molecular basis for integrin $\alpha_M\beta_2$ Ligand binding promiscuity. *Journal of Biological Chemistry* **277**, 48635–48642 (2002).

[11] Podolnikova, N. P., Podolnikov, A. V., Haas, T. A., Lishko, V. K. & Ugarova, T. P. Ligand recognition specificity of leukocyte integrin $\alpha_M\beta_2$ (Mac-1, CD11b/CD18) and its functional consequences. *Biochemistry* **54**, 1408–1420 (2015).

[12] Arnaout, M. A. Biology and structure of leukocyte β_2 integrins and their role in inflammation. *F1000Research* **5**, F1000 Faculty Rev-2433 (2016).

[13] Lee, J.-O., Rieu, P., Arnaout, M. A. & Liddington, R. Crystal structure of the A domain from the a subunit of integrin CR3 (CD11b/CD18). *Cell* **80**, 631–638 (1995).

[14] Lee, J.-O., Bankston, L. A., Arnout,M.A. & Liddington,R.C. Two conformations of the integrin A-domain (I-domain): a pathway for activation? *Structure* **3**, 1333–1340 (1995).

[15] Baldwin, E. T. *et al.* Cation binding to the integrin CD11b I domain and activation model assessment. *Structure* **6**, 923–935 (1998).

[16] Xiong, J.-P., Li, R., Essafi, M., Stehle, T. & Arnaout, M. A. An isoleucine-based allosteric switch controls affinity and shape shifting in integrin CD11b A-domain. *Journal of Biological Chemistry* **275**, 38762–38767 (2000).

[17] McCleverty, C. J. & Liddington, R. C. Engineered allosteric mutants of the integrin αMβ2 I domain: structural and functional studies. *Biochemical Journal* **372**, 121–127 (2003).

[18] Mahalingam, B. *et al.* Stable coordination of the inhibitory Ca^{2+} ion at the metal ion-dependent adhesion site in integrin CD11b/CD18 by an antibody-derived ligand aspartate: Implications for integrin regulation and structure-based drug design. *The Journal of Immunology* **187**, 6393–6401 (2011).

[19] Bajic, G., Yatime, L., Sim, R. B., Vorup-Jensen, T. & Andersen, G. R. Structural insight on the recognition of surface-bound opsonins by the integrin I domain of complement receptor 3. *Proceedings of the National Academy of Sciences* **110**, 16426–16431 (2013).

[20] Jensen, M. R. *et al.* Structural basis for simvastatin competitive antagonism of complement receptor 3. *Journal of Biological Chemistry* **291**, 16963–16976 (2016).

[21] Takada, Y., Ye, X. & Simon S. The integrins. *Genome Biology* **8**, 215 (2007).

[22] Ventura, C. L. *et al.* Identification of a novel *Staphylococcus aureus* two-component leukotoxin using cell surface proteomics. *PLoS ONE* **5**, e11634 (2010).

[23] DuMont, A. L. *et al.* Characterization of a new cytotoxin that contributes to *Staphylococcus aureus* pathogenesis: The cytotoxin LukAB kills human phagocytes. *Molecular Microbiology* **79**, 814–825 (2011).

[24] Rouha, H. *et al.* Five birds, one stone: Neutralization of α-hemolysin and 4 bi-component leukocidins of *Staphylococcus aureus* with a single human monoclonal antibody. *mAbs* **7**, 243–254 (2015).

[25] Janesch, P. *et al.* Selective sensitization of human neutrophils to LukGH mediated cytotoxicity by *Staphylococcus aureus* and IL-8. *Journal of Infection* **74**, 473–483 (2017).

[26] Malachowa, N. *et al. Staphylococcus aureus* leukotoxin GH promotes inflammation. *Journal of Infectious Diseases* **206**, 1185–1193 (2012).

[27] Trstenjak, N. *et al.* Adaptation of the *Staphylococcus aureus* leukocidin LukGH for the rabbit host by protein engineering. *Biochemical Journal* **476**, 275-292 (2019).

[28] Badarau, A. *et al.* Structure-function analysis of heterodimer formation, oligomerization, and receptor binding of the *Staphylococcus aureus* bi-component toxin LukGH. *Journal of Biological Chemistry* **290**, 142–156 (2015).

[29] Badarau, A. *et al.* Context matters: The importance of dimerization-induced conformation of the LukGH leukocidin of *Staphylococcus aureus* for the generation of neutralizing antibodies. *mAbs* **8**, 1347–1360 (2016).

[30] Galdiero, S. & Gouaux, E. High resolution crystallographic studies of α-hemolysin-phospholipid complexes define heptamer-lipid head group interactions: Implication for understanding protein-lipid interactions. *Protein Science* **13**, 1503–1511 (2004).

[31] Tanaka, Y. *et al.* 2-Methyl-2,4-pentanediol induces spontaneous assembly of staphylococcal α-hemolysin into heptameric pore structure. *Protein Science* **20**, 448–456 (2011).

[32] DuMont, A. L. *et al.* Identification of a crucial residue required for *Staphylococcus aureus* LukAB cytotoxicity and receptor recognition. *Infection and Immunity* **82**, 1268–1276 (2014).

[33] Diamond, M. S. & Springer, T. A. A subpopulation of Mac-1 (CD11b/CD18) molecules mediates neutrophil adhesion to ICAM-1 and fibrinogen. *The Journal of cell biology* **120**, 545–556 (1993).

[34] Li, R. *et al.* Activation of integrin αIIbβ3 by modulation of transmembrane helix associations. *Science* **300**, 5 (2003).

[35] Nguyen, V. T., Kamio, Y. & Higuchi, H. Single-molecule imaging of cooperative assembly of γ-hemolysin on erythrocyte membranes. *The EMBO journal* **22**, 4968–4979 (2003).

[36] Fan, Z. *et al.* Neutrophil recruitment limited by high-affinity bent β_2 integrin binding ligand in cis. *Nature Communications* **7**, 12658 (2016).

[37] Sen, M. & Springer, T. A. Leukocyte integrin $\alpha_L\beta_2$ headpiece structures: The αI domain, the pocket for the internal ligand, and concerted movements of its loops. *Proceedings of the National Academy of Sciences* **113**, 2940–2945 (2016).

[38] Xie, C. *et al.* Structure of an integrin with an αI domain, complement receptor type 4. *The EMBO Journal* **29**, 666–679 (2010).

[39] DuMont, A. L. *et al. Staphylococcus aureus* elaborates leukocidin AB to mediate escape from within human neutrophils. *Infection and Immunity* **81,** 1830–1841 (2013).

[40] Malachowa, N., Kobayashi, S. D., Freedman, B., Dorward, D. W. & DeLeo, F. R. *Staphylococcus aureus* leukotoxin GH promotes formation of neutrophil extracellular traps. *The Journal of Immunology* **191**, 6022–6029 (2013).

[41] Gao, M. & Schulten, K. Onset of anthrax toxin pore formation. *Biophysical Journal* **90**, 3267–3279 (2006).

[42] Schittenhelm, L., Hilkens, C. M. & Morrison, V. L. β_2 Integrins as regulators of dendritic cell, monocyte, and macrophage function. *Frontiers in Immunology* **8**, (2017).

[43] Berends, E. T. M. *et al. Staphylococcus aureus* impairs the function of and kills human dendritic cells via the LukAB toxin. *mBio* **10**, e01918-18 (2019).

[44] Badarau, A., Trstenjak, N., Nagy, E. Structure and function of the two-component cytotoxins of *Staphylococcus aureus* – Learnings for designing novel therapeutics. in Protein Reviews: Volume 18 (ed. Atassi, M. Z.) 15–35 (Springer Singapore, 2017).

[45] Gasteiger, E. et al. Protein identification and analysis tools on the ExPASy Server. in The Proteomics Protocols Handbook (ed. Walker, J. M.) 571–607 (Humana Press, 2005). doi:10.1385/1-59259-890-0:571

[46] Anthis, N. J. & Clore, G. M. Sequence-specific determination of protein and peptide concentrations by absorbance at 205 nm: Sequence-specific protein concentration at 205 nm. *Protein Science* **22**, 851–858 (2013).

[47] Blanchet, C. E. *et al.* Versatile sample environments and automation for biological solution X-ray scattering experiments at the P12 beamline (PETRA III, DESY). *Journal of Applied Crystallography* **48**, 431–443 (2015).

[48] Franke, D. *et al. ATSAS 2.8* : a comprehensive data analysis suite for small-angle scattering from macromolecular solutions. *Journal of Applied Crystallography* **50**, 1212–1225 (2017).

[49] Svergun, D. I. Determination of the regularization parameter in indirect-transform methods using perceptual criteria. *Journal of Applied Crystallography* **25**, 495–503 (1992).

[50] Hajizadeh, N. R., Franke, D., Jeffries, C. M. & Svergun, D. I. Consensus Bayesian assessment of protein molecular mass from solution X-ray scattering data. *Scientific Reports* **8**, 7204 (2018).

[51] Svergun, D., Barberato, C. & Koch, M. H. J. *CRYSOL* – a program to evaluate X-ray solution scattering of biological macromolecules from atomic coordinates. *Journal of Applied Crystallography* **28**, 768–773 (1995).

[52] Petoukhov M.V. et al. New developments in the ATSAS program package for small-angle scattering data analysis. *Journal of Applied Crystallography* **45**, 342–350 (2012).

[53] Konarev, P. V., Volkov, V. V., Sokolova, A. V., Koch, M. H. J. & Svergun, D. I. *PRIMUS* : a Windows PC-based system for small-angle scattering data analysis. *Journal of Applied Crystallography* **36**, 1277–1282 (2003).

[54] Siemsen, D. W. *et al.* Neutrophil isolation from nonhuman species. in *Neutrophil Methods and Protocols* (eds. Quinn, M. T. & DeLeo, F. R.) 19–37 (Humana Press, 2014). doi:10.1007/978-1-62703-845-43

[55] Kabsch, W. *XDS*. *Acta Crystallographica Section D Biological Crystallography* **66**, 125–132 (2010).

[56] Tickle, I.J. *et al.* STARANISO (http://staraniso.globalphasing.org/cgi-bin/staraniso.cgi). Cambridge, United Kingdom: Global Phasing Ltd (2018).

[57] Vonrhein, C. *et al.* Data processing and analysis with the *autoPROC* toolbox. *Acta Crystallographica Section D Biological Crystallography* **67**, 293–302 (2011).

[58] Evans, P. Scaling and assessment of data quality. *Acta Crystallographica Section D Biological Crystallography* **62**, 72–82 (2006).

[59] Evans, P. R. & Murshudov, G. N. How good are my data and what is the resolution? *Acta Crystallographica Section D Biological Crystallography* **69**, 1204–1214 (2013).

[60] McCoy, A. J. *et al. Phaser* crystallographic software. *Journal of Applied Crystallography* **40**, 658–674 (2007).

[61] Emsley, P., Lohkamp, B., Scott, W. G. & Cowtan, K. Features and development of *Coot*. *Acta Crystallographica Section D Biological Crystallography* **66**, 486–501 (2010).

[62] Murshudov, G. N., Vagin, A. A. & Dodson, E. J. Refinement of macromolecular structures by the maximum-likelihood method. *Acta Crystallographica Section D Biological Crystallography* **53**, 240–255 (1997).

[63] Murshudov, G. N. *et al.* REFMAC5 for the refinement of macromolecular crystal structures. *Acta Crystallographica Section D* **67**, 355-367 (2011).

[64] Cowtan, K. The *Buccaneer* software for automated model building. 1. Tracing protein chains. *Acta Crystallographica Section D Biological Crystallography* **62**, 1002–1011 (2006).

[65] Cowtan, K. Fitting molecular fragments into electron density. *Acta Crystallographica Section D Biological Crystallography* **64**, 83–89 (2008).

[66] Adams, P. D. *et al. PHENIX* : a comprehensive Python-based system for macromolecular structure solution. *Acta Crystallographica Section D Biological Crystallography* **66**, 213–221 (2010).

[67] Krissinel, E. Stock-based detection of protein oligomeric states in jsPISA. *Nucleic Acids Research* **43**, W314–W319 (2015).

[68] Kabsch, W. A solution for the best rotation to relate two sets of vectors. *Acta Crystallographica Section A* **32**, 922 (1976).

[69] Winn, M. D. *et al.* Overview of the *CCP* 4 suite and current developments. *Acta Crystallographica Section D Biological Crystallography* **67**, 235–242 (2011).

Figure 1

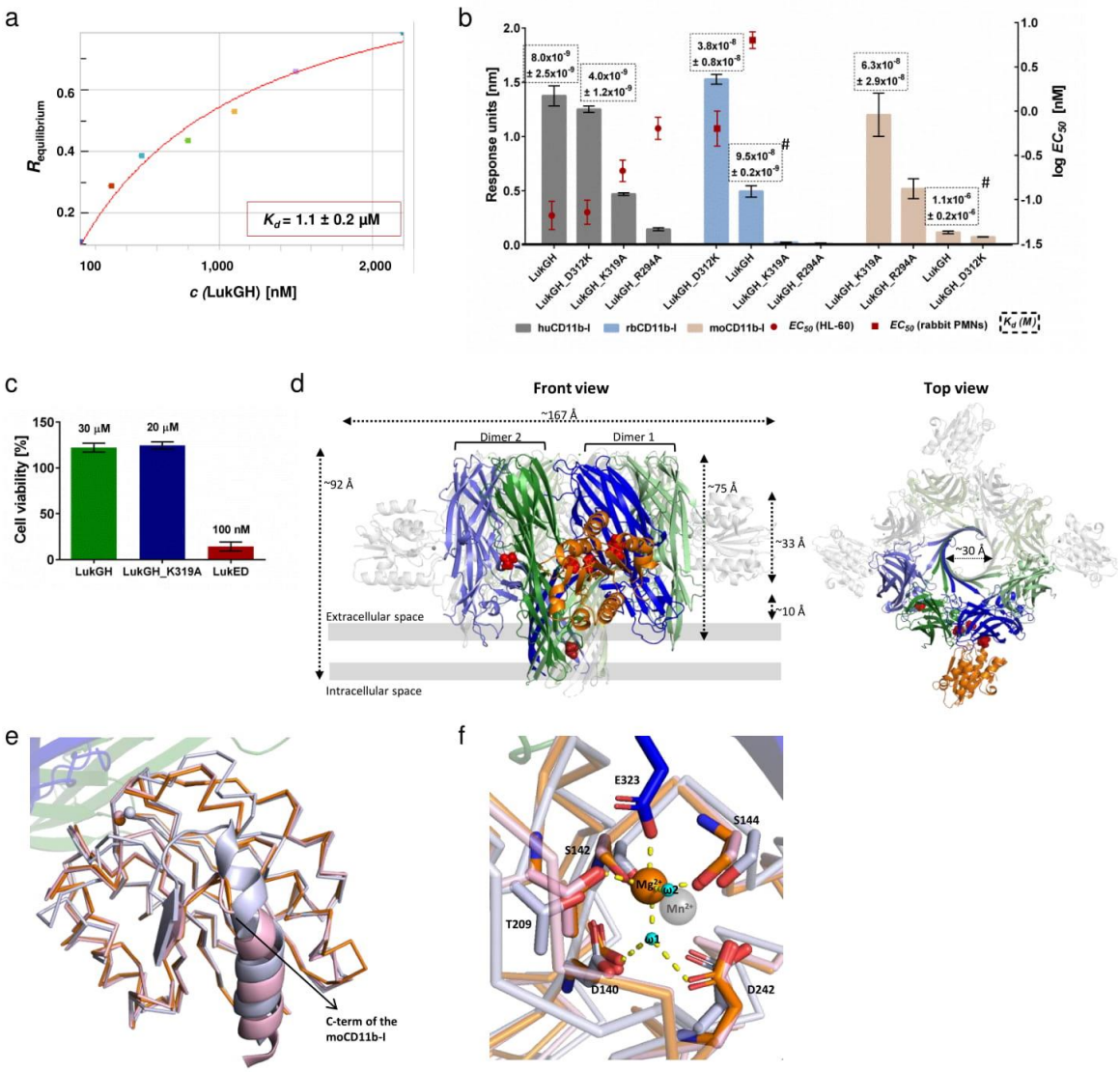

Figure 1. Binding and activity of LukGH wild-type and mutants to CD11b-I and crystal structure of LukGH-CD11b-I.

(a) Steady state analysis of binding of LukGH wild-type to moCD11b-I. The steady state K_d is shown in the insert.

(b) Binding of selected LukGH mutants to hu, rb or moCD11b-I expressed as response units (mean of 2–10 independent experiments ± S.E.M.) and K_d (mean of 2–10 independent experiments ± S.D.). K_d determined by steady state analysis is marked with #. EC_{50} values of LukGH mutants towards differentiated HL-60 cells, rabbit or mouse PMNs assessed in a luminescent cell viability assay measuring cellular ATP content (mean of 2–8 independent experiments ± S.E.M.). For variants that had limited or no cytotoxicity (could not kill >75% of cells at the highest toxin concentration used), EC_{50} is not shown. The data with human and rabbit receptors (both binding and activity) are from reference [27] .

(c) Cytotoxicity of LukGH, LukGH_K319A and LukED towards mouse PMNs assessed in a luminescent cell viability assay measuring cellular ATP content at cytotoxin concentrations of 30 µM, 20 µM and 100 nM, respectively (mean of 3 independent experiments ± S.E.M.).

(d) Front and top view of LukGH_K319A–moCD11b-I crystal structure. Dark blue and light green cartoons represent LukH and LukG from dimer 1 and dark and dark green and light blue cartoon represent LukG and LukH from dimer 2, respectively. moCD11b-I is shown as orange cartoon. Other dimers forming the octamer pore, and bound CD11b-I molecules are shown as grey cartoon. Red spheres represent bound DMSO molecules from one asymmetric unit (dark red sphere represents DMSO 2).

(e) Comparison of moCD11b-I secondary structure and **(f)** MIDAS residues from LukGH_K319A–moCD11b-I structure (orange ribbon) with the active (1IDO, light pink ribbon) and inactive (1JLM, light grey ribbon) form of huCD11b-I. C-terminal α-helix is shown as light pink cartoon (1IDO) and grey cartoon (1JLM). Structures are aligned on moCD11b-I and MIDAS residues in **(e)** and **(f)**, respectively. Metal ion from moCD11b-I structure and inactive form of CD11b-I (1JLM) are shown as orange and grey sphere.

Figure 2

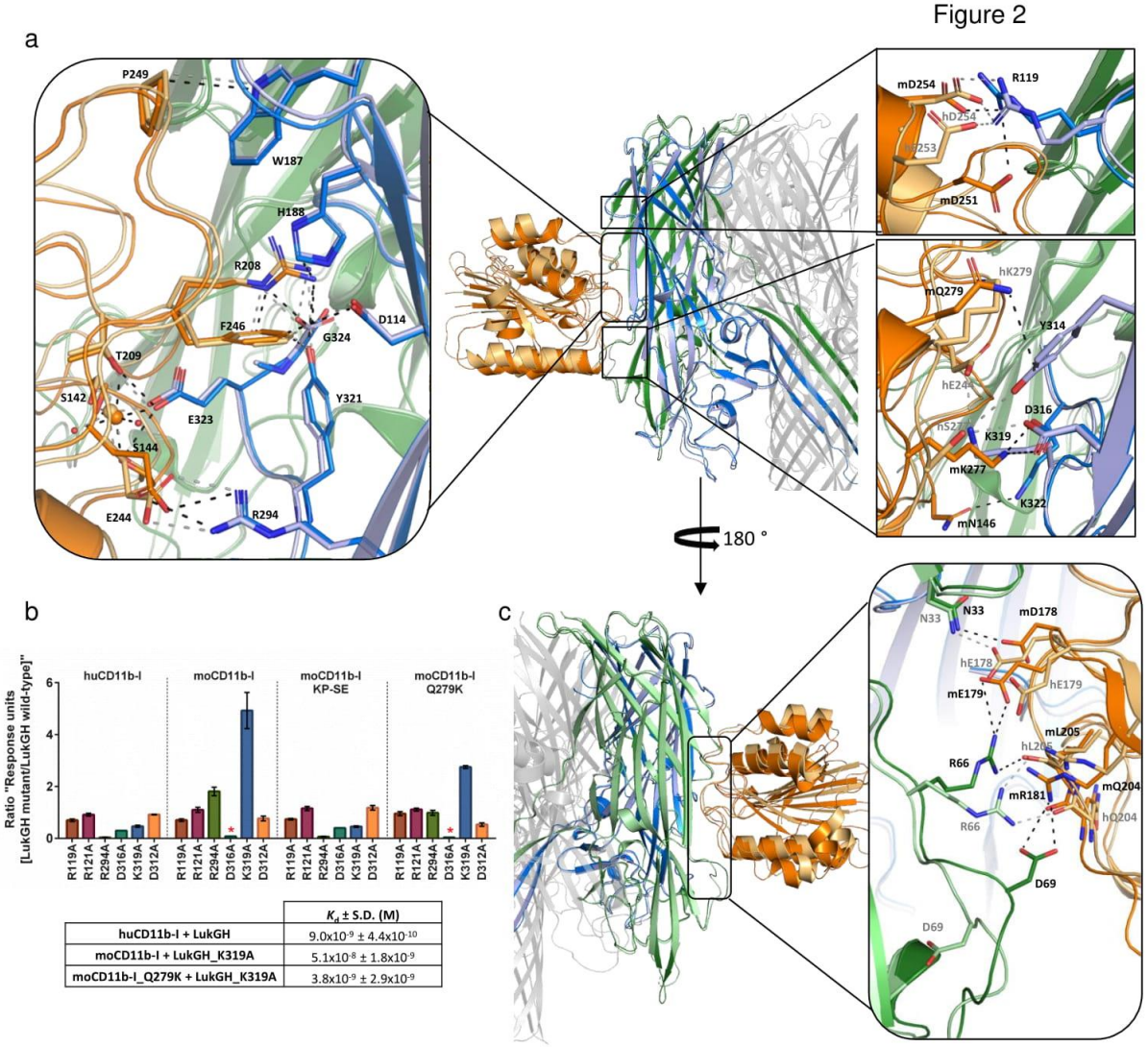

	K_d ± S.D. (M)
huCD11b-I + LukGH	$9.0x10^{-9}$ ± $4.4x10^{-10}$
moCD11b-I + LukGH_K319A	$5.1x10^{-8}$ ± $1.8x10^{-9}$
moCD11b-I_Q279K + LukGH_K319A	$3.8x10^{-9}$ ± $2.9x10^{-9}$

Figure 2. Binding epitope of LukGH-CD11b-I.

(a) Binding epitope of LukH–CD11b-I with detailed views of the specific interactions involved in CD11b-I binding in boxes, aligned on LukH. LukG, LukH and CD11b-I from the LukGH_K319A–moCD11b-I structure are shown in green, blue and orange, respectively. The same protein components from the LukGH–huCD11b-I structure are shown in pale green, pale blue and pale orange. Hydrogen bonds, salt bridges, the coordinate covalent bonds of Mg^{2+} as well as some other selected close contacts are shown as dashed lines coloured black (for the moCD11b-I complex) or grey (for the huCD11b-I complex). The left panel shows conserved interactions and the right top and bottom panels show non-conserved interactions between the human and mouse complex.

(b) Binding of LukGH mutants to CD11b-I variants expressed as values relative to wild-type (mean of 3 independent experiments ± S.E.M, except for LukGH_D316A with one experiment). Asterisk represent samples where no binding was detected (RU < 0.05 nm). Insert table shows K_d of selected LukGH and CD11b-I variants (mean of 2–3 independent experiments ± S.D.).

(c) Binding epitope of LukG-CD11b-I with a detailed view of the specific interactions involved in CD11b-I binding in the box, aligned on LukH. Color coding as in Figure 2a.

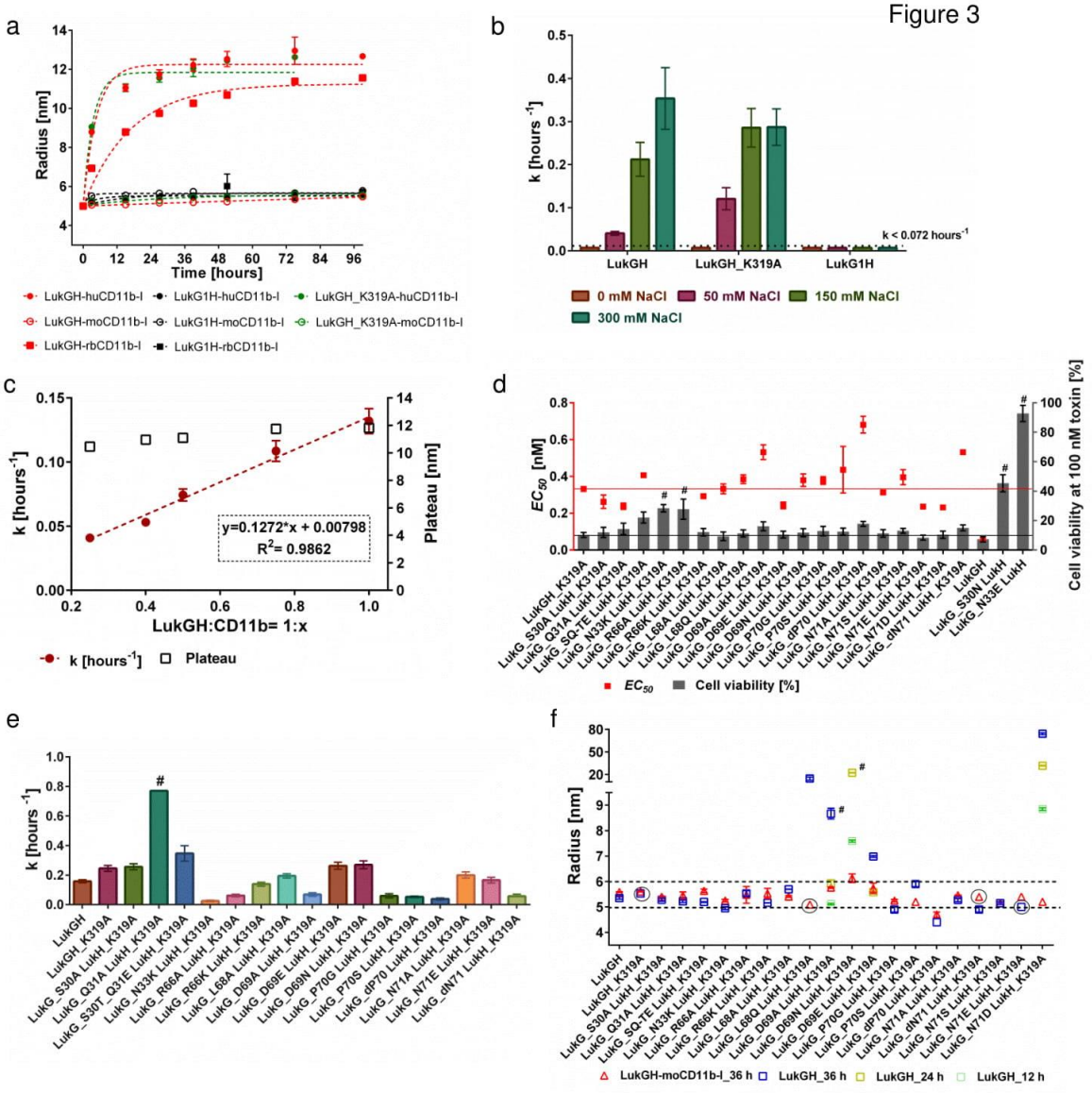

Figure 3. Oligomerization of LukGH in solution, binding and activity of LukGH oligomerisation variants.

(a) Change of LukGH, LukG1H and LukGH_K319A (at 5 mg/ml) plus hu, rb or moCD11b-I (at 2.5 mg/ml) cumulant radius, over time, measured in 25 mM HEPES, pH 7.5, 1 mM $MgCl_2$, 150 mM NaCl (mean of 1–2 replicates ± S.E.M). The dotted lines represent fitting of the data to a one-phase association model with fixed $y_0 = 5$ at $x_0 = 0$ h (GraphPad Prism).

(b) Oligomerization rate constant (*k*) for LukGH, LukGH_K319A and LukG1H (at 5 mg/ml) plus huCD11b-I (2.5 mg/ml) in 25 mM HEPES, pH 7.5, 1 mM $MgCl_2$, 0–300 mM NaCl (mean of 1–2 replicates ± S.E.M.). Data were fitted as in **(a)** giving $R^2 > 0.93$.

(c) Oligomerization rate constant (*k*) of LukGH (4.5 mg/ml) plus increasing amounts of huCD11b-I (2.3 mg/ml) in 25 mM HEPES, pH 7.5, 1 mM $MgCl_2$, 150 mM NaCl (mean of 2 replicates ± S.E.M). Linear regression fit (GraphPad Prism) is shown in red with equation in insert.

(d) Activity of LukGH mutants towards differentiated HL-60 cells expressed as EC_{50} and % cell viability at maximal toxin concentration (100 nM) (mean of 2 independent experiments ± S.E.M.). Red and black line represent EC_{50} value and % cell viability of LukGH_K319A mutant, respectively. Variants that had limited or no cytotoxicity (could not kill >75% of cells at the highest toxin concentration used) are marked with #.

(e) Oligomerization rate constant (*k*) of LukG oligomerization mutants co-expressed with LukH_K319A (at 4.5 mg/ml) plus huCD11b-I (2.3 mg/ml) (mean of 2 replicates ± S.E.M.). Data were fitted as in **(a)**, in all cases, except for LukGH_Q31A LukH_K319A (#ambiguous fit), yielding $R^2 > 0.94$.

(f) Cumulant radius of LukGH_variant–moCD11b-I complexes (at 4.5 mg/ml for LukGH and 2.3 mg/ml for CD11b-I) and individual LukGH variants at 36 h of incubation in 25 mM HEPES, pH 7.5, 1 mM $MgCl_2$,150 mM NaCl (mean of 1 (circled) or 2 replicates ± S.E.M). In case the sample shows increased radius at time 36 h, earlier time points are shown (24 and 12 h). Dotted lines represent ±10 % change from 5.5 nm radius. Samples with *SOS* >10 are marked with #.

Figure 4

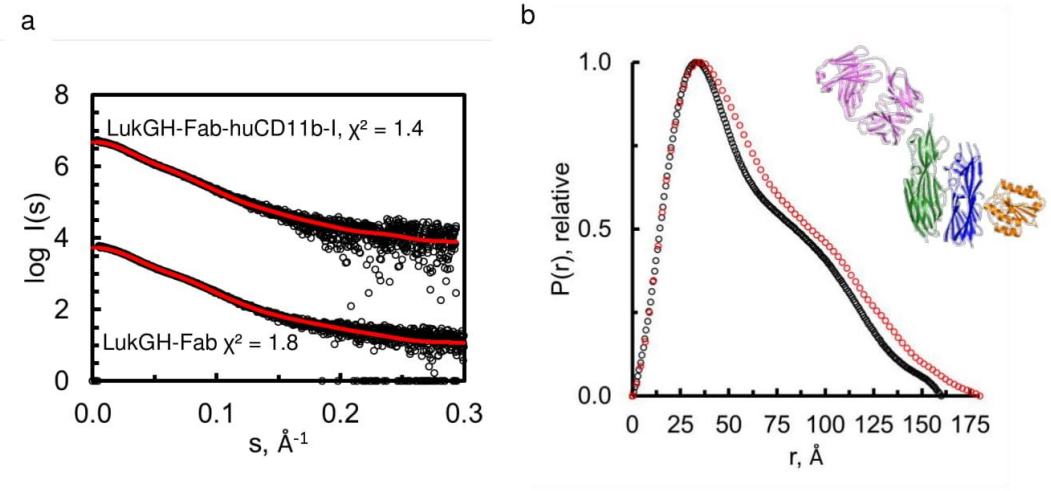

Figure 4. SAXS analysis of complex formation

(a) Scattering data as log*I*(*s*) *vs s* plot compared to the theoretical scattering of the respective models. These comprise the interfaces as retrieved from the crystal structures. χ^2 values are indicated. Curves are shifted along the *y*-axis for better visualization

(b) Distance distribution profile of LukGH-Fab (black) and LukGH–Fab–huCD11b-I (red). The insert shows the expected complex formation as cartoon representation, with the LukG, LukH, huCD11b-I and Fab subunits is green, blue, orange and purple cartoon, respectively.

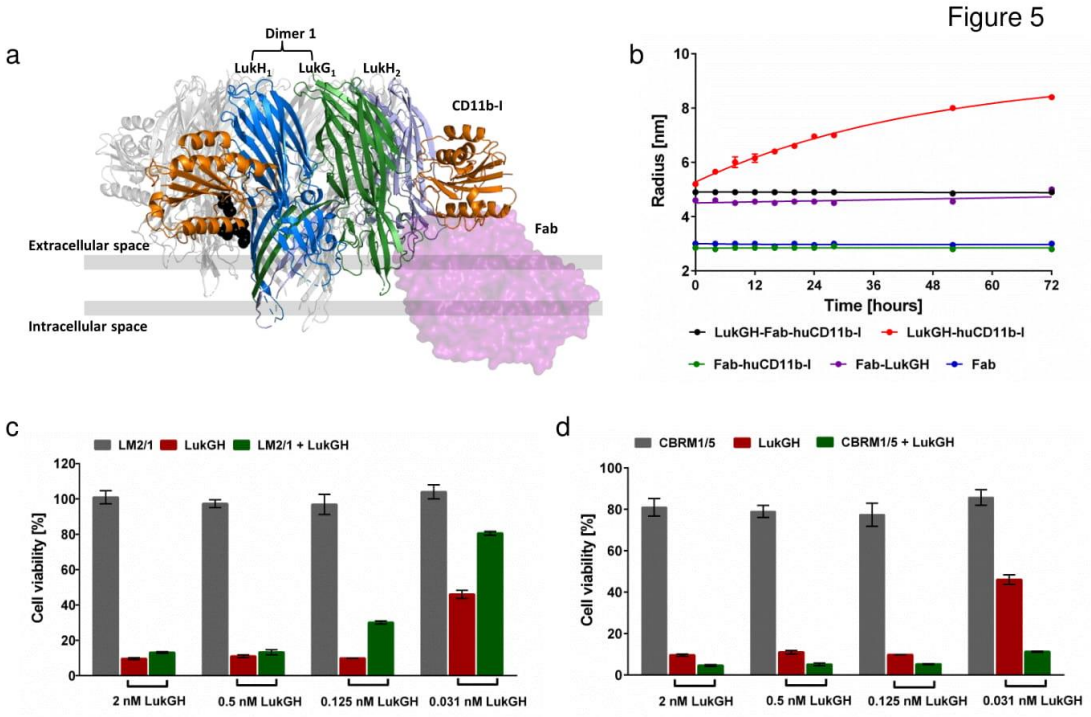

Figure 5. Interaction of LukGH with Fab of aLukGH-mAb#5.H1H2 and activity in presence of LM2/1 and CBRM1/5.

(a) Model of the LukGH–huCD11b-I octamer interacting with CD11b-I and the Fab fragment of αLukGH-mAb#5.H1H2 (PDB 5K59). The Fab is shown as purple surface, CD11b-I domain as orange cartoon, LukH1 and LukG1 forming Dimer 1 as dark blue and green cartoon, respectively, and LukH2 from adjacent dimer as light blue cartoon. The other LukG and LukH protomers and CD11b-I are shown in grey. Residues involved in binding of CBRM1/5 are shown as black spheres.

(b) Change of LukGH plus huCD11b-I and/or αLukGH-mAb#5.H1H2 Fab cumulant radius measured in 25 mM HEPES, pH 7.5, 1 mM $MgCl_2$, 150 mM NaCl at 1 mg/mL (mean of 1-2 replicates ± S.E.M.). The red solid line represents fit of the data to a one-phase association model with fixed $y_0 = 5$ at $x_0 = 0$ h (GraphPad Prism).

(c) and **(d)** Activity of LukGH towards LPS activated human PMNs, in presence and absence of 10 µg/mL LM2/1 **(c)** and CBRM1/5 **(d)** antibodies, assessed in a luminescent cell viability assay measuring cellular ATP content at different LukGH concentrations (mean of 3 replicates ± S.E.M.).

Figure 6

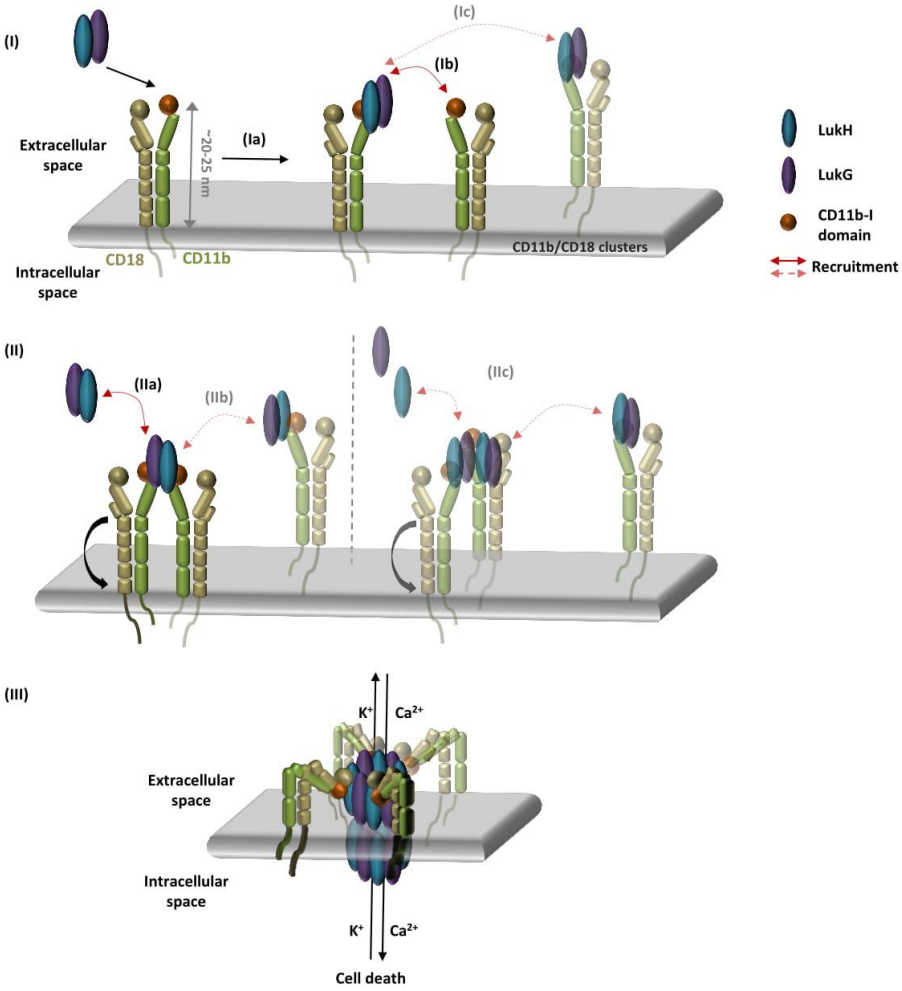

Figure 6. Proposed model of LukGH–CD11b-I interaction and pore formation.

(I) Binding of LukGH to CD11b-I via the LukH protomer **(Ia)** results in recruitment of a second integrin molecule *via* the LukG protomer **(Ib)** or alternatively, recruitment of a second integrin molecule with bound LukGH dimer **(Ic)**.

(II) After recruitment of the second integrin, *via* the LukG protomer, further LukGH dimer molecules are bound either as soluble LukGH dimers **(IIa)** or LukGH dimers bound to integrins **(IIb).** In the alternative version, two LukGH dimers bound to the two integrins **(IIc)** recruit further LukGH dimers in the same way as in **(IIa)** and **(IIb)**.

(III) Bending of the integrin and insertion of the octameric pore containing two to four bound integrins into the membrane.

Molecular mechanism of leukocidin GH - integrin CD11b/CD18 recognition and species specificity - SUPPLEMENTARY INFORMATION

Nikolina Trstenjak[1*], Dalibor Milić[2*], Melissa Ann Graewert[3], Harald Rouha[1§], Dmitri Svergun[3], Kristina Djinović-Carugo[2,4], Eszter Nagy[1§], Adriana Badarau[1#§]

[1]Arsanis Biosciences, Campus Vienna Biocenter, 1030, Vienna, Austria

[2]Department of Structural and Computational Biology, Max Perutz Labs, University of Vienna, 1030 Vienna, Austria

[3]European Molecular Biology Laboratory, Hamburg Unit, c/o DESY, Notkestrasse 85, 22607 Hamburg, Germany, and BioSAXS GmbH, c/o DESY, Notkestrasse 85, 22607 Hamburg, Germany

[4]Department of Biochemistry, Faculty of Chemistry and Chemical Technology, University of Ljubljana, Večna pot 113, SI-1000 Ljubljana, Slovenia

[*] contributed equally to the work

[§] current affiliations: A.B. and H.R. – X4 Pharmaceuticals (Austria) GmbH; E. N. –CEBINA GmbH, Karl-Farkas-Gasse 22, Vienna, Austria

[#] corresponding author: adriana.badarau@x4pharma.com

Supplementary Figure 1

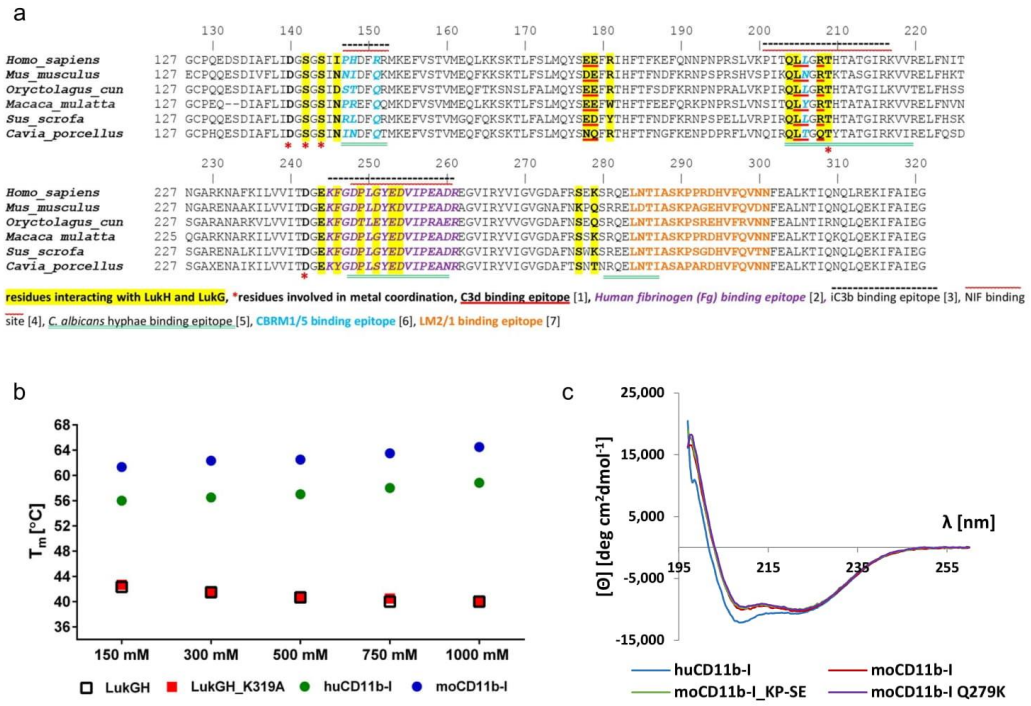

Supplementary Figure 1. Conservation of CD11b-I from different species and stability of CD11b-I variants.

(a) Alignment of CD11b-I residues 127–321 from different species.

(b) Melting temperature of LukGH, LukGH_K319A and CD11b-I variants, measured by DSF, in 25 mM HEPES, pH 7.5, 1 mM $MgCl_2$ with increasing NaCl concentrations (150–1000 mM).

(c) CD spectra of human, mouse CD11b-I and mouse CD11b-I variants in 50 mM sodium phosphate, pH 7.5, 300 mM NaCl.

Supplementary Figure 2

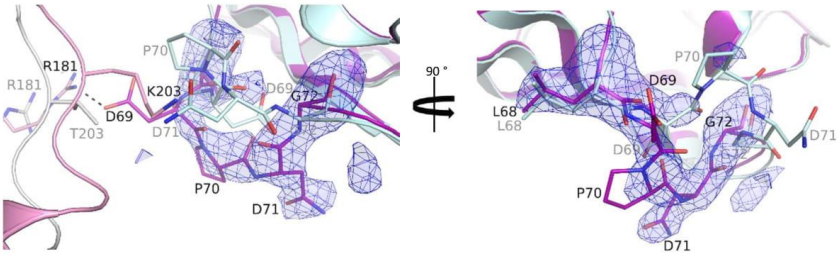

Supplementary Figure 2. Flexible loop in LukG.

The LukG loop 68–72 in the LukGH_K319A–moCD11b-I structure (purple) shows high flexibility and a different conformation from that found in the LukGH–huCD11b-I complex (light cyan). moCD11b-I is represented in pink and huCD11b-I in grey colour. The black residue labels correspond to the LukGH_K319A–moCD11b-I and the grey ones to the LukGH–huCD11b-I structure. The omit σ_A-weighted $mF_o–DF_c$ difference electron density map contoured at 3.0σ level for LukGH_K319A–moCD11b-I is shown as a blue mesh. The salt bridge is highlighted as a dashed line.

Supplementary Figure 3

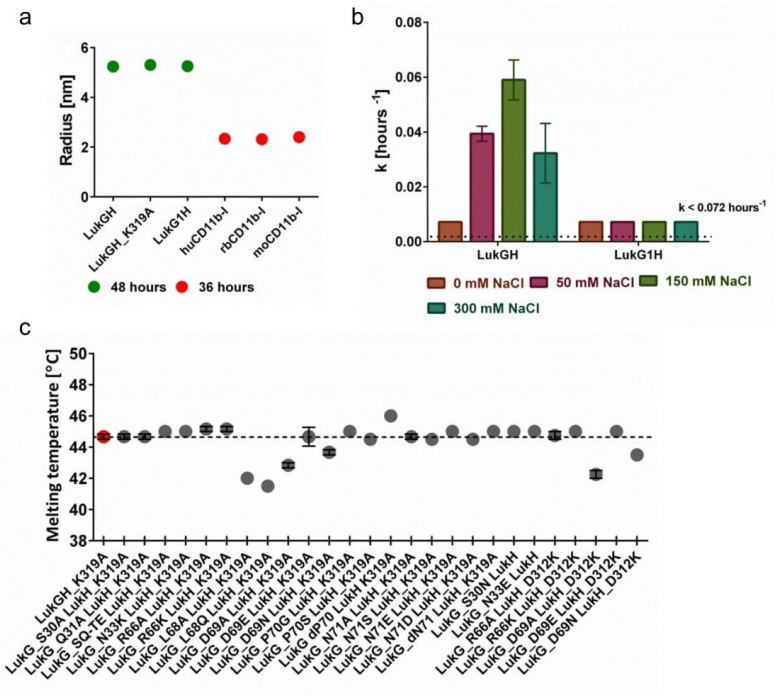

Supplementary Figure 3. Stability of LukGH variants and their oligomerisation in solution.

(a) Cumulant radius of individual LukGH mutants (at 5 mg/ml) and CD11b-I variants (at 2.5 mg/ml), measured by DLS, in 25 mM HEPES, pH 7.5, 1 mM $MgCl_2$, 150 mM NaCl after 48 or 36 h of incubation, respectively (one experiment with two replicates – some replicates are excluded due to poor autocorrelation curve) (mean of 1–2 replicates ± S.E.M).

(b) Oligomerization rate constant (*k*) for LukGH and LukG1H (at 5 mg/ml) in presence of rbCD11b-I (at 2.5 mg/ml) in 25 mM HEPES, pH 7.5, 1 mM $MgCl_2$, 0–300 mM NaCl (mean of 1–2 replicates ± S.E.M.). Data were fitted to a one-phase association model with fixed $y_0 = 5$ at $x_0 = 0$ h (GraphPad Prism), yielding $R^2 > 0.93$.

(c) Melting temperature (T_m) of LukGH variants measured by DSF in 50 mM HEPES, pH 7.5 (mean of 2–3 replicates ± S.E.M). The T_m of LukGH_K319A is marked red.

Supplementary Figure 4

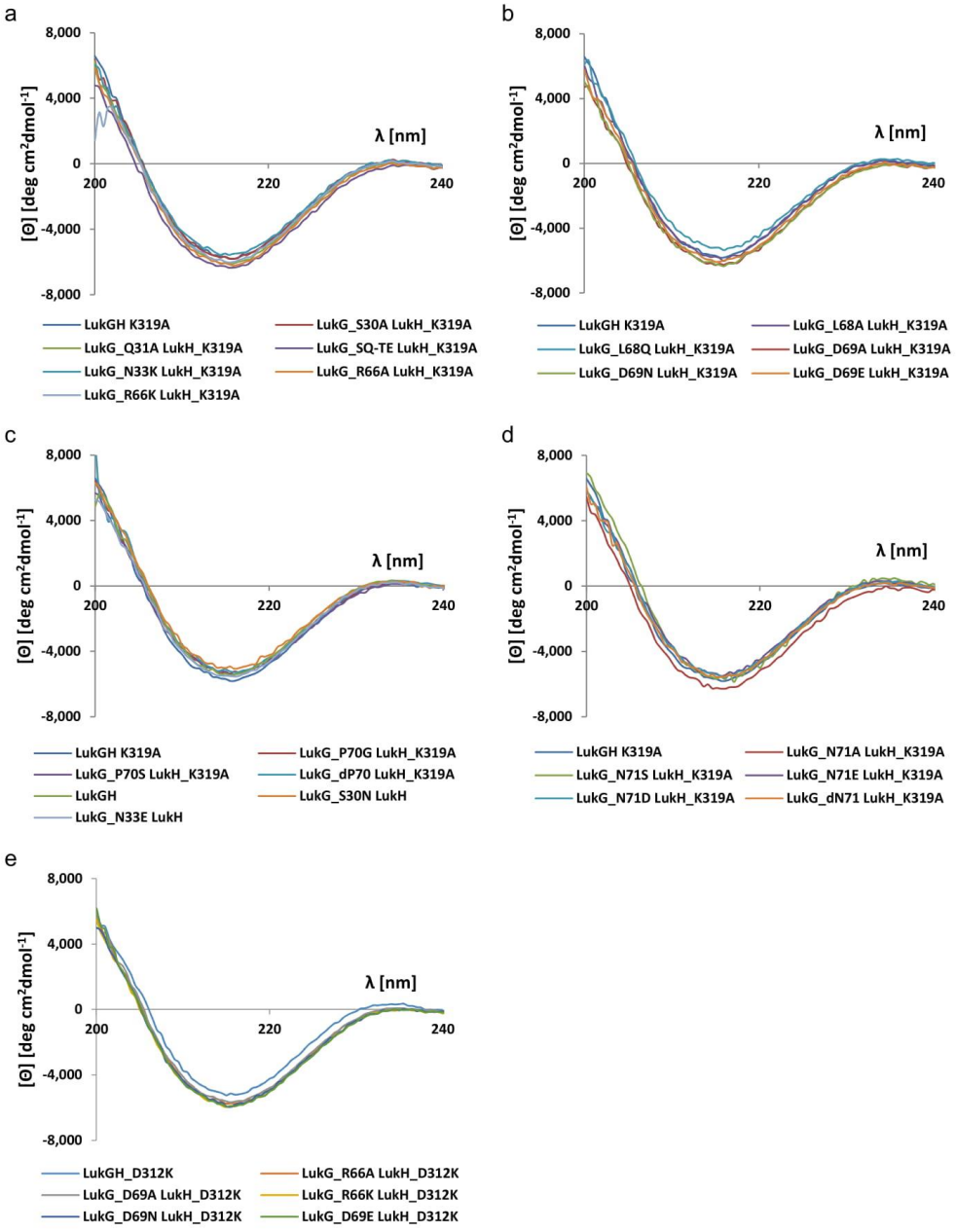

Supplementary Figure 4. Characterization on LukGH oligomerization mutants. (a) – (e) CD spectra of LukGH mutants in 20 mM sodium phosphate, pH 7.5, 150–250 mM NaCl.

Supplementary Figure 5

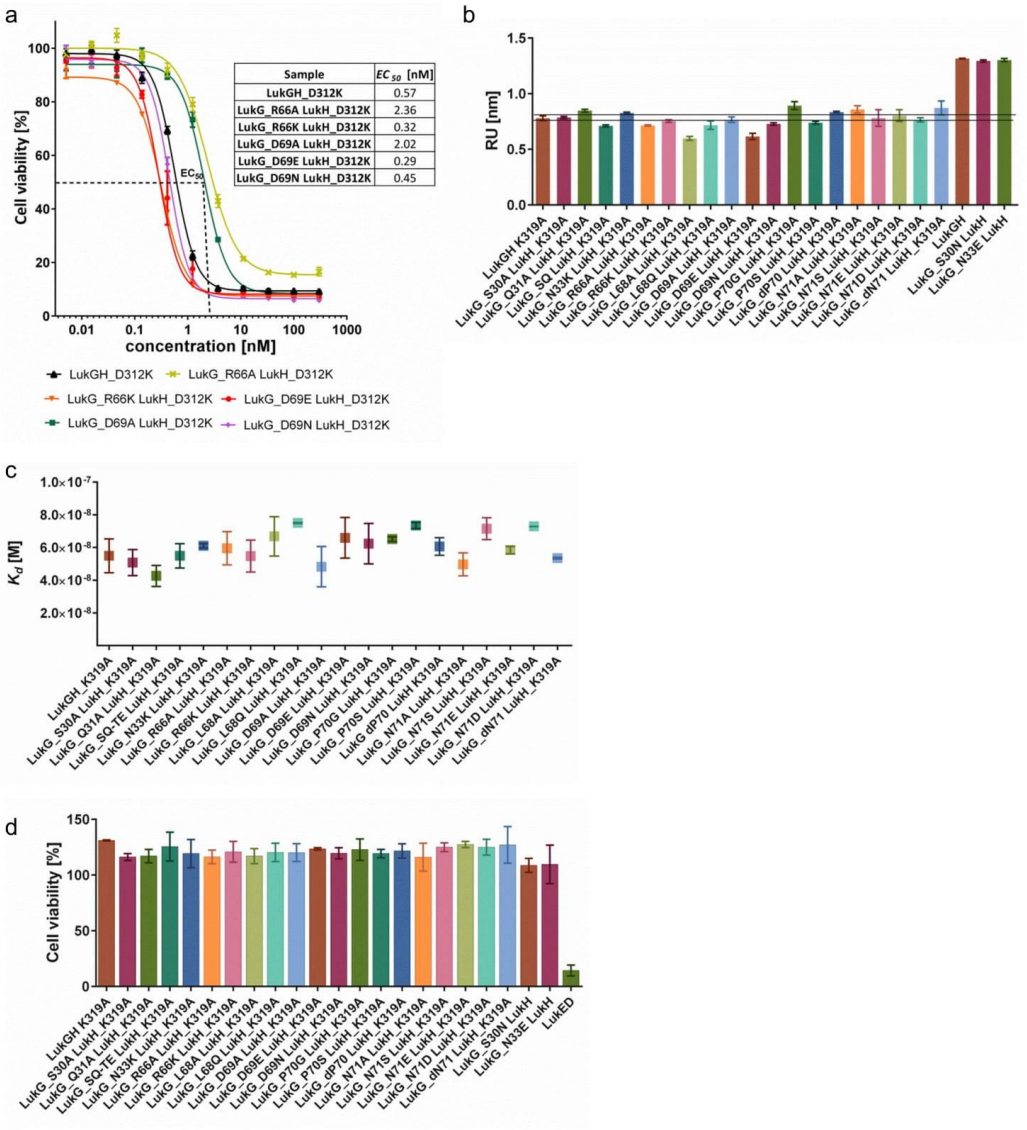

Supplementary Figure 5. Activity and receptor binding of LukGH oligomerization mutants.

(a) Activity of LukG oligomerization mutants (positions 66 and 69), co-expressed with LukH_D312K, towards rbPMNs assessed in a luminescent cell viability assay measuring cellular ATP content at increasing cytotoxin concentrations. Solid lines represent non-linear fit of the data and EC_{50} values are shown in the inserted table (mean of 3 replicates ± S.E.M.).

(b) Binding of LukGH oligomerization mutants in the LukH_K319A or LukH wild-type background (100 and 50 nM, respectively) to huCD11b-I, measured by BLI (mean of 2 independent experiments ± S.E.M). For the experiments with LukGH variants in the LukH wild-type background, the huCD11b-I was biotinylated with the amino specific reagent. Solid lines represent average RU for LukGH_K319A.

(c) Affinity of LukGH oligomerization mutants for moCD11b-I measured by BLI (mean of 2-4 independent experiments ± S.E.M.)

(d) Activity of LukGH variants towards mouse PMNs assessed in a luminescent cell viability assay measuring cellular ATP content at toxin concentration of 800–1000 nM for LukGH variants and 100 nM for LukED (mean of 2 independent experiments ± S.E.M).

Supplementary Figure 6

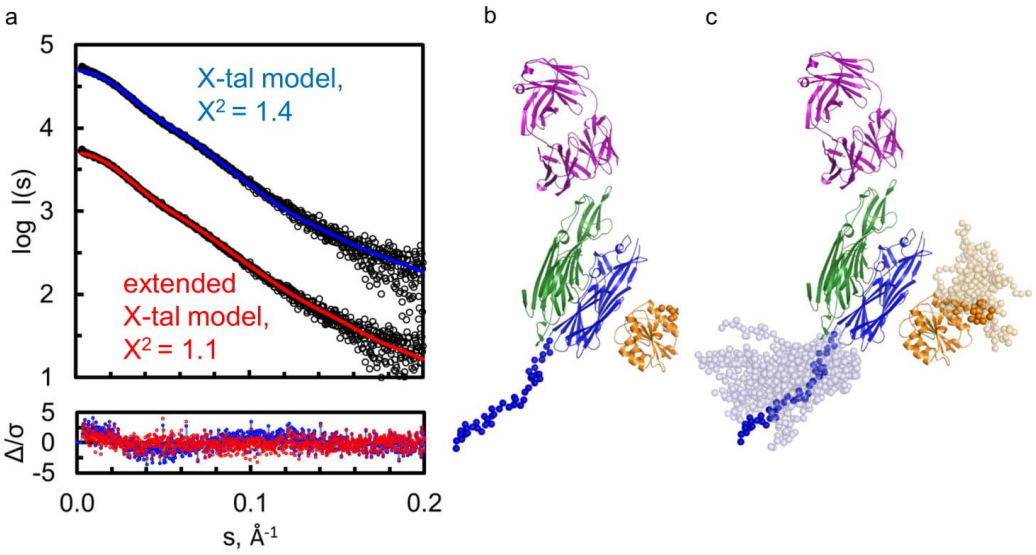

Supplementary Figure 6. SAXS data of FAB–LukGH–huCD11b-I complex and models obtained by CORAL.

(a) Fit and error-weighted residual difference plots of Fab–LukGH – huCD11b-I model with (red) and without (blue) extensions Data are shifted for clarity. X^2 values are indicated. The lower panel shows the residuals (Δ/σ) calculated as I_{exp} (s) – I_{model} (s) normalized with respect to experimental errors (σ).

(b) Representative model obtained with CORAL. Missing residues (44 residues from LukH N-terminus as well as 22 residues from huCD11b-I C-terminus) were modelled as dummy atoms to fit the experimental SAXS data and are shown as spheres. Color coding as in Figure 4.

(c) Overlay of 20 independent CORAL calculations. For clarity the model shown in B is emphasized.

Supplementary Figure 7

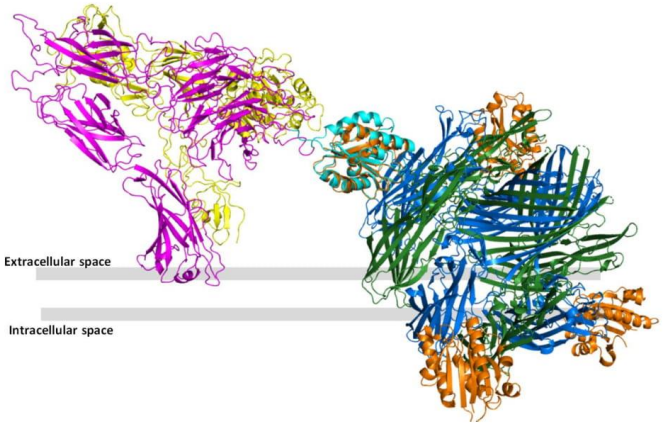

Supplementary Figure 7. Alignment of the LukGH_K319A–moCD11b-I complex with the CD11c/CD18 ectodomain.

(a) Alignment of the CD11b-I from LukGH_K319A–moCD11b-I crystal structure with CD11c-I domain of CD11c/CD18 (PDB 3K71). CD11c/CD18 (magenta and yellow cartoon, respectively, with CD11c-I domain as cyan cartoon) is in bent conformation, i.e. oriented towards the cellular membrane. LukG , LukH and CD11b-I are shown as green, blue and orange cartoon, respectively.

Supplementary Figure 8

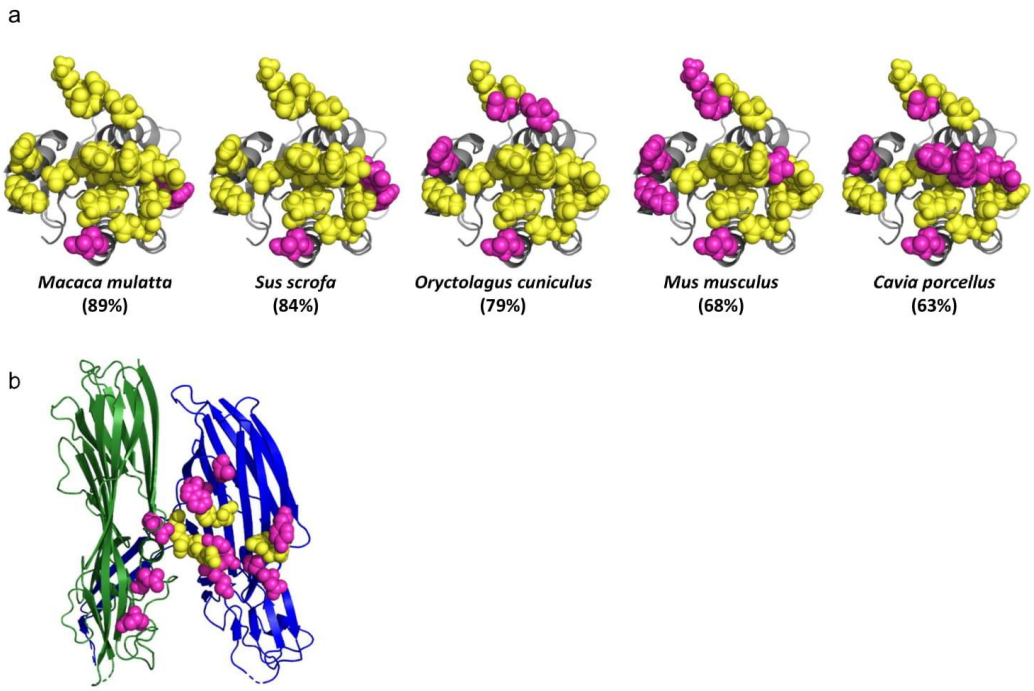

Supplementary Figure 8. Amino acid conservation of CD11b-I and LukGH residues from the binding epitope

(a) Amino acid conservation of the LukGH binding epitope in CD11b-I from rhesus macaque (*Macaca mulatta*), pig (*Sus scrofa*), rabbit (*Oryctolagus cuniculus)*, mouse (*Mus musculus*) and guinea pig (*Cavia porcellus*) CD11b-I compared to huCD11b-I is given as percentage (%) and displayed on the structure of moCD11b-I (grey cartoon). Conserved residues are shown as yellow and non-conserved as magenta spheres.

(b) Amino acid conservation of the LukGH residues involved in CD11b-I binding, among the LukGH sequence variants available in NCBI database (sequences with ≥ 90% coverage and ≥ 87% identity to TCH1516 sequence) displayed on the cartoon representation of the LukGH dimer (PDB 5K59, LukG in green and LukH in blue). Conserved residues are shown as yellow and non-conserved as magenta spheres.

SUPPLEMENTARY TABLES

Supplementary Table 1. Data collection, refinement and validation statistics.

	LukGH_K319A–moCD11b-I	LukGH–huCD11b-I†
Data collection		
Space group	$P42_12$	$P42_12$
Cell dimensions		
a, *b*, *c* (Å)	130.49, 130.49, 109.05	122.11, 122.11, 133.70
α, β, γ (°)	90, 90, 90	90, 90, 90
Resolution (Å)	46.94–2.29 (2.37–2.29)*	45.08–2.75 (2.99–2.75)
R_{meas}	0.206 (2.566)	0.324 (1.739)
Mean $I/\sigma(I)$	7.5 (0.6)	7.8 (1.8)
Completeness (spherical, %)	99.3 (97.6)	53.8 (15.0)
Completeness (ellipsoidal, %)	99.3 (97.6)	92.0 (71.7)
Redundancy	5.6 (4.5)	12.6 (12.5)
$CC_{1/2}$	0.993 (0.212)	0.996 (0.627)
Refinement		
Resolution (Å)	46.94–2.29 (2.37–2.29)	45.08–2.75 (2.85–2.75)
No. reflections	42957 (4124)	14518
R_{work} / R_{free} (%)	18.8 (31.4)/22.7 (34.7)	23.9 (37.7)/28.1 (25.8)
No. non-H atoms		
Protein	6044	5730
Ligand/ion	25	25
Water	356	2
Average *B*-factors (Å^2)		
Protein	54.4	61.1
Ligand/ion	74.1	72.3
Water	49.1	28.3
R.m.s. deviations		
Bond lengths (Å)	0.002	0.003
Bond angles (°)	0.49	0.78
Ramachandran favoured (%)	94.7	94.6
Ramachandran outliers (%)	0.0	0.0

*Values in parentheses are for highest-resolution shell.

†Diffraction data were collected from a crystal that diffracted anisotropically to 2.75 Å along **a***and **b***, and 4.79 Å along **c***.

Supplementary Table 2. Interacting residues between LukH and CD11b-I from LukGH–huCD11b-I and LukGH_K319A–moCD11b-I complexes. Conservation of LukH residues in LukH sequences in the three most divergent sequence variants of TCH1516 (MRSA252, MSHR and H19) and in sequence variants available in NCBI database (only the sequences with ≥90% coverage and ≥87% identity to TCH1516 sequence were analysed).

LukGH_K319A–moCD11b-I		LukGH–huCD11b-I		Amino acid difference in sequence variants H19, MRSA252 or MSHR1132	Amino acids present in other sequence variants (% of sequences with position different from TCH1516)
LukH_K319A	moCD11b-I	LukH	huCD11b-I		
Residues involved in salt-bridge formation					
Gly 324 (C-terminus)	Arg 208	Gly 324 (C-terminus)	Arg 208	conserved	conserved
		Lys 319	Glu 244	Gln (MSHR1132)	Gln (3.6%)
Asp 316	Lys 277			conserved	conserved
Arg 294	Glu 244	Arg 294	Glu 244	conserved	conserved
Lys 183	Asp 178	Lys 183	Glu 178	conserved	conserved
Arg 119	Asp 251	Arg 119	Glu 253	conserved	Ser (7.2%)
Arg 119	Asp 254	Arg 119	Asp 254		
Residues involved in polar and hydrophobic contacts					
Glu 323#	Ser 144#	Glu 323#	Ser 144#	conserved	conserved
Glu 323*	Arg 208	Glu 323*	Arg 208		
Glu 323#	Thr 209#	Glu 323#	Thr 209#		
Glu 323#	Ser 142#	Glu 323#	Ser 142#		
Lys 322	Asn 146			Arg (MSHR1132)	Arg (23.7%)
Tyr 321	Arg 208, Phe 246	Tyr 321	Arg 208, Phe 246	Phe (MSHR1132)	Phe (23%)
Asn 318*	Lys 277			not present (MSHR1132)	not present (3.8%))
Asp 316	Lys 277	Asp 316	Ser 277	conserved	conserved
Tyr314	Gln279	Tyr 314	Ser 277	conserved	His (0.7%)
Arg 294	Glu 244	Arg 294	Glu 244	conserved	conserved
His 188	Arg 208, Phe 246	His 188	Arg 208, Phe 246	conserved	conserved
Trp 187	Pro 249	Trp 187	Pro 249	Arg (MRSA252)	Arg (10.1%)
Asp 114	Phe 246	Asp 114	Phe 246	conserved	conserved

* main chain O; # Mg^{2+}-coordinating residue

Supplementary Table 3. Binding of LukGH (50 nM) to huCD11b-I, measured by BLI, in buffers with different metals.

Buffer	RU (nm)	K_d (M)	k_{on} (M^{-1} s^{-1})	k_{dis} (s^{-1})
PBS + 1% BSA+ 1 mM $MgCl_2$	1.68	$1.2\times10^{-8} \pm 9.4\times10^{-11}$	$6.9\times10^{4} \pm 4.4\times10^{2}$	$7.9\times10^{-4} \pm 4.1\times10^{-6}$
PBS + 1% BSA+ 1 mM $MgCl_2$ + 1 mM $CaCl_2$	0.96	$2.4\times10^{-8} \pm 3.0\times10^{-10}$	$1.0\times10^{5} \pm 1.1\times10^{3}$	$2.4\times10^{-3} \pm 1.1\times10^{-5}$
PBS + 1% BSA+ 1 mM $CaCl_2$	0.02	/	/	/

*RU < 0.05 nm = no binding

Supplementary Table 4. Binding of LukGH or LukGH_K319A to human or mouse CD11b-I in buffer (25 mM HEPES, pH 7.5, 1% BSA and 1 mM $MgCl_2$) with increasing salt concentration (150–1000 mM).

LukGH-huCD11b-I				
NaCl (mM)	**RU (nm)**	**K_d (M)**	**k_{on}(M^{-1} s^{-1})**	**k_{dis}(s^{-1})**
150	1.55 ± 0.18	$1.3\times10^{-8} \pm 7.8\times10^{-11}$	$1.3\times10^{5} \pm 2.0\times10^{4}$	$1.7\times10^{-3} \pm 2.5\times10^{-4}$
300	0.94 ± 0.04	$2.4\times10^{-8} \pm 7.5\times10^{-10}$	$1.4\times10^{5} \pm 2.0\times10^{4}$	$3.4\times10^{-3} \pm 3.8\times10^{-4}$
500	0.62 ± 0.08	$4.6\times10^{-8} \pm 4.5\times10^{-9}$	$1.2\times10^{5} \pm 1.2\times10^{3}$	$5.3\times10^{-3} \pm 5.8\times10^{-4}$
750	0.33 ± 0.05	$8.8\times10^{-8} \pm 5.8\times10^{-9}$	$8.6\times10^{4} \pm 4.1\times10^{2}$	$7.6\times10^{-3} \pm 4.6\times10^{-4}$
1000	0.22 ± 0.03	$1.3\times10^{-7} \pm 5.2\times10^{-9}$	$7.6\times10^{4} \pm 1.1\times10^{3}$	$9.5\times10^{-3} \pm 5.4\times10^{-4}$
LukGH_K319A–moCD11b-I				
150	0.66 ± 0.01	$5.3\times10^{-8} \pm 2.7\times10^{-9}$	$1.3\times10^{5} \pm 1.8\times10^{4}$	$6.7\times10^{-3} \pm 1.3\times10^{-3}$
300	0.28 ± 0.02	$1.1\times10^{-7} \pm 4.4\times10^{-9}$	$1.4\times10^{5} \pm 2.4\times10^{4}$	$1.5\times10^{-2} \pm 2.1\times10^{-3}$
500	0.13 ± 0.001	$1.4\times10^{-7} \pm 4.6\times10^{-8}$	$1.6\times10^{5} \pm 3.0\times10^{4}$	$2.2\times10^{-2} \pm 3.1\times10^{-3}$
750	0.06 ± 0.001*	/	/	/
1000	0.03 ± 0.001*	/	/	/

*RU < 0.05 nm = no binding

Supplementary Table 5. Interacting residues between LukG and CD11b-I from LukGH–huCD11b-I and LukGH_K319A–moCD11b-I complexes. Conservation of LukG residues in LukG sequences in the three most divergent sequence variants of TCH1516 (MRSA252, MSHR and H19) and in sequence variants available in NCBI database (only the sequences with≥ 90% coverage and ≥ 87% identity to TCH1516 sequence were analysed).

LukGH_K319A–moCD11b-I		LukGH–huCD11b-I		Amino acid difference in sequence variants H19, MRSA252 or MSHR1132	Amino acids present in other sequence variants (% of sequences with position different from TCH1516)
LukG	moCD11b-I	LukG	huCD11b-I		
Residues involved in salt bridge formation					
Arg 66	Glu 179			Lys (MSHR1132, MRSA252)	Lys (20.5%)
Asp 69	Arg 181			Glu (H19), Asn (MRSA252)	Glu (13.7%), Asn (11%), Gly (0.7%)
Residues involved in polar and hydrophobic contacts					
Asn 33	Asp 178	Asn 33	Glu 178	Lys (MSHR1132, MRSA252)	Lys (20.5%), Ile (0.7%)
		Arg 66	Gln 204*	Lys (MSHR1132, MRSA252)	Lys (20.5%)
Arg 66	Leu 205* (main-chain O)	Arg 66	Leu 205*		

* main chain O

Supplementary Table 6. Data collection and SAXS derived parameters for LukGH–Fab and LukGH–Fab–huCD11b-I complex.

Data collection parameters		
Radiation source	Petra III (DESY, Hamburg, Germany)	
beamline	EMBL P12	
Detector	Pilatus 2M	
Beam geometry (mm, FWHM)	0.12 × 0.20	
Wavelength (nm)	0.124	
Sample-detector distance (m)	3.1	
Momentum transfer *s* range (nm^{-1})	0.08 - 3.5	
Exposure time (s)	0.045	
Temperature (°C)	20	
Overall parameters	**LukGH–Fab**	**LukGH–Fab–huCD11b-I**
Concentration range (mg/ml)	0.4-4.6	0.4-4.7
R_g from Guinier approximation (nm)	4.7 ± 0.2	5.0 ± 0.2
R_g from PDDF (nm)	4.9 ± 0.1	5.2 ± 0.1
D_{max} (nm)	16 ± 1	18 ± 1
Molecular weight from forward scattering *I*(0), (kDa)	91 ± 15	121 ± 20
Molecular weight from excluded volume (kDa)	110 ± 20	130 ± 20
Molecular weight from DATMOV, (kDa)	110 ± 20	120 ± 20
Molecular weight from volume of correlation (kDa)	90 ± 15	105 ± 20
Molecular weight from sequence (monomer, kDa)	122	143
Software employed		
Primary data reduction	SASFLOW	
Data processing	PRIMUS	
Calculation and comparison of scattering data	Crysol / Oligomer	
Addition of missing residues	CORAL	
SASBDB accession code	SASDF55	SASDF45

Supplementary Table 7. Ligands of CD11b and their affinities as reported in the literature.

Ligand	K_d (M)	Method used
Platelet factor 4 (PF4)	$1.3\times10^{-6} \pm 0.2\times10^{-6}$ [8]	BLI with immobilized PF4 and the I-domain in solution
Hookworm-derived Neutrophil adhesion inhibitor (NIF)	1) 1×10^{-9} [9] 2) $2.1\times10^{-9} \pm 0.5\times10^{-9}$ [4]	1) Binding of biotinylated NIF to CD11b immobilized on the plate 2) Binding of I^{125} labelled NIF to the I-domain expressed on HEK293 cells
Myelin basic protein (MBP)	Three binding events: K_{d1} and $K_{d2}=10^{-4}$, $K_{d3}=10^{-6}$ [10]	SPR with immobilized MBP and the active I-domain in solution
LL-37 (broad spectrum anti-microbial peptide)	1) $5.0\times10^{-6} \pm 0.9\times10^{-6}$ (not 1:1 kinetics so separated into three binding events: $K_{d1}=1\times10^{-6}$, K_{d2} and $K_{d3}=10–100\times10^{-6}$ [11] 2) 4 binding events: K_{d1}= 0.1–0.5×10^{-6}, K_{d2} and $K_{d3}=10–100\times10^{-6}$, $K_{d4}=0.01\times10^{-6}$ [11]	1) SPR with immobilized LL-37 2) BLI with immobilized I-domain and LL-37 in solution
Fibrinogen (Fg)	1) $2.2\times10^{-7} \pm 0.6\times10^{-7}$ [12] 2) 2×10^{-4} [13] 3) $2.5\times10^{-7} \pm 0.7\times10^{-7}$ [14]	1) Binding of ^{125}I labelled fibrinogen to the I-domain immobilized on the plate 2) SPR with the immobilized Fg and active I-domain in the solution 3) SPR with the immobilized Fg binding to CD11b-$I^{123-315}$
C3d	1) 4×10^{-7} [1] 2) 4.5×10^{-7} [1] 3) $1.5\times10^{-6} \pm 0.2\times10^{-6}$ [11]	1) SPR with immobilized C3d and I domain in solution 2) ITC 3) SPR with immobilized C3d and I domain in the solution
iC3b	1) 6×10^{-7} [1] 2) $10^{-7}–10^{-6}$ [1] 3) $4.6\times10^{-7} \pm 1.5\times10^{-7}$ [14] 4) $6.6\times10^{-7} \pm 3.0\times10^{-7}$ [14]	1) ITC 2) SPR with immobilized iC3b binding to I-domain 3) BLI with immobilized binding to CD11b-$I^{123-315}$ 4) SPR with immobilized iC3b binding to CD11b-I^{I316G}
Pleiotrophin (PNT) (cytokine and growth factor)	$1.2\times10^{-6} \pm 0.2\times10^{-6}$ / $3.9\times10^{-6} \pm 0.1\times10^{-6}$ [15]	BLI with PNT immobilized on the surface by two different methods and with active I-domain in the solution
CD54 (ICAM-1)	$2.2\times10^{-7} \pm 0.4\times10^{-7}$ [14]	SPR immobilized CD54 binding to CD11b-$I^{123-315}$

SPR: Surface plasmon resonance, BLI: bio-layer interferometry, ITC: isothermal titration calorimetry

SUPPLEMENTARY REFERENCES:

[1] Bajic, G., Yatime, L., Sim, R. B., Vorup-Jensen, T. & Andersen, G. R. Structural insight on the recognition of surface-bound opsonins by the integrin I domain of complement receptor 3. *Proceedings of the National Academy of Sciences* **110**, 16426–16431 (2013).

[2] Yakubenko, V. P., Lishko, V. K., Lam, S. C.-T. & Ugarova, T. P. A molecular basis for integrin $\alpha_M\beta_2$ Ligand binding promiscuity. *Journal of Biological Chemistry* **277**, 48635–48642 (2002).

[3] Zhang, L. & Plow, E. F. Amino acid sequences within the α subunit of integrin $\alpha_M\beta_2$ (Mac-1) critical for specific recognition of C3bi. *Biochemistry* **38**, 8064–8071 (1999).

[4] Zhang, L. & Plow, E. F. Identification and reconstruction of the binding site within $\alpha_M\beta_2$ for a specific and high affinity ligand, NIF. *Journal of Biological Chemistry* **272**, 17558–17564 (1997).

[5] Forsyth, C. B., Plow, E. F. & and Zhang, L. Interaction of the fungal pathogen *Candida albicans* with integrin CD11b/CD18: Recognition by the I domain is modulated by the lectin-like domain and the CD18 subunit. *The Journal of Immunology* **161**, 6198-6205 (1998).

[6] Oxvig, C., Lu, C. & Springer, T. A. Conformational changes in tertiary structure near the ligand binding site of an integrin I domain. *Proceedings of the National Academy of Sciences* **96**, 2215–2220 (1999).

[7] Violette, S. M., Rusche, J. R., Purdy, S. R., Boyd, J. G. & Cos, J. Differences in the binding of blocking anti-CD11b monoclonal antibodies to the A-domain of CD11b. *The Journal of Immunology* **155**, 3092-3101 (1995).

[8] Lishko, V. K., Yakubenko, V. P., Ugarova, T. P. & Podolnikova, N. P. Leukocyte integrin Mac-1 (CD11b/CD18, $\alpha_M\beta_2$, CR3) acts as a functional receptor for platelet factor 4. *Journal of Biological Chemistry* **293**, 6869–6882 (2018).

[9] Rieu, P., Ueda, T., Haruta, I., Sharma, C. E. & Arnaout, M. A. The A-Domain of β2 integrin CR3 (CDllb/CD18) is a receptor for the hookworm-derived neutrophil adhesion inhibitor NIF. *The Journal of Cell Biology* **127**, 11 (1994).

[10] Stapulionis, R. *et al.* Structural insight into the function of myelin basic protein as a ligand for integrin $\alpha_M\beta_2$. *The Journal of Immunology* **180**, 3946–3956 (2008).

[11] Zhang, X., Bajic, G., Andersen, G. R., Christiansen, S. H. & Vorup-Jensen, T. The cationic peptide LL-37 binds Mac-1 (CD11b/CD18) with a low dissociation rate and promotes phagocytosis. *Biochimica et Biophysica Acta (BBA) - Proteins and Proteomics* **1864**, 471–478 (2016).

[12] Zhou, L., Lee, D. H. S., Plescia, J., Lau, C. Y. & Altieri, D. C. Differential ligand binding specificities of recombinant CDllb/CD18 integrin I-domain. *Journal of Biological Chemistry* **269**, 17075-17079 (1994).

[13] Vorup-Jensen, T. *et al.* Exposure of acidic residues as a danger signal for recognition of fibrinogen and other macromolecules by integrin X 2. *Proceedings of the National Academy of Sciences* **102**, 1614–1619 (2005).

[14] Xiong, J.-P., Li, R., Essafi, M., Stehle, T. & Arnaout, M. A. An isoleucine-based allosteric switch controls affinity and shape shifting in integrin CD11b A-domain. *Journal of Biological Chemistry* **275**, 38762–38767 (2000).

[15] Shen, D. *et al.* Pleiotrophin, a multifunctional cytokine and growth factor, induces leukocyte responses through the integrin Mac-1. *Journal of Biological Chemistry* **292**, 18848–18861 (2017).

3. CONCLUDING DISCUSSION

Leukocidins, the main virulence factors of *S. aureus*, display significant host tropism (Table 1) that hinders studying their role in *S. aureus* pathogenesis in humans and results in ambiguous data from commonly used animal models with rabbits, mice and rats. To circumvent the host specificity of wide range of human specific bacterial factors, including *S. aureus* leukocidins, the most common approach is employing humanized animal models. The humanized animal models are, without a doubt, important and informative research tools, but as pathogens typically bind to the host molecules of complex biological function, humanizing such molecules may result in unforeseen secondary effects. The aim of the dissertation was to gain understanding on molecular mechanisms and structural requirements of leukocidin-host interactions in order to design leukocidin variants that will surpass species specificity, thus providing an alternative tool for humanized animal models in *S. aureus* research.

3.1. LukGH-CD11b-I interaction and its effect on the immune system

We hypothesized that LukGH can be adapted for different species by mapping the LukGH-CD11b-I interface and introducing minimal changes to LukGH, thus resulting in improved affinity for the receptor and subsequently improved cytotoxicity. As the LukGH-CD11b-I binding epitope was unknown when this PhD project was initiated, we first applied site-directed mutagenesis to map the LukH residues involved in interaction with CD11b-I. The binding epitope was subsequently confirmed with crystal structures of LukGH in complex with the human and the mouse CD11b-I domain. Contrary to other leukocidins where the binding epitope is part of the rim domain (Reyes-Robles et al, 2013; Laventie et al, 2014; Peng et al, 2018), the interacting residues of the main binding epitope (found on LukH) are located in the cap domain and they extend to the rim domain in the second binding interface (found on LukG). The crystal structures provided further insight into the molecular mechanism of LukGH-receptor interaction. LukGH dimerization in solution, before binding to the cellular receptor (DuMont et al, 2014; Badarau et al, 2015), was proposed to be responsible for the very high cytotoxic activity of LukGH, which is significantly correlated with the upregulation and activation of CD11b on target cells (Badarau et al, 2015; Janesch et al, 2017). This correlation can be explained by the presence of a second binding interface on the LukG protomer and binding of LukGH to active form of CD11b. As LukGH is binding to the activated form of CD11b, the observed receptor upregulation in presence of *S. aureus* infection-relevant stimuli (Janesch et al, 2017), further emphasises the importance of studying LukGH in the relevant *in vivo* models. Proposed model of pore formation illustrates how a single receptor molecule is able to bind two adjacent LukGH dimers in the octamer, and implicitly a single LukGH dimer can bind two receptor molecules,

via separate LukH and LukG interfaces (Manuscript I). The observed multivalent interaction can explain the high cytotoxic potency of the LukGH, similarly to *Bordetella pertussis* adenylate cyclase toxin (CyaA)-glycans (Hasan et al, 2015) or cholera toxin-gangliosides interactions (Kuziemko et al, 1996), where the multivalent interactions of the toxins with their receptors amplify the toxins' cytotoxicity by increasing the overall affinity. It remains to be seen whether the same principle can be translated to other leukocidins, especially LukSF-PV. The recently identified low affinity interaction of LukF-PV and its receptor CD45 (Table 1; Tromp et al, 2018), besides the other, high-affinity LukSF-PV/receptor interaction (Table 1; with C5Ra and C5L2 receptors) and localization of LukSF-PV in the receptor clusters (Haapasalo et al, 2019) could support such multivalent interactions of LukSF-PV for initiation of the pore formation. The leukocidin receptors and F-components appear to have more important role in the initiation of the oligomerisation and pore formation than believed previously.

The binding of ligands to CD11b/CD18 results in signal transduction across the plasma membrane and triggers intracellular signalling pathways that control diverse cell functions, like survival, migration or phagocytosis activation (Legate et al, 2009; Dupuy & Caron, 2008). Bacterial toxins can hijack CD11b functions, e.g. the CyaA binds the bent form of integrin and by blocking the downstream signalling, prevents activation of phagocytosis (Osicka et al, 2015). As LukGH is binding to the extended, active integrin, where I-domain is located at around 20 nm from the cell membrane (Figure 2A), the integrin has to bend for LukGH to insert into the membrane. By promoting integrin bending, LukGH may render CD11b-I inaccessible for the natural ligands and potentially alter downstream signalling, thus modulating the immune response to *S. aureus* infection. LukGH is binding to CD11b-I at the MIDAS site and its binding epitope overlaps with binding epitope of some natural ligands, e.g. C3d, iC3b or human fibrinogen (Zhang & Plow, 1999; Yakubenko et al, 2002; Bajic et al, 2013, Manuscript I). Considering the high LukGH-CD11b-I affinity, one can speculate that in certain conditions, e.g. high LukGH concentration during *S. aureus* infection, LukGH can potentially compete for binding with the natural ligands of CD11b-I. So far none of the studies have looked at the interplay between LukGH and natural ligands of CD11b-I, potentially an important aspect in LukGH contribution to *S. aureus* pathogenesis.

The extremely high specificity of LukGH-CD11b-I interaction and the availability of structural information on the interaction can aid the development of alternative methods to combat *S. aureus* infections. Receptor-based inhibitory approaches can be used to design small molecule antagonists or receptor-mimicking peptides neutralizing the toxin, as demonstrated for LukED and HIV antagonist (Alonso et al, 2012) and for Gram-negative bacterial toxin LtxA and peptides mimicking binding site on receptor CD11a/CD18 (Krueger et al, 2018), respectively. Furthermore, high

specificity and defined binding epitope render LukGH a feasible candidate for engineering potential therapeutic candidates for targeting the integrin to limit inflammatory responses in CD11b/CD18 mediated autoimmune diseases such as systemic lupus erythematosus or rheumatoid arthritis (Schittenhelm et al, 2017; Manuscript I).

While this dissertation provides structural and molecular basis of LukGH-CD11b-I interaction, additional studies from structural, cell signalling, immunological and functional aspect (e.g. role of lipids in binding, binding of LukGH to inactive form of integrin, effects of integrin bending on integrin downstream signalling, interplay between LukGH and natural ligands of CD11b-I) are necessary to fully understand this complex interaction and its consequences on the immune system. The dissertation also adds to the recent data on the role of receptors in the initiation of the leukocidin pore formation and contribution to their cytotoxicity. These data, taken together with currently available structural and biochemical data on other leukocidins (Reyes-Robles & Torres, 2016; Badarau et al, 2017; Spaan et al, 2017), provide a basis for detailed computational analysis of the mechanism of pore formation that can help to understand the dynamics and energy of the oligomerisation initiation and the pore formation mechanism.

3.2. Species specificity of leukocidins and adaptation of LukGH for the rabbit host

Following determination of the binding epitope, we set out to adapt LukGH for animal hosts by protein engineering of the binding epitope. As there is a measurable but weak interaction between LukGH and the rabbit receptor, accompanied by detectable PMN cytotoxicity *in vitro*, and as rabbits are also sensitive to other pore forming leukocidins (Table 1), we decided to adapt LukGH for rabbits. By introducing one or two mutations in the LukH epitope determined by site-directed mutagenesis, we have modified the LukGH-CD11b-I interface for increased LukGH affinity for the rabbit receptor and cytotoxicity towards rabbit PMNs when expressed recombinantly or from the *S. aureus* chromosome. Even though these data suggest that rabbit adapted strains have a potential for studying LukGH role in *S. aureus* pathogenesis, additional *in vitro* experiments (e.g. visualization of the LukGH binding to the cell surface, activity towards different cells not expressing CD11b/CD18) have to be done to exclude expansion of LukGH pathogenic properties, as it was observed for murine adapted lnlA from *Listeria monocytogenes* (Tsai et al, 2013). Furthermore, contribution of the rabbit-PMN adapted LukGH to *S. aureus* pathogenesis in rabbits in relevant animal models has to be assessed (e.g. rabbit infection model with *S. aureus* wild-type and rabbit-PMN adapted LukGH-expressing strain, testing of different *S. aureus* strains expressing different LukGH variants *in vivo*). While we did increase the sensitivity of rabbit PMNs for LukGH, the sensitivity was still one order of magnitude lower than in humans. The crystal structures of LukGH-receptor complexes

additionally clarified the observed LukGH species specificity and will aid in further improvement of LukGH cytotoxicity in rabbits, as well as in different, more cost-effective animal models; like mouse, rat and guinea pig. The possibility of additional animal models should be considered, as rabbits are more sensitive to LukED that is present in the majority of *S. aureus* strains (Diep et al, 2016) and as leucocidin-mediated red blood cell lysis is much more pronounced with rabbit compared to human RBCs (Trstenjak et al, 2019). The process of LukGH species adaptation by protein engineering can potentially be adjusted for expanding host range of other leukocidins where low cytotoxicity towards certain species is the result of molecular incompatibility between the receptor and cognate leukocidin (i.e. LukSF-PV-C5aR or HlgCB-C5aR in mouse (Spaan et al, 2015a; Trstenjak et al, 2019)). Importantly, it can also be used when obtaining structural information on leukocidin-receptor interaction is challenging, as other leukocidins are binding to transmembrane receptors (Table 1; Trstenjak et al, 2019).

Mouse PMNs are, in our hands using different assay readouts (measuring LDH release (data not shown) or produced ATP), fully resistant to recombinant LukGH wild-type and variants. Weak LukGH cytotoxicity towards mouse PMNs was previously observed using LukGH purified from *S. aureus* culture supernatants (Malachowa et al, 2012), potential consequence of impurities acquired during LukGH purification from the culture supernatants. Based on the LukGH-CD11b-I crystal structures and the supporting experiments, lack of LukGH cytotoxicity towards mouse PMNs, despite the increased affinity of modified leukocidin for the mouse receptor (LukGH_K319A variant), is likely the result of LukGH oligomerisation deficiency in the presence of moCD11b-I in solution. Additional experiments have to be done to confirm lack of LukGH oligomerisation when CD11b-I is expressed on the cell surface (e.g. cryogenic electron microscopy, single-molecule localization microscopy). Despite the mutagenesis efforts of the binding epitope based on the LukGH_K319A-moCD11b-I crystal structure, we were not able to surpass the LukGH oligomerisation deficiency or increase cytotoxicity towards mouse PMNs, suggesting there is more to LukGH-CD11b-I mechanism of interaction than we currently understand. As the binding of the LukGH to CD11b-I doesn't seem to be the restrictive step in the pore formation, one of the subsequent steps (Figure 1) can potentially limit the LukGH cytotoxicity towards mouse cells.

Important aspects of LukGH-CD11b interaction that were also not considered in species specificity so far are CD11b/CD18 glycosylation pattern and the potential contribution of the CD18 subunit. While it was shown that human CD11b subunit alone is sufficient to render cells susceptible to LukGH (DuMont et al, 2013b), same has never been shown for mouse subunit or subunit from other species. An interesting aspect to follow up with is the different predicted glycosylation pattern in full length human and mouse CD11b/CD18 (UniProtKB P11215 and P05555). Even though none of

the CD11b/CD18 predicted glycosylation sites is located in the I-domain, glycans close to the I-domain could potentially sterically hinder the LukGH oligomer formation in mice. Additional experiments with full length and/or glycosylated CD11b/CD18 or mouse-human receptor chimera could aid in further understanding of the observed host tropism.

The emergence of multi-drug resistant *S. aureus* strains and their spread in the hospital and community settings increased the need for effective therapeutics. Due to our limited knowledge on *S. aureus* pathogenesis in humans and non-predictive animal models, there are no available therapeutics up to date other than antibiotics. The research presented in this dissertation provides molecular and structural basis of LukGH-receptor interaction and illustrates how this data can be used to surpass the observed LukGH species specificity, thus providing an alternative tool to existing animal models and can potentially be used to expand to other species-specific virulence factors.

4. REFERENCES

Adair, B. D., Xiong, J.-P., Alonso, J. L., Hyman, B. T. & Arnaout, M. A. EM Structure of the ectodomain of integrin CD11b/CD18 and localization of its ligand-binding site relative to the plasma membrane. *PLoS One* **8**, e57951 (2013).

Adhikari, R. P. *et al.* Antibodies to *S. aureus* LukS-PV attenuated subunit vaccine neutralize a broad spectrum of canonical and non-canonical bicomponent leukotoxin pairs. *PLOS One* **10,** e0137874 (2015).

Aires-de-Sousa, M. Methicillin-resistant *Staphylococcus aureus* among animals: current overview. *Clinical Microbiology and Infection* **23**, 373–380 (2017).

Alonzo III, F. *et al.* CCR5 is a receptor for *Staphylococcus aureus* leukotoxin ED. *Nature* **493,** 51–55 (2012).

Alonzo, F. & Torres, V. J. The bicomponent pore-forming leucocidins of *Staphylococcus aureus*. *Microbiology and Molecular Biology Reviews* **78,** 199–230 (2014).

Arnaout, M. A. Biology and structure of leukocyte β2 integrins and their role in inflammation. *F1000Research* **5**, (2016).

Badarau, A. *et al.* Structure-function analysis of heterodimer formation, oligomerization, and receptor binding of the *Staphylococcus aureus* bi-component toxin LukGH. *Journal of Biological Chemistry* **290,** 142–156 (2015).

Badarau, A. *et al.* Context matters: The importance of dimerization-induced conformation of the LukGH leukocidin of *Staphylococcus aureus* for the generation of neutralizing antibodies. *mAbs* **8,** 1347–1360 (2016).

Badarau, A., Trstenjak, N. & Nagy, E. Structure and function of the two-component cytotoxins of *Staphylococcus aureus* – Learnings for designing novel therapeutics. in *Protein Reviews: Volume 18* (ed. Atassi, M. Z.) 15–35 (Springer Singapore, 2017).

Bajic, G., Yatime, L., Sim, R. B., Vorup-Jensen, T. & Andersen, G. R. Structural insight on the recognition of surface-bound opsonins by the integrin I domain of complement receptor 3. *Proceedings of the National Academy of Sciences* **110**, 16426–16431 (2013).

Berube, B. & Wardenburg, J. *Staphylococcus aureus* α-toxin: Nearly a century of intrigue. *Toxins* **5**, 1140–1166 (2013).

Brown, E. L. et al. The Panton–Valentine leukocidin vaccine protects mice against lung and skin infections caused by *Staphylococcus aureus* USA300. *Clinical Microbiology and Infection* 15, 156-164 (2009).

Campbell, I. D. & Humphries, M. J. Integrin structure, activation, and interactions. *Cold Spring Harbor Perspectives in Biology* **3**, a004994–a004994 (2011).

Chambers, H. F. & DeLeo, F. R. Waves of resistance: *Staphylococcus aureus* in the antibiotic era. *Nature Reviews Microbiology* **7,** 629–641 (2009).

Colin, D. A., Mazurier, I., Sire, S. & Finck-Barbancon, V. Interaction of the two components of leukocidin from *Staphylococcus aureus* with human polymorphonuclear leukocyte membranes: sequential binding and subsequent activation. *Infection and Immunity* **62,** 3184–3188 (1994).

Coxon, A., Rieu, P., Barkalow, F. J., Askari, S. & Sharpe, A. H. A novel role for the β2 integrin CD11b/CD18 in neutrophil apoptosis: A homeostatic mechanism in inflammation. *Immunity* **5**, 653-666 (1996).

Dalla Serra, M. *et al. Staphylococcus aureus* bicomponent γ-hemolysins, HlgA, HlgB, and HlgC, can form mixed pores containing all components. *Journal of Chemical Information and Modeling* **45**, 1539–1545 (2005).

Diamond, M. S., Garcia-Aguilar, J., Bickford, J. K. & Springer, T. A. The I domain is a major recognition site on the leukocyte integrin Mac-1 (CDllb/CD18) for four distinct adhesion ligands. *The Journal of Cell Biology* **120**, 1031-1043 (1993).

Diep, B. A. *et al.* Improved protection in a rabbit model of community-associated methicillin-resistant *Staphylococcus aureus* necrotizing pneumonia upon neutralization of leukocidins in addition to alpha-hemolysin. *Antimicrobial Agents and Chemotherapy* **60,** 6333–6340 (2016).

Ding, Z.M. *et al.* Relative contribution of LFA-1 and Mac-1 to neutrophil adhesion and migration. *The Journal of Immunology* **163**, 5029 –5038 (1999).

DuMont, A. L. *et al.* Characterization of a new cytotoxin that contributes to *Staphylococcus aureus* pathogenesis: The cytotoxin LukAB kills human phagocytes. *Molecular Microbiology* **79,** 814-825 (2011).

DuMont, A. L. *et al. Staphylococcus aureus* elaborates leukocidin AB to mediate escape from within human neutrophils. *Infection and Immunity* **81,** 1830–1841 (2013a).

DuMont, A. L. *et al. Staphylococcus aureus* LukAB cytotoxin kills human neutrophils by targeting the CD11b subunit of the integrin Mac-1. *Proceedings of the National Academy of Sciences* **110,** 10794–10799 (2013b).

DuMont, A. L. *et al.* Identification of a crucial residue required for *Staphylococcus aureus* LukAB cytotoxicity and receptor recognition. *Infection and Immunity* **82,** 1268–1276 (2014).

Dupuy, A. G. & Caron, E. Integrin-dependent phagocytosis - spreading from microadhesion to new concepts. *Journal of Cell Science* **121**, 1773–1783 (2008).

Fan, Z. *et al.* Neutrophil recruitment limited by high-affinity bent β2 integrin binding ligand in cis. *Nature Communications* **7**, 12658 (2016).

Fowler, V. G. & Proctor, R. A. Where does a *Staphylococcus aureus* vaccine stand? *Clinical Microbiology and Infection* **20**, 66–75 (2014).

Gillet, Y. *et al.* Association between *Staphylococcus aureus* strains carrying gene for Panton-Valentine leukocidin and highly lethal necrotising pneumonia in young immunocompetent patients. *The Lancet* **359**, 753–759 (2002).

Graves, S. F. *et al.* Sublytic concentrations of *Staphylococcus aureus* Panton-Valentine leukocidin alter human PMN gene expression and enhance bactericidal capacity. *Journal of Leukocyte Biology* **92**, 361–374 (2012).

Guerra, F. E., Borgogna, T. R., Patel, D. M., Sward, E. W. & Voyich, J. M. Epic immune battles of history: Neutrophils vs. *Staphylococcus aureus*. *Frontiers in Cellular and Infection Microbiology* **7**, (2017).

Guillet, V. et al. Crystal structure of leucotoxin S component: New insight into the staphylococcal β-barrel pore-forming toxins. *Journal of Biological Chemistry* **279**, 41028–41037 (2004).

Haapasalo, K. *et al. Staphylococcus aureus* toxin LukSF dissociates from its membrane receptor target to enable renewed ligand sequestration. *The FASEB Journal* **33**, 3807–3824 (2019).

Hasan, S. *et al.* Interaction of *Bordetella* adenylate cyclase toxin with complement receptor 3 involves multivalent glycan binding. *FEBS Letters* **589**, 374–379 (2015).

Ho, M.K. & Springer, T.A. Mac-1 antigen: quantitative expression in macrophage populations and tissues, and immunofluorescent localization in spleen. *The Journal of Immunology* **128**, 2281–2286 (1982).

Janesch, P. *et al.* Selective sensitization of human neutrophils to LukGH mediated cytotoxicity by *Staphylococcus aureus* and IL-8. *Journal of Infection* **74,** 473–483 (2017).

Kobayashi, S. D. *et al.* Comparative analysis of USA300 virulence determinants in a rabbit model of skin and soft tissue infection. *The Journal of Infectious Diseases* **204**, 937–941 (2011).

Koop, G. *et al.* Identification of LukPQ, a novel, equid-adapted leukocidin of *Staphylococcus aureus*. *Scientific Reports* **7,** 40660 (2017).

König, B. et al Composition of staphylococcal bi-component toxins determines pathophysiological reactions. *Journal of medical microbiology* **46**, 479–485 (1997).

Krueger, E., Hayes, S., Chang, E. H., Yutuc, S. & Brown, A. C. Receptor-based peptides for inhibition of leukotoxin activity. *ACS Infectious Diseases* **4**, 1073–1081 (2018).

Kuziemko, G. M., Stroh, M. & Stevens, R. C. Cholera toxin binding affinity and specificity for gangliosides determined by surface plasmon resonance. *Biochemistry* **35**, 6375–6384 (1996).

Labandeira-Rey, M. et al. Panton-Valentine leukocidin causes necrotizing pneumonia. *Science* **315**, 1130-1133 (2007).

Latger-Cannard, V., Duma, D., Bensoussan, D., Stoltz, J.F. Spatial distribution of the beta2 integrin (CD11b/CD18) and L-selectin (CD62L) adherence receptors on human neutrophils by Conventional Optical Scanning Microscopy (COSM). *Biorheology* **40**, 167-172 (2003).

Laventie, B. J. *et al.* Residues essential for Panton-Valentine leukocidin S component binding to its cell receptor suggest both plasticity and adaptability in its interaction surface. *PLoS One* **9,** e92094 (2014).

Lee, J.-O., Rieu, P., Arnaout, M. A. & Liddington, R. Crystal structure of the A domain from the a subunit of integrin CR3 (CD11 b/CD18). *Cell* **80,** 631–638 (1995a).

Lee, J.-O., Bankston, L. A. & Robert C Liddington, M. A. A. and. Two conformations of the integrin A-domain (I-domain): a pathway for activation? *Structure* **3**, 1333–1340 (1995b).

Legate, K. R., Wickstrom, S. A. & Fassler, R. Genetic and cell biological analysis of integrin outside-in signaling. *Genes & Development* **23**, 397–418 (2009).

Lina, G. *et al.* Involvement of Panton-Valentine leukocidin producing *Staphylococcus aureus* in primary skin Infections and pneumonia. *Clinical Infectious Diseases* **29**, 1128–1132 (1999).

Lipinska, U. *et al.* Panton-Valentine leukocidin does play a role in the early stage of *Staphylococcus aureus* skin infections: A rabbit model. *PLoS One* **6**, e22864 (2011).

Löffler, B. et al. *Staphylococcus aureus* Panton-Valentine leukocidin is a very potent cytotoxic factor for human neutrophils. *PLoS Pathogens* **6**, e1000715 (2010).

Lubkin, A. *et al. Staphylococcus aureus* leukocidins target endothelial DARC to cause lethality in mice. *Cell Host & Microbe* **25**, 463-470 (2019).

Lynn, W.A., Raetz C.R., Qureshi, N. & Golenbock, D.T. Lipopolysaccharide-induced stimulation of CD11b/CD18 expression on neutrophils. Evidence of specific receptor-based response and inhibition by lipid A-based antagonists. *The Journal of Immunology* **147**, 3072-3079 (1991).

Malachowa, N. *et al. Staphylococcus aureus* leukotoxin GH promotes inflammation. *Journal of Infectious Diseases* **206,** 1185–1193 (2012).

Malachowa, N., Kobayashi, S. D., Freedman, B., Dorward, D. W. & DeLeo, F. R. *Staphylococcus aureus* leukotoxin GH promotes formation of neutrophil extracellular traps. *The Journal of Immunology* **191**, 6022–6029 (2013).

Monecke, S. *et al.* Diversity of *Staphylococcus aureus* isolates in European wildlife. *PLOS One* **11**, e0168433 (2016).

Monma, N. *et al.* Essential residues, W177 and R198, of LukF for phosphatidylcholine-binding and pore-formation by staphylococcal-hemolysin on human erythrocyte membranes. *Journal of Biochemistry* **136**, 427–431 (2004).

Naimi, T. S. *et al.* Comparison of community- and health care–associated methicillin-resistant *Staphylococcus aureus* infection. *JAMA* **290**, 2976-2984 (2003).

Nguyen, V. T., Kamio, Y. & Higuchi, H. Single-molecule imaging of cooperative assembly of γ-hemolysin on erythrocyte membranes. *The EMBO journal* **22**, 4968–4979 (2003).

Nocadello, S. *et al.* Crystal structures of the components of the *Staphylococcus aureus* leukotoxin ED. *Acta Crystallographica Section D Structural Biology* **72,** 113–120 (2016).

Olson R., Nariya H., Yokota K., Kamio Y., & Gouaux E. Crystal structure of staphylococcal LukF delineates conformational changes accompanying formation of a transmembrane channel. *Nature Structural Biology* **6**, 134–140 (1999).

Osicka, R. et al. Bordetella adenylate cyclase toxin is a unique ligand of the integrin complement receptor 3. *eLife* **4**, e10766 (2015).

Pédelacq, J.-D. *et al.* The structure of a *Staphylococcus aureus* leucocidin component (LukF-PV) reveals the fold of the water-soluble species of a family of transmembrane pore-forming toxins. *Structure* **7,** 277–287 (1999).

Peng, Z. et al. Rim domain loops of staphylococcal β-pore forming bi-component toxin S-components recognize target human erythrocytes in a coordinated manner. *The Journal of Biochemistry* **164**, 93–102 (2018).

Pilsczek, F. H. *et al.* A novel mechanism of rapid nuclear neutrophil extracellular trap formation in response to *Staphylococcus aureus*. *The Journal of Immunology* **185**, 7413–7425 (2010).

Podolnikova, N. P., Podolnikov, A. V., Haas, T. A., Lishko, V. K. & Ugarova, T. P. Ligand recognition specificity of leukocyte integrin α_M β_2 (Mac-1, CD11b/CD18) and its functional consequences. *Biochemistry* **54,** 1408–1420 (2015).

Potrich, C. *et al.* The influence of membrane lipids in *Staphylococcus aureus* gamma-hemolysins pore formation. *Journal of Membrane Biology* **227,** 13–24 (2009).

Prince, A., Wang, H., Kitur, K. & Parker, D. Humanized mice exhibit increased susceptibility to *Staphylococcus aureus* pneumonia. *Journal of Infectious Diseases* **215**, 1386-1395 (2017).

Rao, Q., Rao, X., Hu, X. & Shang, W. *Staphylococcus aureus* ST121: a globally disseminated hypervirulent clone. *Journal of Medical Microbiology* **64**, 1462–1473 (2015).

Reyes-Robles, T. *et al. Staphylococcus aureus* leukotoxin ED targets the chemokine receptors CXCR1 and CXCR2 to kill leukocytes and promote infection. *Cell Host & Microbe* **14,** 453–459 (2013).

Reyes-Robles T. & Torres V.J. *Staphylococcus aureus* pore-forming toxins. In: Bagnoli F., Rappuoli R., Grandi G. (eds) *Staphylococcus aureus*. Current Topics in Microbiology and Immunology, vol 409. Springer, Cham (2016).

Rigby, K. M. & DeLeo, F. R. Neutrophils in innate host defense against *Staphylococcus aureus* infections. *Seminars in Immunopathology* **34**, 237–259 (2012).

Roblin, P. *et al.* A covalent S-F heterodimer of leucotoxin reveals molecular plasticity of β-barrel pore-forming toxins. *Proteins: Structure, Function, and Bioinformatics* **71,** 485–496 (2008).

Rouha, H. *et al.* Five birds, one stone: Neutralization of α-hemolysin and 4 bi-component leukocidins of *Staphylococcus aureus* with a single human monoclonal antibody. *mAbs* **7,** 243–254 (2015).

Salgado-Pabón, W. & Schlievert, P. M. Models matter: the search for an effective *Staphylococcus aureus* vaccine. *Nature Reviews Microbiology* **12**, 585–591 (2014).

Schittenhelm, L., Hilkens, C. M. & Morrison, V. L. β2 integrins as regulators of dendritic cell, monocyte, and macrophage function. *Frontiers in Immunology* **8**, 1866 (2017).

Sen, M., Yuki, K. & Springer, T. A. An internal ligand-bound, metastable state of a leukocyte integrin, α X β 2. *The Journal of Cell Biology* **203**, 629–642 (2013).

Sen, M. & Springer, T. A. Leukocyte integrin α L β 2 headpiece structures: The αI domain, the pocket for the internal ligand, and concerted movements of its loops. *Proceedings of the National Academy of Sciences* **113**, 2940–2945 (2016).

Sengelov, H., Kjeldsen, L. & Diamond, M. S. Subcellular localization and dynamics of Mac-1 ($\alpha_m\beta_2$) in human neutrophils. *Journal of Clinical Investigation* **92**, 1467-1476 (1993).

Shimaoka, M., Takagi, J. & Springer, T. A. Conformational regulation of integrin structure and function. *Annual Review of Biophysics and Biomolecular Structure* **31**, 485–516 (2002).

Spaan, A. N., Surewaard, B. G. J., Nijland, R. & van Strijp, J. A. G. Neutrophils versus *Staphylococcus aureus*:A biological tug of war. *Annual Review of Microbiology* **67**, 629–650 (2013a).

Spaan, A. N. *et al.* The staphylococcal toxin Panton-Valentine leukocidin targets human C5a receptors. *Cell Host & Microbe* **13,** 584–594 (2013b).

Spaan, A. N. *et al.* The staphylococcal toxins γ-haemolysin AB and CB differentially target phagocytes by employing specific chemokine receptors. *Nature Communications* **5,** 5438 (2014).

Spaan, A. N. *et al.* Differential interaction of the staphylococcal toxins Panton–Valentine leukocidin and γ-Hemolysin CB with human C5a receptors. *The Journal of Immunology* **195,** 1034–1043 (2015a).

Spaan, A. N. *et al. Staphylococcus aureus* targets the Duffy antigen receptor for chemokines (DARC) to lyse erythrocytes. *Cell Host & Microbe* **18,** 363–370 (2015b).

Spaan, A. N., van Strijp, J. A. G. & Torres, V. J. Leukocidins: staphylococcal bi-component pore-forming toxins find their receptors. *Nature Reviews Microbiology* **15**, 435-447 (2017).

Tan, S. The leucocyte β2 (CD18) integrins: the structure, functional regulation and signalling properties. *Bioscience Reports* **32**, 241–269 (2012).

Tong, S. Y. C., Davis, J. S., Eichenberger, E., Holland, T. L. & Fowler, V. G. *Staphylococcus aureus* infections: Epidemiology, pathophysiology, clinical manifestations, and management. *Clinical Microbiology Reviews* **28,** 603–661 (2015).

Tromp, A. T. *et al.* Human CD45 is an F-component-specific receptor for the staphylococcal toxin Panton–Valentine leukocidin. *Nature Microbiology* **3,** 708–717 (2018).

Trstenjak, N. *et al.* Adaptation of the *Staphylococcus aureus* leukocidin LukGH for the rabbit host by protein engineering. *Biochemical Journal* **476**, 275-292 (2019).

Tsai, Y.-H., Disson, O., Bierne, H. & Lecuit, M. Murinization of internalin extends its receptor repertoire, altering *Listeria monocytogenes* cell tropism and host responses. *PLoS Pathogens* **9**, e1003381 (2013).

Vandenesch, F., Lina, G. & Henry, T. *Staphylococcus aureus* hemolysins, bi-component leukocidins, and cytolytic peptides: A redundant arsenal of membrane-damaging virulence factors? *Frontiers in Cellular and Infection Microbiology* **2,** (2012).

Ventura, C. L. *et al.* Identification of a novel *Staphylococcus aureus* two-component leukotoxin using cell surface proteomics. *PLoS One* **5,** e11634 (2010).

Viana, D. et al. A single natural nucleotide mutation alters bacterial pathogen host tropism. *Nature Genetics* **47**, 361–366 (2015).

Voyich, J. M. *et al.* Is Panton-Valentine leukocidin the major virulence determinant in community-associated methicillin-resistant *Staphylococcus aureus* disease? *The Journal of Infectious Diseases* **194**, 1761–70 (2006).

Vrieling, M. *et al.* Bovine *Staphylococcus aureus* secretes the leukocidin LukMF' to kill migrating neutrophils through CCR1. *mBio* **6**, e00335-15 (2015).

Wollert, T. *et al.* Extending the host range of *Listeria monocytogenes* by rational protein design. *Cell* **129,** 891–902 (2007).

Woodin, A. M. Fractionation of a leucocidin from *Staphylococcus aureus*. *Biochemical Journal* **73**, 225–237 (1959).

Woodin, A. M. Purification of the two components of leucocidin from *Staphylococcus aureus*. *Biochemical Journal* **75,** 158–165 (1960).

Wright, S. D. et al. Identification of the C3bi receptor of human monocytes and macrophages by using monoclonal antibodies. *Proceedings of the National Academy of Sciences* **80**, 5699-5703 (1983).

Wright, S. D. et al. Complement receptor type three (CD11b/CD18) of human polymorphonuclear leukocytes recognizes fibrinogen. *Proceedings of the National Academy of Sciences* **85**, 7734–7738 (1988).

Xie, C. et al. Structure of an integrin with an αI domain, complement receptor type 4. *The EMBO Journal* **29**, 666–679 (2010).

Yakubenko, V. P., Lishko, V. K., Lam, S. C.-T. & Ugarova, T. P. A Molecular basis for integrin αM β2 ligand binding promiscuity. *Journal of Biological Chemistry* **277**, 48635–48642 (2002).

Yamashita, K. *et al*. Crystal structure of the octameric pore of staphylococcal γ-hemolysin reveals the β-barrel pore formation mechanism by two components. *Proceedings of the National Academy of Sciences USA* **108**, 17314-17319 (2011).

Yamashita, D. *et al.* Molecular basis of transmembrane beta-barrel formation of staphylococcal pore-forming toxins. *Nature Communication* **5**, 4897 (2014).

Yanai, M. et al. Separately or combined, LukG/LukH is functionally unique compared to other staphylococcal bicomponent leukotoxins. *PLoS One* **9**, e89308 (2014).

Yokota K. & Kamio, Y. Tyrosine 72 residue at the bottom of rim domain in LukF crucial for the sequential binding of the staphylococcal γ-hemolysin to human erythrocytes. *Bioscience, Biotechnology and Biochemistry* **64**, 2744–2747 (2000)

Yoong, P. & Pier, G. B. Immune-activating properties of Panton-Valentine leukocidin improve the outcome in a model of methicillin-resistant *Staphylococcus aureus* pneumonia. *Infection and Immunity* **80**, 2894–2904 (2012).

Yoong, P. & Torres, V. J. Counter inhibition between leukotoxins attenuates *Staphylococcus aureus* virulence. *Nature Communications* **6**, 8125 (2015).

Zhang, L. & Plow, E. F. Amino acid sequences within the α subunit of integrin αM β2 (Mac-1) critical for specific recognition of C3bi. *Biochemistry* **38**, 8064–8071 (1999).